Controls on intrusion-related gold mineralisation in the Lisle/Golconda area northeast Tasmania

Nicholas J. Fitzpatrick BSc

UNIVERSITY
OF TASMANIA

A research thesis submitted as partial fulfilment of a
Bachelor of Science with Honours

CODES SRC
Centre for Ore Deposit Research

Abstract

The Enterprise and Potoroo prospects are located in the historical mining district of the Lisle/Golconda area of northeast Tasmania, 30km northeast of Launceston, and gold at both is hosted predominantly in and immediately adjacent to granitic intrusions. Mineralisation at the Enterprise prospect is hosted in Devonian granodiorite of the Scottsdale Batholith, and occurs in several sub-vertical 0.1 – 0.5 metre wide continuos quartz veins, whereas the Potoroo prospect hosts disseminated and vein hosted sulphide mineralisation in pervasively altered granodiorite. Typical mineralised intersections at Enterprise included 0.4 metres at 14.4g/t Au, and at Potoroo 106.5 metres at 0.2g/t Au. These sites occur on the subsurface extension of the Scottsdale Batholith, which projects 11km west of the main granite mass.

Geological logging found that initially a 300 metre diameter circular stock of feldspar-biotite-quartz granodiorite was intruded, and is chemically one of the most primitive magmas in the Scottsdale Batholith. It was followed by at least two additional phases and a series of 'vein' dykes and quartz veins. Mineralogy and geochemical data indicate that a cryptic Si-Na alteration pervasively modified all of these rocks, prior to the development of the Au bearing veins with haloes of secondary biotite ± pyrrhotite, and subsequent baron quartz veins.

Magmatic hydrothermal features (quartz-layered textures, aplite 'vein' dykes, greisen and myrmekitic textures) in the feldspar-biotite-quartz granodiorite, suggest the evolution of a volatile phase during its crystallisation. However there is no specific evidence to indicate gold-bearing quartz formed from these precise fluids. Rather the subsequent alteration of these rocks provides evidence that similar volatile development continued at depth across the period of gold formation. The fluid inclusions at this structural level therefore provide a guide but not a direct measure of fluids active at the time of gold precipitation. The inclusions in both magmatic and hydrothermal lithologies comprise three types: *Type 1* CO_2-rich, high temperature (290° to 450°C), and low salinity (<14 wt % NaCl equiv); *Type 2* H_2O-rich, moderate temperature (160° to 420°C), low salinity (<12.2 wt % NaCl equiv); and *Type 3* NaCl rich, with decrepitation temperatures (T_d) up to 420°C and salinities of at least 26.5 wt

% NaCl equiv. The CO_2-rich nature and high temperature are consistent with a magmatic origin. Moreover, sulphides directly related to ore have $\delta^{34}S$ = -0.36 to 2.43‰, which is consistent with a magmatic origin, and is significantly different to most Mathinna Group-hosted gold vein system values.

Based on major and trace element characteristics, the Enterprise and Potoroo granodiorites are geochemically distinct from the Scottsdale Batholith. Phase proportions in CO_2-rich fluid inclusions, and aluminium-in-hornblende barometry, estimated pressures of emplacement of up to 1000 bars or 4 km for the Enterprise intrusion. By contrast, data for the bulk of the Scottsdale Batholith (as published elsewhere) is 100 to 2400 bars, or 5 to 9km depth, supporting a much deeper emplacement depth. The pressure of emplacement and chemistry of the Enterprise pluton is distinct from the Scottsdale Batholith, supporting that the Enterprise forms a distinct intrusive body, although the two may be linked along the aforementioned granite ridge.

Several important features including physiochemical characteristics of the fluids, depth of emplacements and distribution/style of alteration and mineralisation make the Enterprise and Potoroo prospects very similar to well characterised intrusion-related gold deposits, such as Fort Knox and Pogo, Alaska, USA, rather than classic metamorphic gold systems emplaced into granite. The large resources in some of these deposits provide optimism, and geometric guides, for future exploration of the Scottsdale Batholith.

Declaration

This theses contains no material which has been accepted for the award of any other degree or diploma in any university, and to the best of the authors knowledge, contains no material previously published or written by any other person, except where due reference is made in the text.

Nicholas Justin Fitzpatrick

November 2004

Acknowledgements

First and for most I would like to thank my two supervisors Garry Davidson and Anthony Harris for their wisdom, advice and support throughout the year.

I extend my gratitude to TasGold limited for the opportunity to conduct this project, and for the logistical and financial support. In particular, I wish to thank Rob Reid for his assistance.

This would not have been possible if it was not for the assistance provided by the technical staff including Christine Cook and Keith Harris (sulphur isotopes), Katie McGoldrick (rock preparation), Phil Robinson (analytical), David Steel (microprobe) and Simon Stephens (petrology).

I would also like to thank Tom and Tim for the loan of their digital cameras, allowing me to go through the year without purchasing one of my own.

Thanks to all my fellow honours students: Ben, Hugh, Kerrin, Kate, Choppa, Trent, Ned, Derek, Mick, John and Grace for a great year.

Finally, my family: Mum, Dad, Jason and Andrew, for their continued support over the last four years, making all this possible.

Table of Contents

List of Figures

List of Plates

List of Tables

1. Introduction

1.1 Preamble

Gold at the Enterprise and Potoroo gold prospects occurs within and immediately adjacent to, granitic intrusions. Mineralisation at the Enterprise prospect is in Devonian granodiorite, occurring as quartz veins, whereas the Potoroo prospect hosts disseminated and vein hosted sulphide mineralisation in pervasively altered granodiorite. TasGold Ltd is evaluating these prospects, and several others in the area, for their economic potential. Paragenetic studies incorporating a variety of petrographic techniques (including microthermometry) help to better constrain exploration models. One hypothesis is that the mineralisation is an example of an 'Intrusion-related gold' style deposit. Several important features (e.g. physiochemical characteristics of the fluids, depth of emplacements and distribution/style of alteration and mineralisation) make the Enterprise and Potoroo prospects very similar to well characterised intrusion-related gold deposits, such as Fort Knox and Pogo, Alaska, USA (Table 1.1).

1.2 Prospect Location and Access

The Enterprise and Potoroo prospects form part of exploration licence (EL) 2/92, located south of Golconda, approximately 30 km northeast of Launceston (Figure 1.1), Tasmania. Access to the study area is via the B81, beginning approximately 7 km north of Launceston at an intersection with the East Tamar Highway. Approximately 30 km along B81 a sign posted 'Golconda' leads to several prospects, including the Enterprise and Potoroo. Tracks are unsealed with 4WD transport recommended on some and others only accessible on foot. The maximum relief of the area is 400m. The landscape is covered by open sclerophyll woodland to dense wet sclerophyll forest, with minor cleared areas. Due to the long history of mining in the district, the countryside is covered with abandoned workings including shafts and pits, although many are now in filled they still pose a significant hazard to those using the area.

TABLE 1.1 Characteristics of Intrusion-Related Gold Deposits with Resources >0.5 M oz (after Baker, 2002)

Deposit	Size (Mt)	Grade(g/t Au)	Host intrusion	Deposit Style	Metal suite	Au/Bi r[2]	Ore minerals	Alteration	Fluids (T=°C, S= wt%NaCl equiv)	(kbar)/ Depth (km)	References
Korri Kollo, Bolivia	64	2.3	Dacite domes, I?	Sheeted veinlets	Ag, As, Sb, Sn, Bi, Cu, Zn, Pb, W	?	Py, Apy, Ccp, Gal, Bim, Sbn, Sph	Argillic	Early H_2O-NaCl brine S = 8-45, T >300; later H_2O-NaCl S =5-15. T =200-350	<0.5/0.4-0.8	Peterson and Fitzmeyer (1998)
Brewery Creek, Yukon	13.3	1.4	Monzonite sills, I>M	Disseminated and veinlets	As, Sb, (Hg)	Abs	Py, Po, Apy, Sbn	Qtz, Ser, Carb, Clay	Immiscible H_2O-NaCl brine S > 40, vapour (CO_2) S < 3, T >450; later H_2O-CO_2-NaCl, S < 10, T <250	~0.5/~2.0	Diment (1996); Dunne (1995)
Donlin Creek, Alaska	323	2.9	Rhyolite sills/dikes, I	Veins, veinlets	Ag, As, Sb, Hg	Abs	Py, Apy, Sbn	Qtz, Ser, Carb, Clay	Immiscible H_2O-NaCl brine and vapour (CO_2) T >550; later H_2O-CO_2-NaCl, T =150-260	~0.5/~2.1	Ebert et al. (2000)
Shotgun, Alaska	~1 M oz		Granite stock, I	Stockwork and breccia	Bi, Te, Mo, As, Cu	0.73	Apy, Po, Lo, Py, Ccp, Sch	Ab, Ser, Qtz, Carb	Immiscible H2O-NaCl brine S >40, vapour (CO2) T =350-650	~0.5/~2.2	Rombach and Newberry (2001)
Kidston, Australia	94	1.48	Rhyolite porphyry stock, I>M	Breccias and sheeted veins	Bi, Mo, W, As, Te, Zn, Cu, Pb, Sn	?	Py, Po, Apy, Bim, Ccp, Sph, Mol, Gal	Qtz, Ser, Carb	Immiscible H_2O-NaCl brine and vapour (CO_2) T ~400-540; late H_2O-NaCl, S < 10, T =170-350	~0.8/~3.0	Baker and Andrew (1991)
Vasilkovskoe, Kazakstan	60	3.7	Granodiorite pluton, I	Sheeted	As, Sb, W, Pb, Cu, Bi, Te	?	Py, Po, Bim, Ccp, Sph, Gal, Mol, Sbn, Sch	Ab, Ser, Qtz, Carb	CO_2-H_2O-NaCl, S = <11, T =150-250	>1.0/>3.0	Spiridonov (1996)
Dublin Gulch, Yukon	50.3	0.93	Granodiorite pluton, I	Sheeted	Bi, Te, Mo, As, Sb,W, Pb, Cu	0.89	Py, Po, Apy, Bim, Sch, Gal, Pb-Bi-Te-S	Ksp>Ab, Qtz, Ser, Carb	Early CO_2-H_2O-NaCl-CH_4, T =250-350; late low XCO_2,H_2O-NaCl S =5-15, T =150-250	>1.1/>3.5	Maloof et al. (2001)
Mokrsko, Czech Rep.	66	1.5	Granodiorite pluton, I	Sheeted	As, Bi, Te, Mo, W, Sb	?	Py, Po, Apy, Mol, Sch, Bim	Ab, Amp, Bt, Qtz	CO_2-H_2O-NaCl, S = <10, T =330 ± 20	~1.5/~5.0	Boiron et al. (1995)
Fort Knox, Alaska	158	0.83	Porphyritic granite pluton, I	Sheeted	Bi, Te, Mo, As, Sb,W	0.86	Apy, Py, Sbn, Sch, Po, Lo, Mol, Bim	Ab, Qtz, Ser, Carb	CO_2-H_2O-NaCl-CH_4, S = 2-8, T =300-480	>1.5/>5.0	McCoy et al. (1997)
Pogo, Alaska	10	~15	Granite, aplites, I	Flat lenses	Bi, Te, As, Ag, Cu, Pb	0.89	Apy, Py, Po, Lo, Bim	Bi, Qtz, Ser, Carb	CO_2-H_2O-CH_4, S < 10, T =300-600	>1.7/>5.0	Smith et al. (1999)
Salave, Spain	~15	~2	Granodiorite pluton, I	Disseminated (greissen)	As, Sb, Mo, W, Zn, Cu	?	Mol, Sph, Gal, Cep	Ab, Ser, Carb	CO_2-H_2O-NaCl	?	Harris (1990)
Timbarra, Australia	13	0.95	Granodiorite pluton, I>M	Disseminated	Bi, Mo, Sb, As, Ag	0.69	Mol, Bim, Py, Apy	Ab, Qtz, Ser, Carb	CO_2-H_2O-NaCl, S < 10, T =200-400	~2.0/~7.0	Mustard (2001)
Jilau, Tajikstan	54	1.1	Granodiorite pluton, I	Sheeted	Bi, Te, W, As, Cu	?	Bim, Sch, Cpy, Py, Apy	Qtz, Fsp, Carb, Ser	Early CO_2-H_2O-NaCl-CH_4, T =300-450; late H_2O-NaCl S =2-14, T =130-300	~2.2/~8.0	Cole et al. (2000)

Abbreviations: Ab=Albite, abs = no bismuth reported, Apy = arsenopyrite, Bim = bismuthinite, Bt = biotite, Carb = carbonate, Ccp = chalcopyrite, Fsp = felspar, Gal = galena, I = ilmenite series, I>M = ilmenite series more abundant than magnetie series, Ksp = K felspar, Lo = loellingite, M = magnetite series, Mol = molybdenite, Po = pyrrhotite, Py = pyrite, Qtz = quartz, S = salinity, Sbn = stibnite, Sch = scheelite, Ser = sericite, Sph = sphalerite, T = temperature, ? Au/Bi not reported

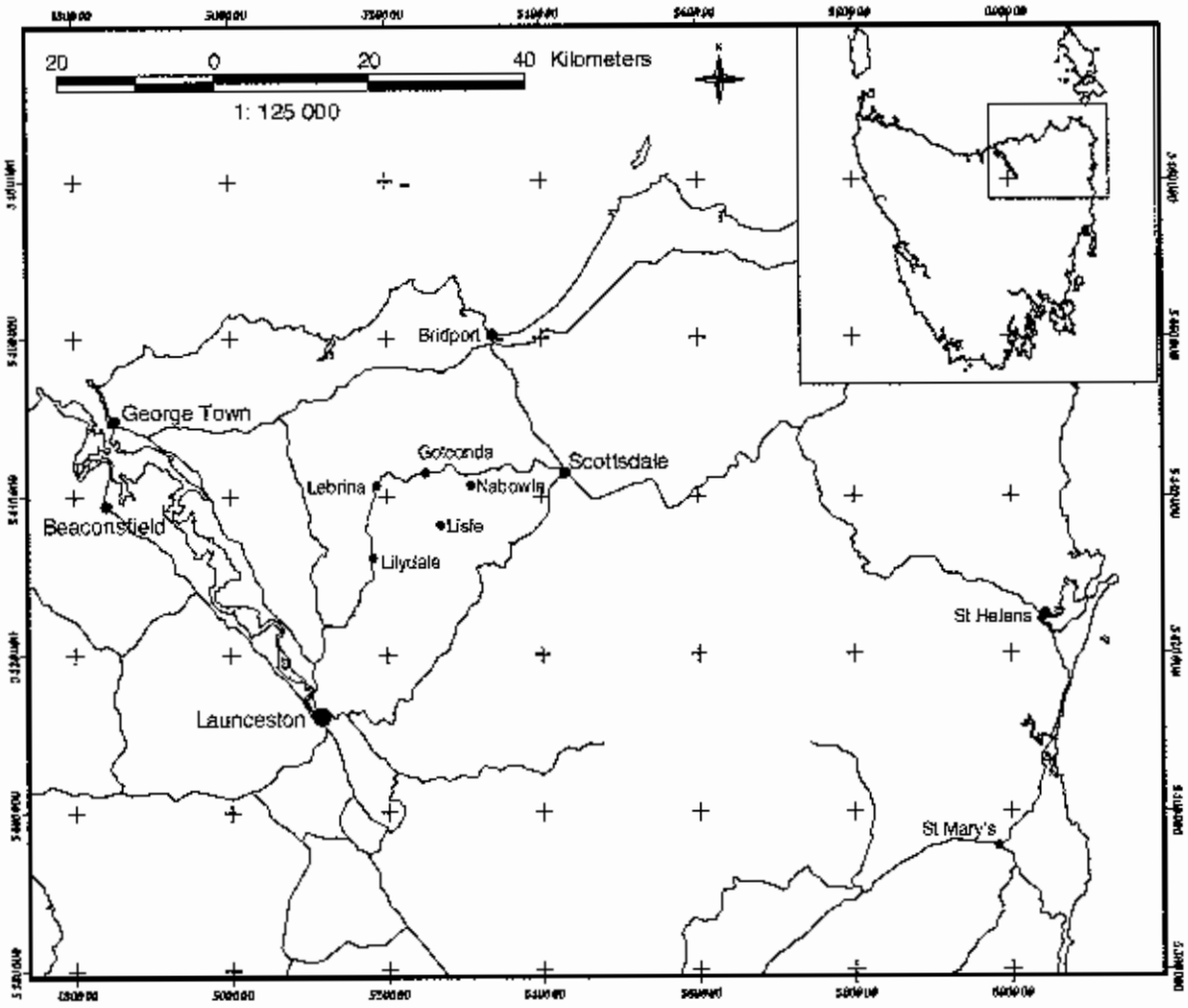

Figure 1.1 Location map of the Lisle/Golconda area northeast Tasmania.

1.3 Tenement Details, History and Previous Exploration

The Denison and Golconda alluvial fields were discovered in 1872 (Coroneus, 1993) and the Lisle alluvial field in 1878, following the discovery of the Tobacco Creek Goldfield in 1877 (Dickens, 1991). The majority of production, although sporadic, occurred between 1878 and 1909, with an estimated production of 250,000 ounces of gold (Twelvetrees, 1909). Minor alluvial mining continued until recent years (Bottrill et al., 1992). Hard rock mining in the Golconda and Panama goldfields continued periodically until the 1920's.

Modern mineral exploration in the area has been conducted since the mid 1970's with an emphasis of targeting high grade and/or high tonnage sources of the alluvial gold. A number of exploration licenses have been held by a variety of companies/organisations. Between 1976 and 1978 Comalco undertook a brief review of the area including a pancon survey, geological mapping and bedrock sampling. Subsequently, CRA Exploration (CRAE) undertook stream silt sampling, identifying arsenic anomalies in the southern part of the Lisle area (Broadbent, 1982). These anomalies were not followed up. B.P. Minerals (BP) and Seltrust carried out a program of geological mapping, rock chip and stream silt sampling, aeromagnetic geophysical surveying and percussion drilling between 1983 and 1986. Argyle Minerals carried out an aerial photograph interpretation between 1986 and 1988 (Cromer, 1987) followed by limited rock chip sampling and bulk sampling of alluvial material from the Denison River goldfield. Billiton completed a number of programmes, from 1990 to 1991 including regional and comprehensive Bulk Leach Extraction Gold (BLEG) stream sediment and soil geochemical surveys. Although two exploration targets were delineated these were not followed up in any detail. Between 1993 and 2001 Macmin completed soil geochemical sampling, power auger sampling and rock chip geochemical sampling. This was followed by drilling 4 diamond core holes (for 195.3 m), and 4 RC holes (for 359 m). In addition, several costeans were trenched across the prospects.

EL 2/92 includes sites of historical mining including Panama, Virginia Ridge, Gold Crest, Enterprise, Cradle Creek and Bessells deposits/prospects (Figure 1.1). EL 2/92 encompasses an area of 12 km^2 and lies within the larger EL 41/02. In addition to those listed above, EL 41/02 also includes Lebrina East, Lebrina, Trevors, Titmus, Wild Knife, Watts, New Bonanza, Lone Star, and Patersonia deposits/prospects. TasGold Ltd has identified seven new prospects based on detailed gold and or arsenic soil anomalies. These include Potoroo, Potoroo North, Potoroo West in EL2/92; and Wild Knife Ridge, Lone Star South (East), Lone Star South (West) and Lebrina South Prospects in EL 41/02.

TasEx completed an RC drilling program at the Enterprise and Potoroo prospects on the EL 2/92 in 2002. 15 RC holes (for 571.5 m) at Potoroo identified gold associated with disseminated sulphide mineralisation and quartz veining hosted in altered granitoids. 5 RC holes (for 247 m) and one diamond tail (for 122.5 m) at Enterprise produced best intersections of 2 m at 2.9 g/t including 0.4 m at 14.4 g/t. More recently (2003 to present) TasGold Ltd has acquired two licences (EL 2/92 and EL 41/02) from TasEx and is continuing to evaluate them for their economic potential. Since listing on the Australian Stock Exchange in April 2003, TasGold has completed extensive RC drilling, diamond drilling and trenching programs at the Enterprise, Potoroo, Junction Star, Panama and Kelly's prospects. Diamond drilling at Enterprise in 2003 returned best drill intersection of 0.8 m at 11.2 g/t gold from the West Vein. Diamond drilling at Potoroo in August 2004 returned intersections of 106.5 m at 0.19 g/t gold, including a higher-grade zone containing 6.9 m of 1.8 g/t gold, in altered granodiorite.

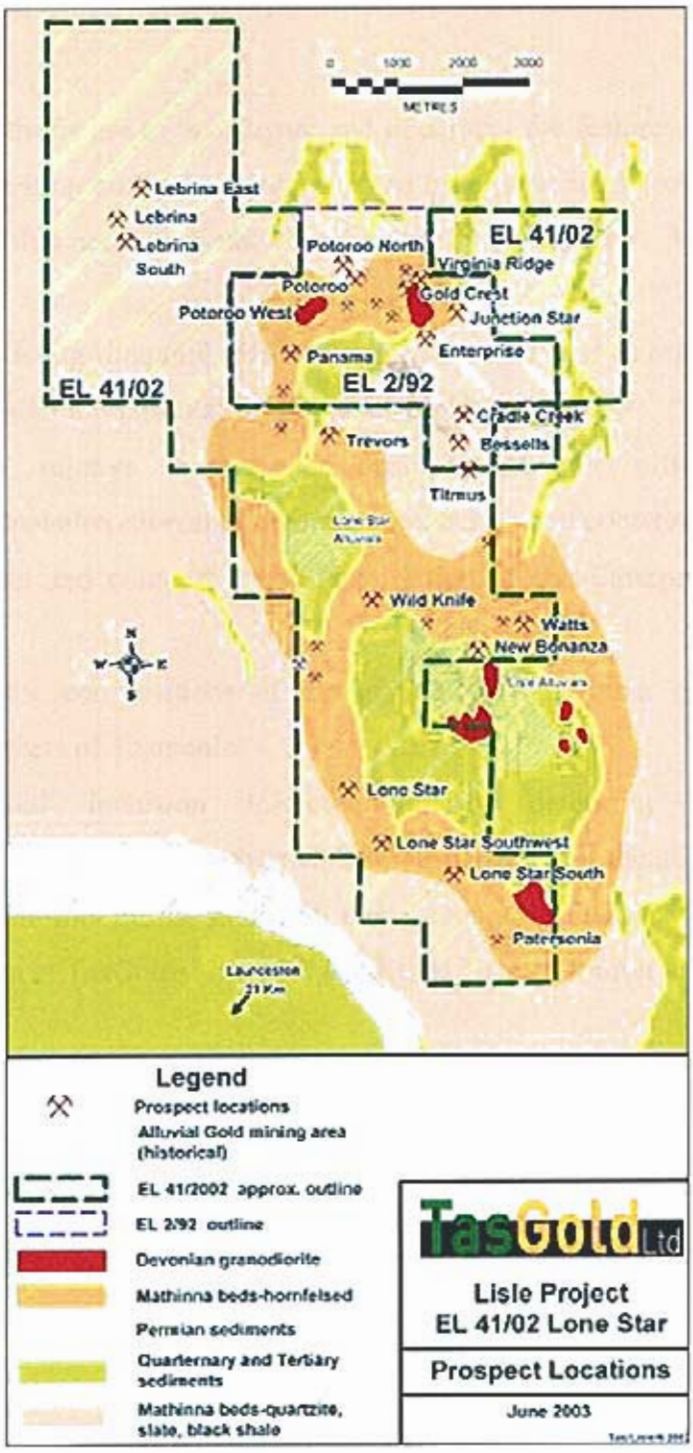

Figure 1.2 Map of the Lisle area showing the locations of the prospects relative to the EL 2/1992 and EL 41/2002 exploration licences (TasGold).

1.4 Objectives

The aims of this thesis are to investigate and document the features that characterise hydrothermal alteration and mineralisation at the Enterprise and Potoroo prospects. A detailed study of this nature has not been previously undertaken. The specific aims are to:

- log the existing diamond drill holes for structure, mineralogy, lithology and timing of alteration, mineralisation and veining events;
- determine relative timing relationships between different intrusive, hydrothermal alteration and mineralisation events and construct a paragenesis;
- characterise and compare the mineralisation of the Enterprise and Potoroo prospects;
- compare the compositions of the granodiorites to other granitoids in the northeast parts of Tasmania;
- using fluid inclusion microthermometry determine physiochemical characteristics of the hydrothermal fluid responsible for the mineralised veins;
- based upon the thesis findings, make recommendations to assist further exploration at TasGolds' EL 2/92 and EL 41/02 exploration licences.

1.5 Methods

Six diamond drill holes totalling 460 metres were geologically logged. Constrained sample material was used to make 35 polished thin sections. Prospects were scouted for outcrops and mine exposures, with relationships documented by photography and sketches, but no detailed mapping was possible due to the sparse and recessive outcrop. Polished thin sections were used for mineral identification, mineral chemistry, composition estimations and paragenetic relationships. In addition, 7 fluid inclusion thick sections were used for petrography and microthermometric experiments on fluid inclusion populations. Hand drilled sulphide samples were prepared for $\delta^{34}S$ analyses at the Central Science Laboratory, University of Tasmania. 16 whole rock geochemical analyses were prepared from crushed and pulverised (1-2 kg) samples, these samples were used to chemically characterise the intrusive phases. Five of these whole-rock samples were also analysed for ferrous iron to better constrain the oxidation state of the granitoids. Data from this study has been integrated with other geochemical analyses from other granitic rocks from northeast Tasmania (obtained from Mineral Resources Tasmania, personal communication M. McClenaghan). A reconnaissance magnetic susceptibility survey of each of the logged cores was used to evaluate magnetic methods as an exploration tool; this has lead to the establishment of a second honours level research study (Benjamin Hey), and no further magnetics research was undertaken in this project.

2. Regional geology of northeast Tasmania, with emphasis on occurrences of gold mineralisation.

2.1 Introduction

The Palaeozoic geology of northeast Tasmania is dominated by Early Ordovician to Early Devonian turbiditic sedimentary rocks (called the Mathinna Group); and Late Devonian to Early Carboniferous granitic rocks (400-350 Ma; Black, 2001, 2004). The Devonian-Carboniferous intrusions include the Scottsdale Batholith in the west, and the Blue Tier Batholith in the east. These are unconformably overlain by late Carboniferous to Triassic Parmeener Supergroup sedimentary rocks, which are intruded by thick sheets of Jurassic dolerite. Tertiary basalt is dispersed throughout the northeast and Tertiary sediments are widespread in lower relief areas. Quaternary alluvium is common in river valleys and coastal plains. Figure 2.1 is a generalised geologic map of northeast Tasmania.

Mineralisation in northeast Tasmania is widespread. Figure 2.2 is a generalised map of the mineralisation in the northeast, showing some of the estimated gold production (tonnes) for a number of gold fields (Bottrill et al., 1992). Gold has historically been mined from lode/vein deposits hosted in the Mathinna Group sedimentary rocks and the contact aureoles to intrusions (e.g., Mathinna, Mangana, and Hogans Road/Golden ridge), from veins in granotoid host rocks (e.g., Enterprise), or from Quaternary alluvium (e.g. Lisle). Hardrock gold predominantly occurs in quartz ± pyrite and arsenopyrite veins, but recent exploration has identified significant examples of disseminated sandstone-hosted gold in the Denison area. Disseminated gold-bearing sulphide mineralisation hosted in granodioritic rocks has been discovered at Potoroo. Other economic resources include tin-tungsten mineralisation directly related to intrusions (e.g. Anchor Mine), and base metal sulphides (copper, lead, zinc and silver) associated with zoned mineral fields (e.g. the Scamander field, including mineralisation at Pyramid Hill).

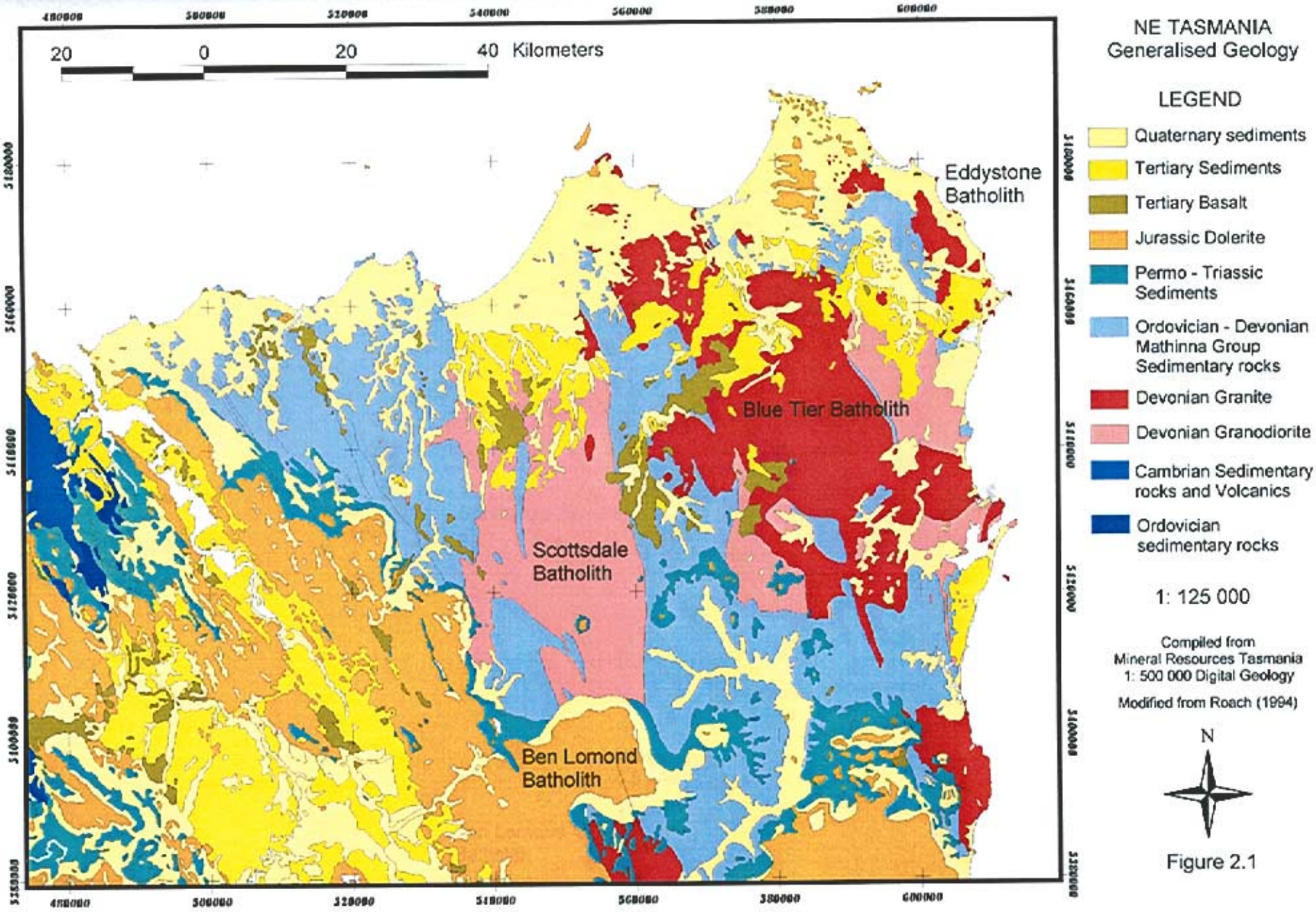
20 0 20 40 Kilometers
Eddystone Batholith
Blue Tier Batholith
Scottsdale Batholith
Ben Lomond Batholith
NE TASMANIA
Generalised Geology
LEGEND
Quaternary sediments
Tertiary Sediments
Tertiary Basalt
Jurassic Dolerite
Permo - Triassic Sediments
Ordovician - Devonian Mathinna Group Sedimentary rocks
Devonian Granite
Devonian Granodiorite
Cambrian Sedimentary rocks and Volcanics
Ordovician sedimentary rocks
1: 125 000
Compiled from
Mineral Resources Tasmania
1: 500 000 Digital Geology
Modified from Roach (1994)
N

Figure 2.1

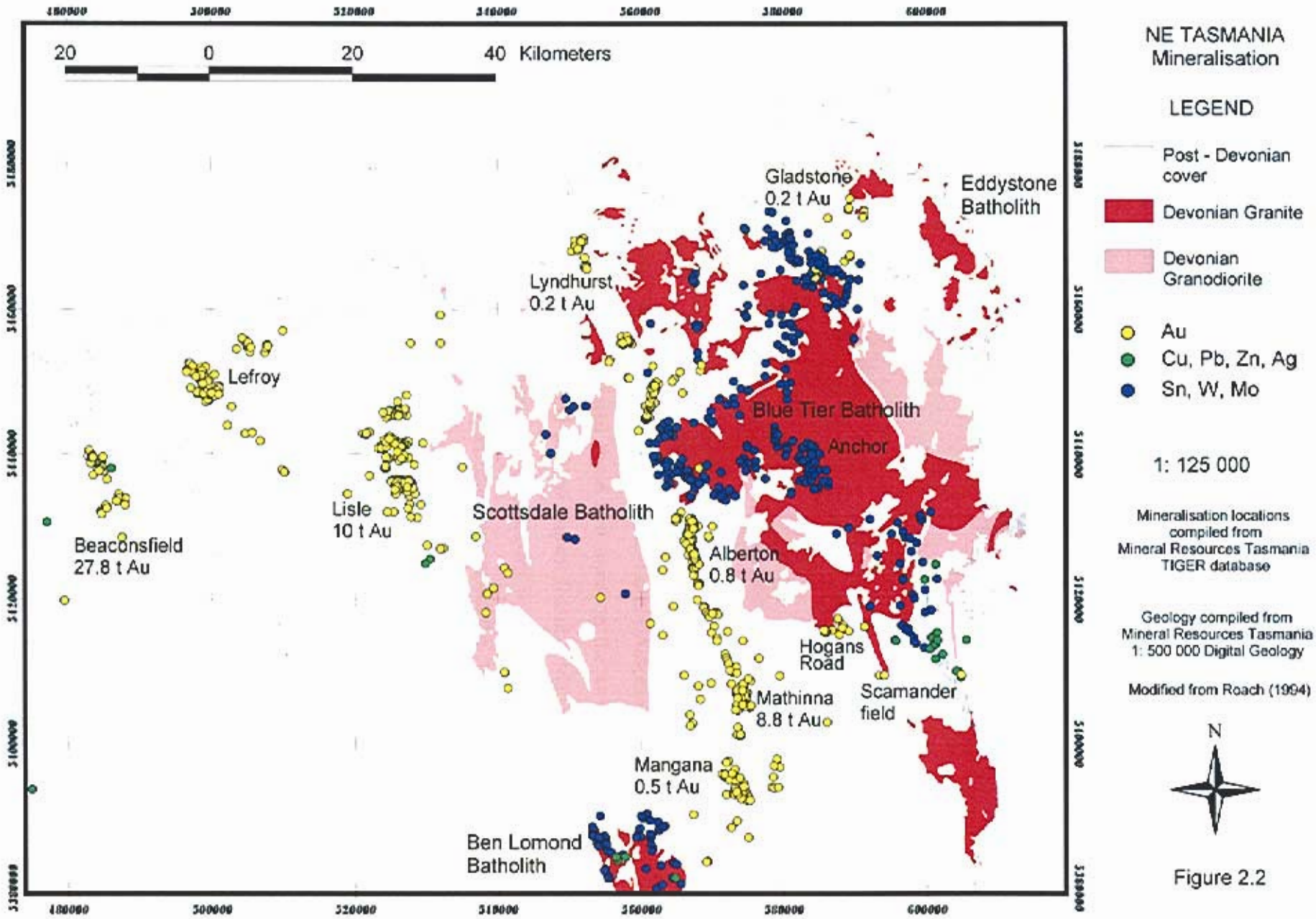
20 0 20 40 Kilometers
Gladstone
0.2 t Au
Eddystone
Batholith
Lyndhurst
0.2 t Au
Lefroy
Blue Tier Batholith
Anchor
Lisle
10 t Au
Scottsdale Batholith
Beaconsfield
27.8 t Au
Alberton
0.8 t Au
Hogans
Road
Mathinna
8.8 t Au
Scamander
field
Mangana
0.5 t Au
Ben Lomond
Batholith
NE TASMANIA
Mineralisation
LEGEND
Post - Devonian
cover
Devonian Granite
Devonian
Granodiorite
Au
Cu, Pb, Zn, Ag
Sn, W, Mo
1: 125 000
Mineralisation locations
compiled from
Mineral Resources Tasmania
TIGER database
Geology compiled from
Mineral Resources Tasmania
1: 500 000 Digital Geology
Modified from Roach (1994)
N

Figure 2.2

Lode gold deposits are the predominant source of gold mineralisation in northeast Tasmania (which are all shown on Figure 2.2). Deposits are typically located in districts occurring along NNW and to a lesser extent NE trending structures that are interpreted to relate to thrust features (Reed, 2002). Districts include the Mangana-Alberton-Lyndhurst, Hogans Road (Brilliant Creek), Gladstone, Denison-Lisle-St. Patrick's River, Lefroy-Den-Back Creek and Beaconsfield. The Tasmania reef at Beaconsfield is the largest lode gold deposit in Tasmania, with a pre-mining resource of nearly 2 x 10^6 ounces (Jones, 2001). The reef is characterised by deformed Ordovician turbiditic sedimentary host rocks, NE-striking geometry and a sulphide-rich mineralogy

2.2 The Mathinna Group

The Mathinna Group consists of a sequence of turbiditic sandstone, siltstone and mudstone ranging in age from Cambro Ordovician to Early Devonian. Banks (1962) divided the Mathinna Group into two subdivisions, a western Ordovician 'Lutite Association' and eastern Siluro-Devonian 'Arenite–Lutite Association'. Turner (1980) interpreted that a fault separated these two units on the basis of structural trends, apparent lithological change and lack of known fossils. Mapping by Powell and Baillie (1992) in the Bellingham area has shown a conformable relationship between the two associations. They have also suggested the Mathinna Group be further subdivided into at least three units (probably four) on the basis of their mapping.

The Lutite Association consists of argillaceous rocks with lesser arenite, which outcrops between the Tamar River and Nabowla. These rocks are distinguished by a strong tectonic cleavage that is commonly flat lying, and predates a strong north-westerly-trending upright crenulation cleavage. Powell et al. (1993) proposed a conformable stratigraphy of ~6km thick for the western part, based on outcrops between Georgetown and the western margin of the Scottsdale Batholith. Banks and Smith (1968) documented a single fossil locality containing Ordovician graptolites (*Loganograptus cf. logani*) of Arenig age.

The Arenite–Lutite association comprise all Mathinna Group sediments to the east of Golconda and consist of interbedded fine to medium grained sandstone and siltstone deposited by turbidity currents (Williams, 1959). Powell et al. (1993) inferred Siluro-Devonian age for the Arenite–Lutite Association, based upon Devonian graptolite ages from near Scamander and Beaconsfield. Silurian graptolites are also known from the central east at Golden Ridge (Rickards et al., 1993).

2.3 The Granitoids

The granitoids of Tasmania have been divided in the eastern Bassian and western Taswegian zones on the basis of minor compositional differences (Chappell et al., 1988), and interpretations of gravity data (Leaman and Richardson, 1989; Leaman et al., 1980). The Bassian zone of the east Tasmanian terrain comprises S- and I-type granitoids that were emplaced between 400 and 350 Ma (Black, 2001, 2004). These zones are broadly associated with Eastern and Western mineral provinces of Tasmania, respectively. According to Groves (1977), Cocker (1982), and Williams (1959) the granitoids, which have narrow contact metamorphic aureoles, appear to have been passively emplaced, although Rickards et al. (1993) documented substantial reorientation of D_2 folds around the New Haleys Country Pluton. The Bassian Zone granitoids form composite tabular bodies outcropping over an area of approximately 2500 km^2. Outcrop is dominated by generally NNE trending batholiths that have intruded the Ordovician-Devonian Mathinna Group. The main batholiths are the Ben Lomond, Scottsdale, Blue Tier, Eddystone, and Furneaux.

Based on gravity interpretations, Leaman et al. (1980) showed that the granitoid bodies in the Bassian Zone Batholiths amalgamate at depth to form a single batholith. The outcropping batholiths are mostly made up of four main types (Higgins et al., 1985; Mackenzie et al., 1988; McClenaghan, 1984, 1989; McClenaghan and Williams, 1982). The order of intrusion according to Gee & Groves (1971) and McClenaghan (1989) appears to be first: I-type, magnetite-bearing hornblende granodiorites; followed by peraluminous, cordierite-bearing S-type, biotite granites, then non-cordierite-bearing biotite granites of both I and S-type; and finally peraluminous alkali feldspar granites.

The Scottsdale Batholith is dominated by granodiorites whereas the Blue Tier and Eddystone batholiths are predominantly composed of granite and adamellite. The granitoids of the Scottsdale Batholith are I-type, whereas those of Eddystone Batholith and the Furneaux Islands are mostly S-type. The Blue Tier Batholith is composed of both I and S-type intrusions.

Goscombe et al. (1994) used four different geobarometric methods from several sites to conclude that the pressures during emplacement of the Scottsdale Batholith averaged 1200 ± 500 bars. Varne and Fulton (1994) used the aluminium-in-hornblende barometer to estimate pressures for the Scottsdale Batholith, with results ranging between 100 and 2400 bars, with an average of 1300 bars. Patison (1999) noted that the Pyengana Pluton possessed a similar cordierite-dominant contact metamorphic assemblage in the Mathinna Group to the Scottsdale batholith. Pressures based on the contact metamorphic assemblage in the Pyengana Pluton averaged 2460 bars. The St Mary's Porphyrite indicates that at least some of the Tasmanian granites have erupted equivalents, testifying to some very shallow emplacement conditions.

2.4 Deformation

The Mathinna Group sediments have been metamorphosed to sub- to mid-greenschist facies (Patison et al., 2001). Field relationships suggest the Mathinna Group has undergone at least two regional folding events. The first, D_1, is interpreted to have occurred during the Ordovician to Devonian. It is characterised by NE-E directed thrusts (Powell and Baillie, 1992; Taylor, 1992). S_1 occurs as a penetrative cleavage best preserved in pelitic units. Patison et al. (2001) described the S_1 cleavage as defined by white mica in both sandstone (spaced to fracture cleavage) and pelite (slaty cleavage) at a locality near Scamander. The second fold event, D_2, occurs as SW directed thrusts and upright folds, interpreted to be Middle Devonian in age (Cocker, 1982; Powell and Baillie, 1992). D_2 is interpreted to be associated with the first phase of the Tabberabberan Orogeny (Reed, 2001), and is represented by S_2, a closely spaced disjunctive cleavage not clear in outcrop.

The granitic intrusions produced distinct hornfelsed zones in to ~1 km of the surrounding Mathinna Group. According to McClenaghan et al. (1982) the granitic rocks appear to post date the folding and syntectonic metamorphism in the Mathinna Group, however some workers suggested that the presence of pervasive NW oriented cleavage in some granitoids is consistent with their emplacement during D_2 (Varne and Fulton, 1994).

2.5 Gold Mineralisation

The principle areas of primary gold production in northeast Tasmania occur in several districts: (1) Mangana-Alberton-Lyndhurst; (2) Hogans Road (Brilliant Creek); (3) Gladstone; (4) Denison-Lisle-St. Patricks River; (5) Lefroy-Den-Back Creek; and (6) Beaconsfield (Bottrill et al., 1992). The Mangana-Lyndhurst district forms a strongly linear belt referred in some literature as 'The Main Slide' or the 'Mangana-Lyndhurst Trend' (Figure 2.2). Keele et al. (1993) found that mineralisation in this trend was emplaced post-development of regional S_2, through dextral reactivation of this structure.

Most of the gold mineralisation in northeast Tasmania occurs in the Mathinna Group sediments as structurally controlled quartz ± sulphide veins. In some areas mineralisation is spatially associated with and/or hosted in intrusions of hornblende granodiorite (e.g. Golden Ridge). In other areas field relationships, gravity and magnetics interpretations indicate that there is no clear relationship between mineralisation and the granitoids (e.g. Mangana-Lyndhurst district; Roach, 1994). The Tasmania Reef, Beaconsfield, sits within the structural zone that separates the eastern and western Tasmania terrains. The reef itself is hosted in the Ordovician Denison and Gordon Groups. The NE striking Tasmania Reef is unlike the dominant NNW structural trend of central, northern, and NE Tasmania. Jones (2001) concluded that the Tasmania Reef is an unusual lode gold deposit, with several unusual features that make it difficult to fit into the existing scheme for lode gold deposits.

The most recent $^{40}Ar/^{39}Ar$ dating by Bierlein et al. (2004) from a number of sedimentary rock-hosted orogenic lode gold deposits in northeastern Tasmania constrained most ore formation to between 395 and 385 Ma. Bierlein et al. (2004) suggested that most therefore formed late in the Tabberabberan Orogeny, and correlated in time with the second major gold mineralising phase in Victoria, which formed deposits such as Fosterville.

Bierlein et al. (2004) provide age constraints on the emplacement of granites that show a spatial relationship to gold mineralisation. Gold mineralisation in the Denison area was constrained to 385.4 ± 2 Ma, from $^{40}Ar/^{39}Ar$ dating by Bierlein et al. (2004). Mineralisation in the Denison area is hosted in Mathinna Group turbidites well outside the contact aureole associated with Devonian granitoids to the southeast. The Lisle and Golconda goldfields are located several kilometres to the south of the Denison area, mineralisation here occurs in veins and disseminations within the Mathinna Group turbidites, contact aureoles and the granitoids. In comparison existing zircon ages for the Scottsdale Batholith obtained from the Mineral Resources Tasmania database range between 386.6 ± 2.7 and 390.8 ± 2.2 Ma. Black (2001) has also determined ages for the Scottsdale Batholiths using U-Pb SHRIMP. Ages for the Scottsdale Batholith ranged from 388.7 ± 2.6 to 391.5 ± 2.5 Ma (OZCHRON database Geoscience Australia website).

The Trafalgar deposit occurs within the contact aureole of the Halcys New Country Pluton at the southern margin of the Blue Tier Batholith. Gold bearing quartz veins are hosted primarily in hornfelsed Mathinna Group turbidites, with some veins extending into and hosted by the granitoids. Ar/Ar dating by Bierlein et al. (2004) determined timing for vein emplacement at Trafalgar of 386.6 ± 2.1 Ma.

Bierlein et al. (2004) used their new age data to suggest a difference in formation age between granite-related gold at Denison and Trafalgar and deposits in the Lyndhurst-Mangana district that show no field relationship to the granitoids. Their evidence illustrated granite-related gold at Denison and Trafalgar to have occurred slightly later (382 – 385 Ma) than deposits in the Lyndhurst-Mangana district (389 – 394 Ma).

However, McClenaghan and Higgins (1993) found that the southern portion of the Blue Tier Batholith was emplaced from ~398 to ~388 Ma (K-Ar and Rb-Sr emplacement ages), providing evidence that granitic intrusions were being emplaced across most of the two intervals nominated by Bierlein et al. (2004). Balck (2001) has also determined ages from the Blue Tier Batholith using U-Pb SHRIMP. Analyses from the Poimena Pluton gave results of 383.8 ± 2.9 Ma.

2.6 Summary

The Early Ordovician to Early Devonian turbiditic Mathinna Group sedimentary rocks and Late Devonian to Early Carboniferous granitic rocks dominate the geology of northeast Tasmania. The Mathinna Group is the oldest exposed basement rock in the northeast terrain. The granitoids intrude the Mathinna Group sediments in a series of batholiths. This intrusion of the granitoids corresponds to the genesis of intrusion-related gold mineralisation as supported by age constraints from Bierlein et al (2004). In a number of occurrences gold has been noted occurring within intrusions and recovered at some locations (eg. Enterprise and Trafalgar). Historically the majority of gold has been recovered from within the Mathinna Group and its associated hornfelsed carapace. In some areas no relationship exists between the intrusion of the granitoids and mineralisation (eg. Lyndhurst-Mangana district) and Bielein et al. (2004) has shown this mineralisation event to be earlier than the latter. Intrusions can potentially provide a heat engine and/or fluids to generate mineralisation, and this could be a factor controlling the distribution of gold in northeast Tasmania.

3. Igneous and alteration petrology of the Enterprise Prospect.

3.1 Introduction

At the Enterprise prospect, gold is predominantly hosted in two main veins: the Enterprise and West veins as illustrated in Figure 3.1. The veins are interpreted to relate to NS trending SW directed thrusts, which are associated with regional D_2 in the northeast of Tasmania. At the Potoroo prospect, gold is hosted in veins or occurs as disseminations in hydrothermally altered granodiorite. Veins cut, and are associated with hydrothermal alteration of the intrusions. The Enterprise and Potoroo prospects are centred on multiple granitic to dioritic intrusives that form part of the Scottsdale Batholith. These intrusive bodies occur as small dykes, cupolas or porphyritic apophyses that emanate from larger stocks. These bodies intrude the surrounding Mathinna Group turbidites and locally have hornfelsed them. Intrusion textures vary from equigranular, plagioclase feldspar-biotite-quartz granodiorites to porphyritic, plagioclase feldspar-hornblende-biotite diorites. Numerous inclusions (xenoliths) of hornfelsed Mathinna Group sediments and diorite enclaves are common in the intrusions.

Surface exposure in the vicinity of the gold bearing veins at the Enterprise and Potoroo prospects is poor, with a subdued topography likely the result of both Tertiary and Quaternary weathering. Typically granitic bodies underlie the weathered valleys, whereas Mathinna Group hornfels forms surrounding more resistant ridges. Access to the mineralised veins at the Enterprise prospect was via shafts and pits, though most are now filled or have collapsed. The Enterprise vein is hosted in an approximately NS striking (350°) moderately west dipping (40-50°) thrust fault. The extent of the Enterprise vein at depth and along strike was unknown until recent drilling programs. The results of this drilling showed that the vein extends over a strike length of 400m and to a depth of 80m below surface. The vein remains open at depth. Furthermore drilling identified a second vein not discovered by historical prospectors, the West Vein, with intervals of up to 0.8 metres at 11.2 g/t gold (Figure 3.1).

Geochemical soil sampling initially discovered the potoroo prospect with the only bedrock discovered through trenching. An RC drilling program in 2003, and diamond drilling between June and September 2004 has further defined mineralisation at Potoroo. The lack of easy access has made assessing structural, lithological controls of gold mineralisation and hydrothermal alteration difficult.

Diamond drill core intersects the veins in a number of holes and these were logged as part of this project (Appendix C). Although this core was not oriented during drilling, it allowed relationships between intrusive phases, vein-dykes, vein stages and alteration assemblages to be investigated. The diamond drill core provided the material for 35 polished thin sections used in the detailed petrographic descriptions presented here. Detailed petrographic descriptions of the mineralised intrusives from EL 2/92 were previously lacking.

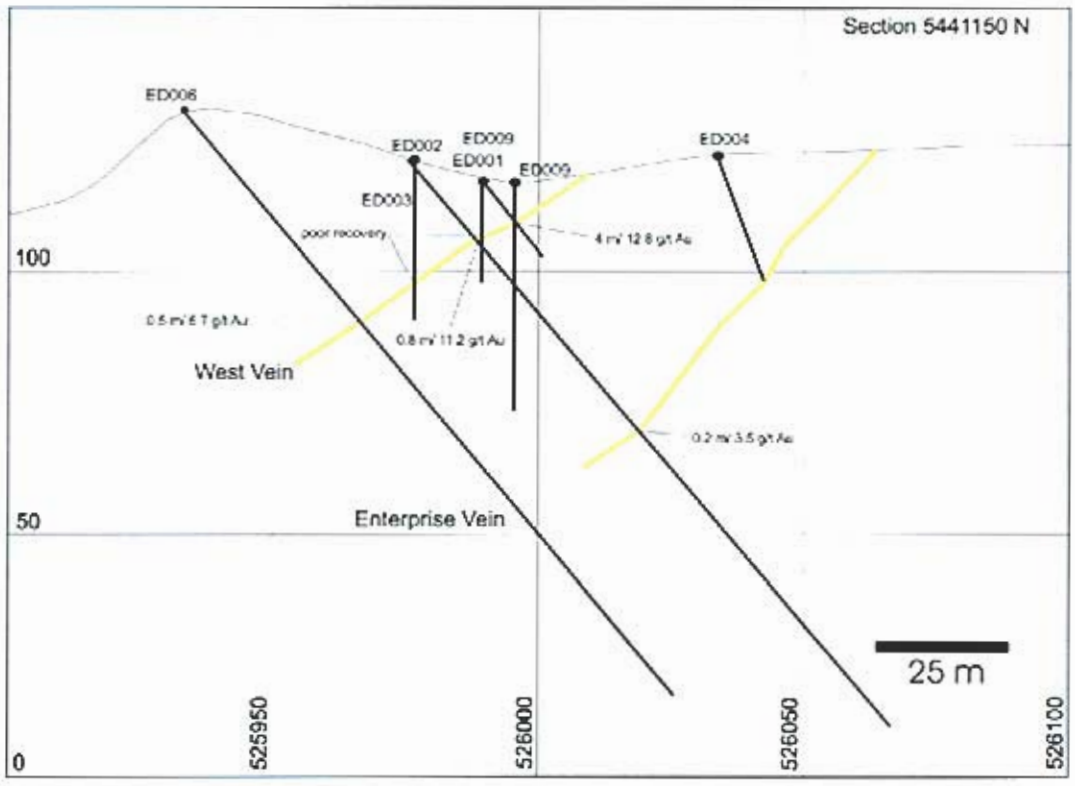

Figure 3.1 Cross section through the Enterprise prospect (northing 5441150). This section shows the position of the Enterprise Vein and West Vein, relative to the position of various drill holes. Grid spacing is 50 metres (Modified after TasGold, 2003).

3.2 Terminology

The following explanations were deemed to be warranted because of the specialised terminology that has developed in the description of magmatic-hydrothermal textures. It was not deferred to an appendix because it is essential to the description of the Enterprise and Potoroo lithologies.

Myrmekitic texture is a common feature in pegmatitic granites (Marmo, 1971); i.e., those granites rich in a volatile phase. It refers to a microscopic intergrowth of 'worm-like' or vermicular quartz in plagioclase feldspar, and commonly occurs in contact with K-feldspar (Phillips, 1974). In sections perpendicular to the worm-like rods, quartz may appear as 'tear drop' shaped crystals in feldspar. Myrmekitic textures may vary significantly in their appearance, which has led to a number of explanations for their origin; however, the commonly reported model is that myrmekites reflect subsolidus replacement affects. Other ideas on myrmekitic texture genesis include processes such as exsolution, metasomatic replacement and direct magmatic crystallisation (Hippertt and Valarelli, 1998).

A range of other textures characterise the magmatic-hydrothermal transition. These include *miarolitic cavities*, *interconnected miarolitic textures*, *unidirectional solidification textures*, *pegmatite's* and *aplitic vein-dykes*. These textures imply that intrusives exsolved volumes of a volatile phase (Candela and Blevin, 1995). These textures have been documented in granites associated with some granite-associated gold deposits, for example, Timbarra, Australia (Candela and Blevin, 1995; Mustard, 2001, 2003b, a; Mustard and Ulrich, 2004). If in sufficient amounts magmatic volatiles may flow through cavities (preserved as miarolitic cavities) and accumulate in the roof zone of the magma chamber (preserved as unidirectional solidification textures). These exsolved magmatic fluids can potentially carry ore-forming elements (e.g. Au, Cu, Pb, Zn). Thus, these textures commonly are characteristic of the margin and apical zones of intrusions. Recognition of these textures is important, as they link intrusion-related ore deposits to the magma from which the ore metals were sourced.

Quartz-layered textures are a type of unidirectional solidification texture, whereby crystals are oriented approximately perpendicular to the planes of layering. These textures are characterised by morphological features indicative of mineral growth in one direction from a solid substrate (Shannon et al., 1982b). Quartz-layered textures form during the crystallisation of the host magma, producing layers and multilayer sequences, predominantly in apical and marginal parts of intrusions. This layering is generally concordant with the intrusive contacts of the stocks in which they formed. Quartz-layered textures represent one of the magmatic-hydrothermal transition textures that provide evidence for their host intrusions exsolving large volumes of aqueous fluids (Candela and Blevin, 1995; Lowenstern and Sinclair, 1996).

Voluminous *greisens* are also suggestive of the host intrusion exsolving large volumes of aqueous fluids. Greisens are aggregates of quartz and muscovite with accessory amounts of topaz, fluorite, tourmaline, rutile, cassiterite and wolframite formed by the alteration of rock, or crystallising of minerals from late stage fluids exsolved from a solidifying magma. Therefore voluminous greisens suggest intrusions exsolved volatiles.

3.3 Methods

The following descriptions from the Enterprise prospect are based on macroscopic observations made from drill core intersections and microscopic observations and petrographic descriptions from thin sections. Unknown accessory minerals were identified by David Steel using the Energy Dispersive Spectrometer (EDS) on a Cameca SX100 electron microprobe at the Central Science Laboratory, University of Tasmania. Use of a portable infrared spectrometer (PIMA) was also trialled and aided in the identification of alteration mineral assemblages. Compositions were estimated for each of the units by visual observation (point counting) under microscope from thin sections.

3.4 Intrusive characteristics

Three main phases of intrusions have been distinguished at the Enterprise prospect on the basis of their primary textural, compositional and morphological features. Their modal mineral abundances are shown in Figure 3.2 and their textural and compositional characteristics are summarised in Table 3.1. A Schematic cross section constructed from logging drill holes shows estimated relationships between the intrusive phases, mineralised veins and position of a quartz-layered texture, is shown in Figure 3.3.

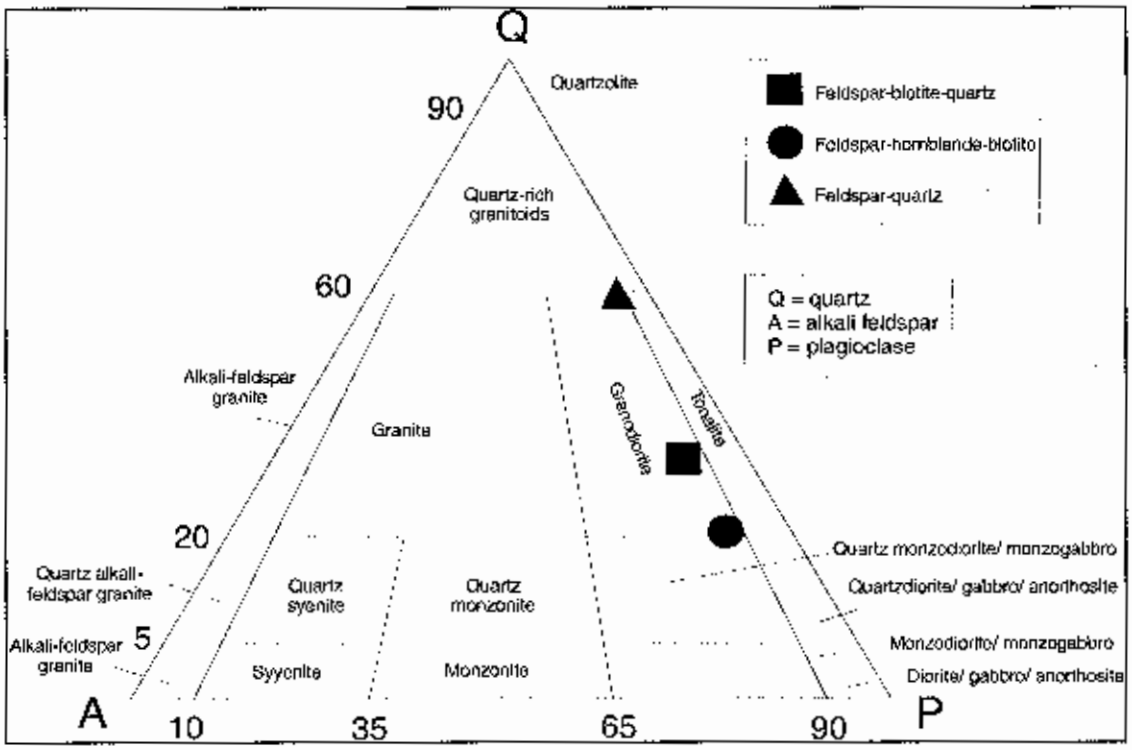

Figure 3.2 Modal mineral abundances for the three intrusive phases at the Enterprise prospect. The classification used is from that recommended by the IUGS Subcommission of the Systematics of Igneous Rocks (Streckeisen, 1973).

Table 3.1 Summary and Comparison of the Textural Characteristics of the Various Intrusive Phases from the Enterprise and Potoroo prospects

Type	Prospect	%Phenos	% Mafic	Hbl	Bi	Mag	Accessory/trace minerals	% Plag	Sub Plag	Euh Plag	%Kfs	Megacryst (phenocrysts >5mm)	% Qtz
FBQ	Enterprise	semi-porph	<20	=	+	=	Apatite, zircon, mag	~50	++	=	10	+ (plagioclase)	30
FBQ	Potoroo	10	10	=	=	=	Apatite, zircon, mag	60	++	+	=	++ (plagioclase)	30
FHB	Enterprise	20-30	>25	+	=	=	Apatite	~30	+	+	10	++ (plagioclase, biotite, hornblende)	20-50
QF	Enterprise	equi	~0			=	Apatite	30-40	+	=	<10	+ (plagioclase)	60

Abbreviations: FBQ = feldspar-biotite quartz granodiorite, FHB = feldspar-hornblende-biotite granodiorite, QF = quartz-feldspar granodiorite, Bi = biotite, equi = equigranular, Euh = euhedral, Hbl = hornblende, Kfs = K-feldspar, mag = magnetite, mg = medium grained (1-2mm), Phenos = phenocrysts, semi-porph = semi porphyritic, Sub = subhedral, ++ = dominant, + = abundant, "=" = present

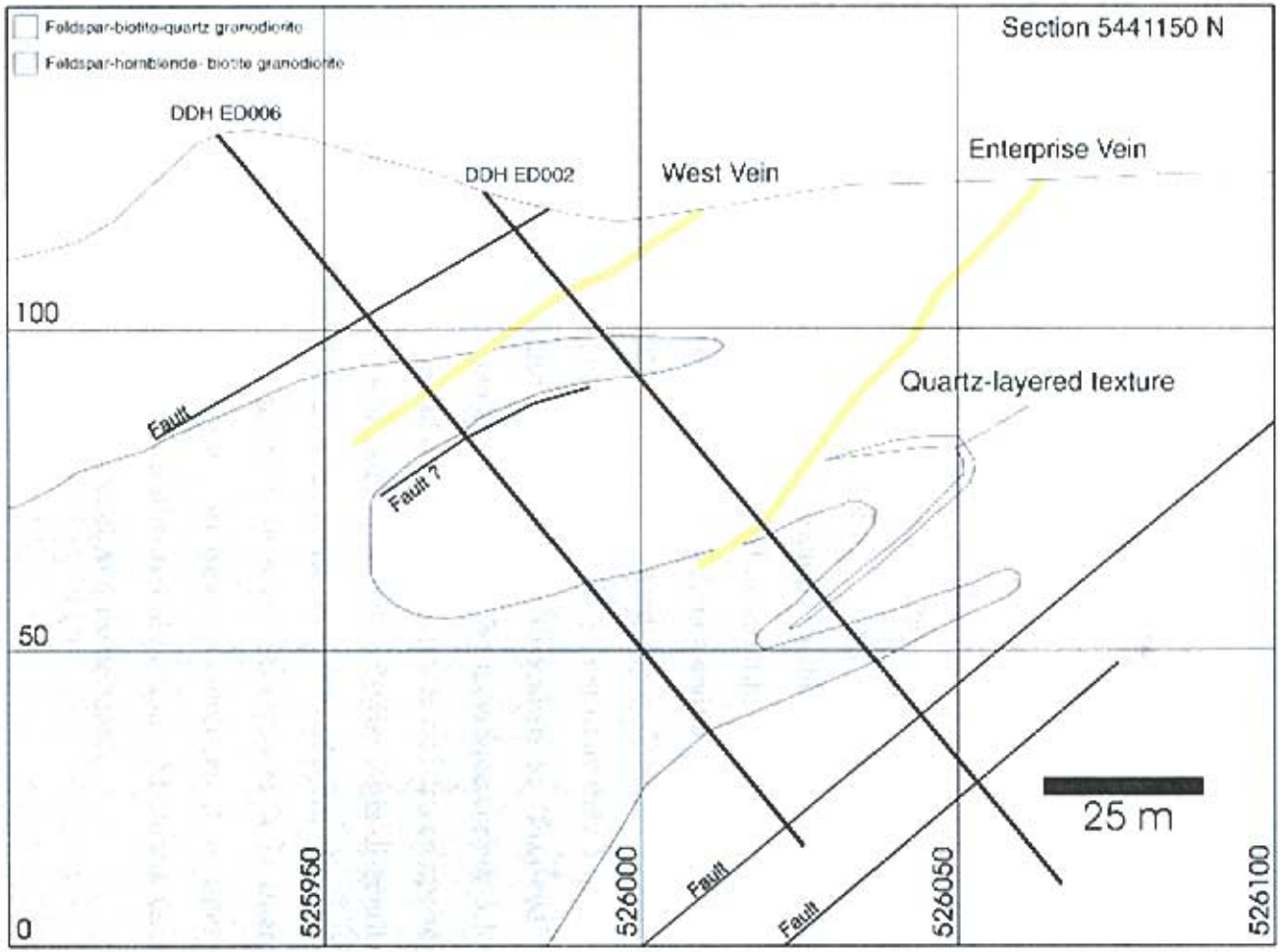

Figure 3.3 Schematic cross section through the Enterprise prospect. Plot shows an estimated view of the feldspar-hornblende-biotite granodiorite intruding the feldspar biotite-quartz granodiorite and the position of a quartz-layered texture.

3.4.1 Feldspar-biotite-quartz granodiorite

Feldspar-biotite-quartz granodiorite (FBQ) is the earliest and most abundant intrusive phase exposed in drill core from the Enterprise prospect (Plates 3.1 A and B). The stock is broadly fine- to medium-grained (1mm-3mm) composed to subhedral grains, with an equigranular to sub-porphyritic texture. It has an estimated composition of 50% plagioclase (although variable trace amounts of K-feldspar also occur), 30% quartz and ~20% biotite. Accessory minerals include apatite, zircon, and magnetite. Trace amounts of finely disseminated magnetite are present and to a lesser extent aggregates of magnetite associated with biotite 'clots' (Plate 3.1 C). Feldspars are the dominant crystal phase with an average crystal size of approximately 2 mm up to 5 mm. Plagioclase shows well developed oscillary zoning (Plate 3.1 D). Myrmekitic texture (Plate 3.3A) occurs and is particularly well developed along the contacts with other units. Background gold concentrations in the FBQ average 0.08 ppm. The feldspars are weakly to moderately altered to sericite, with sericite occurring as both 'cross hatched' growths throughout entire crystals and/or as selective alteration along growth zones (Plate 3.2). Biotite occurs interstitially to dominant crystal phases (both as primary and secondary growths), and as 'clots' approximately 5 mm in diameter of secondary 'shredded' biotite. Phlogopite (also known as 'foxy-red' biotite) was identified from hand specimen and thin section by its unique copper colour and using PIMA. Phlogopite is common in the FBQ granodiorite and can comprise >50% of the biotite component in the rock in some intervals. Pyrrhotite is disseminated in trace amounts throughout, however, in some zones up to 2 % of pyrrhotite is observed. The origin of the pyrrhotite is uncertain; in some occurrences it is interpreted to be primary thus magmatic in origin. In other occurrences it is interpreted to be secondary, resulting from later hydrothermal alteration. Mathinna Group xenoliths (up to 10cm in diameter) and dioritic enclaves are common.

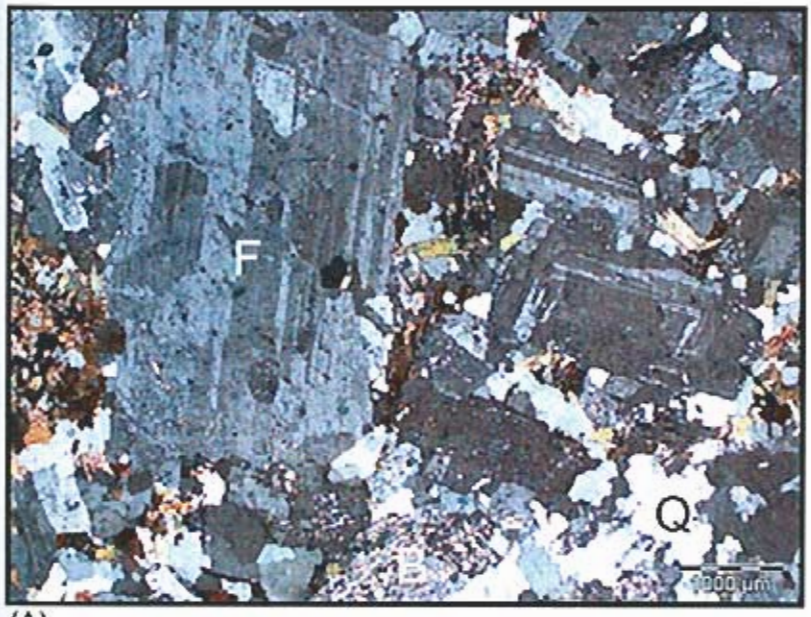

(A)

(B)

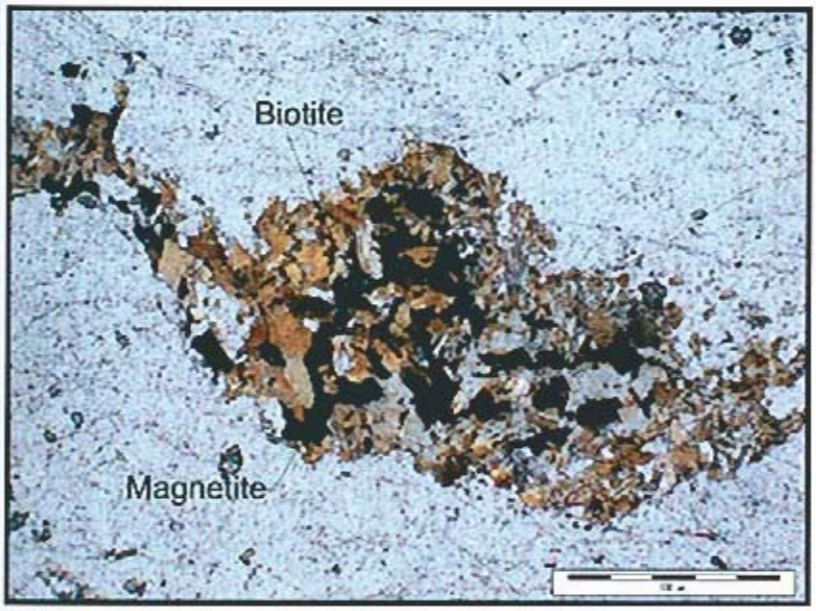

(C)

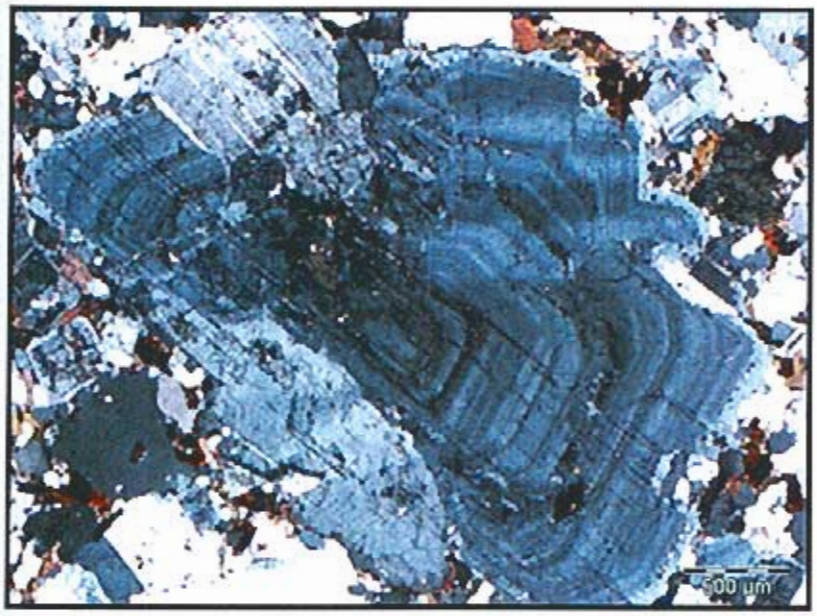

(D)

Plate 3.1 (A) Photomicrograph under cross polarised light of the FBQ. Note the subporphyritic texture (E5.13). (B) Photograph of the FBQ. (E5.13) Scale bar is in cm. (C) Photomicrograph of an aggregate ('clot') of secondary 'shredded' biotite and magnetite from the FBQ under normal light (E5.3). (D) Photomicrograph under cross polarised light of an alkali-feldspar phenocryst showing oscillary zoning and some internal complexity (E5.13).

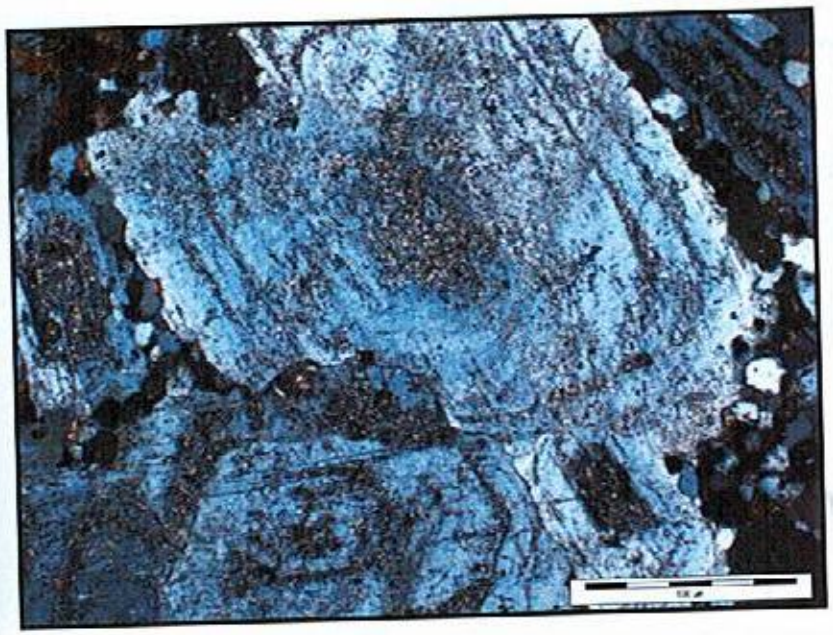

(A)

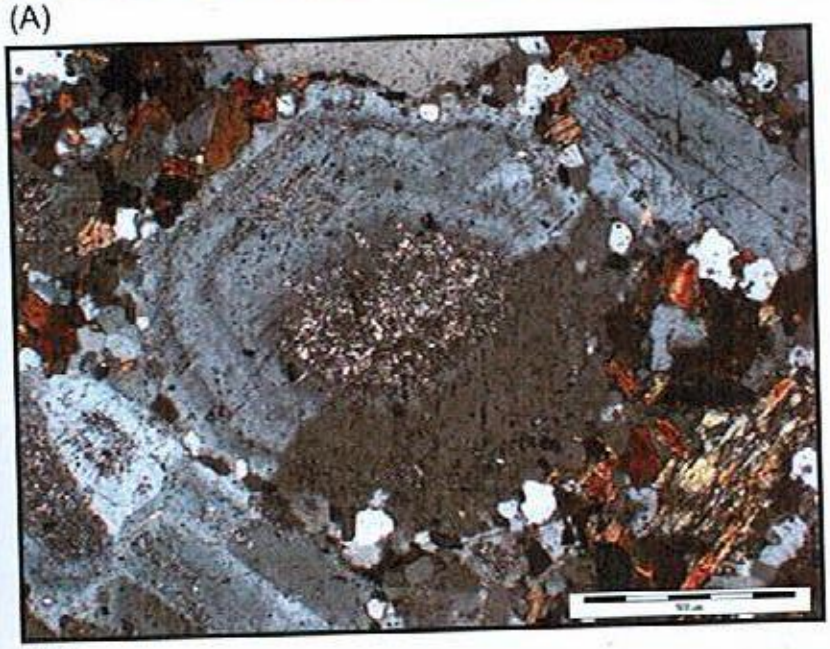

(B)

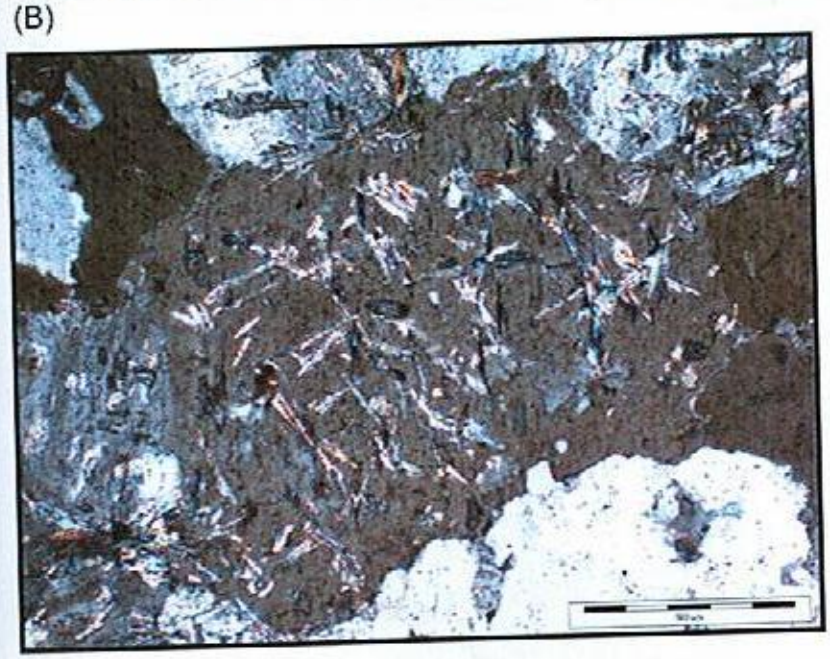

(C)

Plate 3.2 (A) Photomicrograph of sericite replacing a plagioclase feldspar phenocryst in the FBQ under cross-polarised light (E5.8). (B) Photomicrograph of sericite replacing the core of a potassium feldspar phenocryst under cross-polarised light (ED2.13). (C) Photomicrograph of 'cross-hatched' sericite replacing an unrecognisable feldspar phenocryst under cross polarised light (E5.9).

(A)

(B)

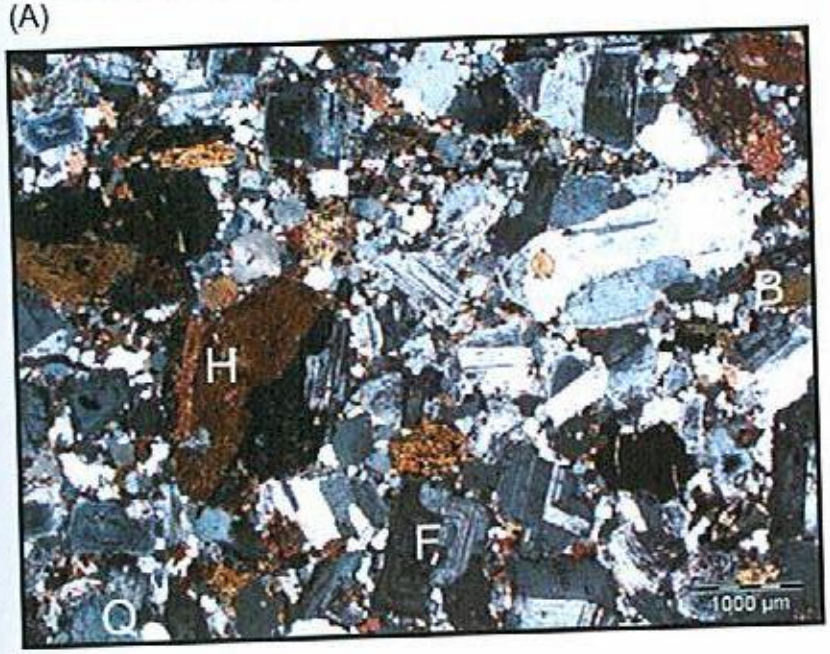

(C)

(D)

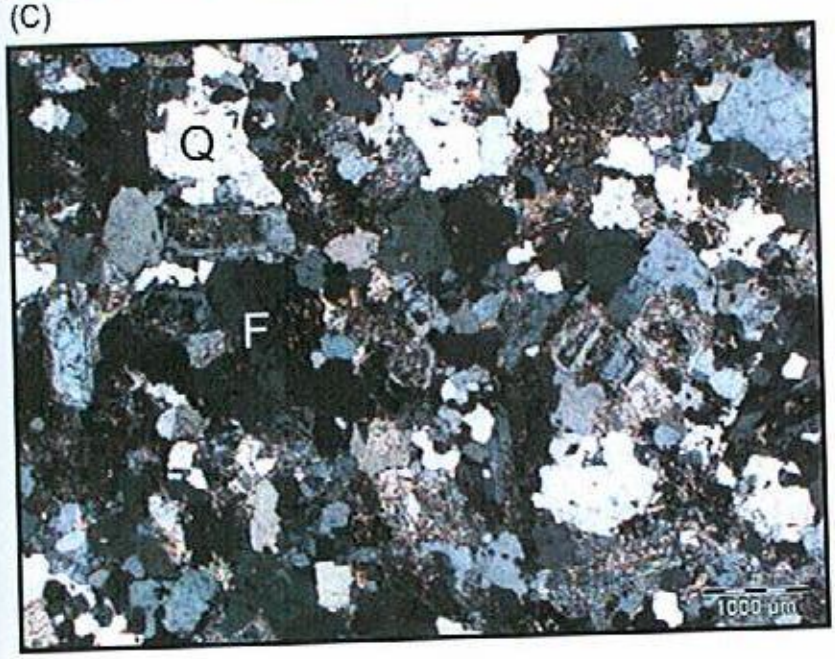

(E)

Plate 3.3 (A) Photomicrograph of a typical myrmekitic texture from in the FHB under cross-polarised light (E5.4). (B) Photograph of the FHB. Scale is in cm (ED2.4). (C) Photomicrograph of the FHB (ED6.1) (D) Photograph of the QF. Scale is in cm (E5.4). (E) Photomicrograph under cross polarised light of the QF (E5.12)

3.4.2 Feldspar-hornblende-biotite granodiorite

Feldspar-hornblende-biotite -granodiorite (FHB) occurs as variable intersections in drill core, metres to tens of metres wide (Plate 3.3 B and C). Based on observations, the FHB apparently intrudes the FBQ granodiorite (Figure 3.3). Through drill core, it is interpreted that the FHB is intruding the FBQ in a series of 'fingers' or dykes of approximately 3m wide and a strike length of approximately 75m. The FHB has an equigranular to porphyritic texture. The FHB granodiorite has an estimated composition of 50% plagioclase feldspar, 20% quartz, 15% hornblende and 10% biotite. Groundmass comprises approximately 30% feldspar, 30% quartz, 30% biotite and less than 10% hornblende. Accessory minerals include apatite and to a lesser extent magnetite. Feldspars occur up to 4 mm in length (when occurring as phenocrysts) and exhibit well developed oscillary zoning.

Most advanced hydrothermal alteration obscures primary mineralogy. Feldspars have been weakly altered to sericite, most commonly along growth zones but also as cross-hatched laths throughout entire crystals. Rare feldspars have been partially to completely altered to sericite, and only a pseudomorph of the original crystal shape remains. Secondary 'shredded' biotite alteration occurs and is especially well developed surrounding hornblendes. Hornblende and biotite form discrete clumps/clots of approximately 3mm in diameter. Approximately ~40% of the biotite has been altered to chlorite.

3.4.3 Quartz–feldspar granodiorite

Quartz-feldspar granodiorite (QF) is the youngest and least abundant (in drill core) of the intrusive phases (Plate 3.3 D and E). The longest intersections of the QF granodiorite are approximately 1m in DDH E005 and ED002 (appendix C). The QF is equigranular with an average grain size of between 100 and 500 μm, approximately 10% of the rock is comprised of megacrysts of plagioclase feldspar up to 700μm l length. The QF has an estimated composition of 60% Quartz and 40% feldspar (90% of which is plagioclase with remainder K-feldspar).

The QF is moderately to intensely hydrothermally altered, however it is very weakly mineralised. Approximately 50% of the feldspars have been moderately altered to sericite, particularly well developed along growth zones. Greisen has been observed along the margins/contacts of the QF, although not in any significant volume (<5cm, 63.53m down drill hole E005; E5.5). Myrmekitic feldspar-quartz intergrowths are best observed along contacts with other phases, especially the FBQ, it is also moderately developed within the interior of the QF.

3.5 Vein dykes

3.5.1 Narrow 'vein' dykes

Narrow 'vein' dykes (Plate 3.4 A and B), typically 5 to 10 cm in wide, have been observed to cut the FBQ and to a lesser extent the FHB. At hand specimen scale they appear to have a mafic composition. In section these 'vein' dykes have a weakly porphyritic texture composed of <20% phenocrysts of hornblende (up to 4mm) and biotite (up to 2mm). The fine grained groundmass (0.02 mm) is estimated to compose 30% feldspar, 40% biotite and 30% quartz. The dykes are characterised by diagnostic chilled margins (typically 3mm wide) that distinguish them from being xenoliths, with phenocrysts oriented in one direction indicative of a flow emplacement. The margin has an equigranular texture that differentiates it from the coarser porphyritic dyke core. All phenocrysts are shaped as elongate needles (i.e. acicular).

Biotite is partially altered by chlorite. Secondary hydrothermal 'shredded' biotite occurs in distinct 'clumps/clots'. In a single case a quartz-pyrrhotite vein cross cuts a narrow-dyke.

(A)

(B)

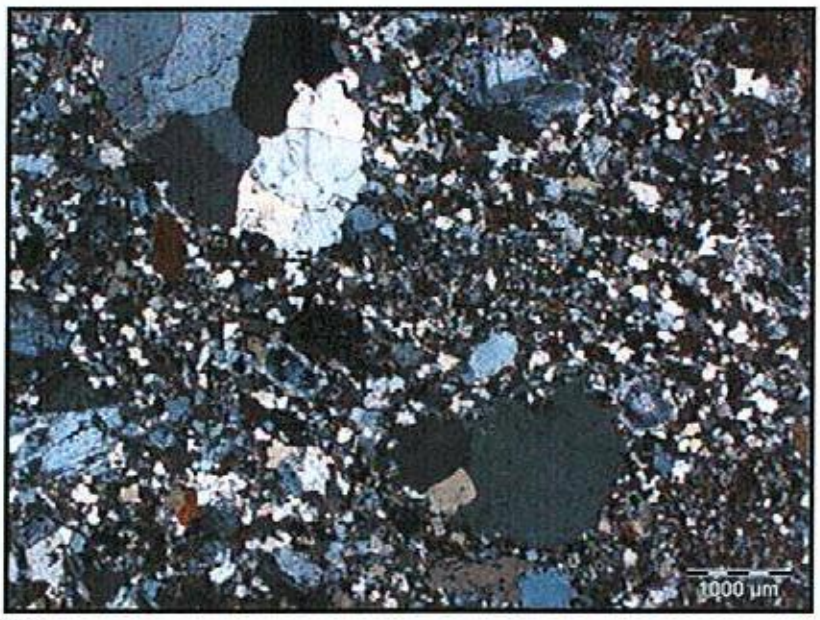

(C)

Plate 3.4 (A) Photomicrograph under cross polarised light of a narrow 'vein' dyke. Note characteristic chilled margin, 'rip up' clasts of host granodiorite and elongate phenocrysts (E5.7). (B) Photograph of a narrow 'vein' dyke (E5.7). (C) Photomicrograph under cross polarised light of a narrow porphyritic 'vein' dyke. Phenocrysts of quartz and feldspar in a fine grained groundmass (ED6.11).

3.5.2 Narrow porphyritic 'vein' dykes

Narrow porphyritic 'vein' dykes (Plate 3.4 C) are typically 10 cm wide, but may be up to 5 metres wide (as seen in drill hole ED006; Appendix C). Characteristic chilled margins are present (typically 3 mm wide). Phenocrysts comprise 60% of the rock and are composed of equal proportions of quartz and plagioclase feldspar. Subhedral to anhedral quartz phenocrysts occur up to 0.5cm in diameter. Quartz also occurs as anhedral clusters. Quartz clusters exhibit rounded margins suggestive of a degree of remobilisation after growth. Their origin is unclear, with likely explanations being an existing vein, or a coarse intrusive host. Xenoliths of granitic rock up to 3 cm are common. Feldspars show well-developed compositional zoning and their interiors are altered to sericite. The groundmass is equigranular and has an estimated groundmass composition of 45% quartz, 40% biotite and 15% feldspar was made, however due to the fine grain size this is uncertain. The groundmass also includes zones or clots of biotite (secondary 'shredded' biotite).

3.5.3 Aplite 'vein' dykes

Aplite vein dykes (Plate 3.5 A and B) averaging 2 cm wide were intersected in all the diamond drill cores logged. The irregular aplite vein dykes are composed of saccharoidal (also referred to as equigranular 'sugary' texture), alkali feldspar and quartz. Typically quartz is more abundant than feldspar (~70:30). The dykes are characterised by well-developed myrmekitic intergrowths of alkali feldspar and quartz along the contacts with the surrounding granodiorite. This myrmekitic texture is also weakly developed within the interior of the vein in rare cases. A single observation was made of pyrrhotite along the centre of an aplite vein dyke, the result of a later hydrothermal overprinting or indicating the fluid responsible for the formation of the dyke was also carrying metals. The dykes exhibit a similar orientation to the quartz veinlets and are not cut by any other unit. Aplite vein dykes are present typically cutting the FBQ granodiorite. It is estimated from these relationships that they formed during the late magmatic to magmatic-hydrothermal transition stage of the intrusion.

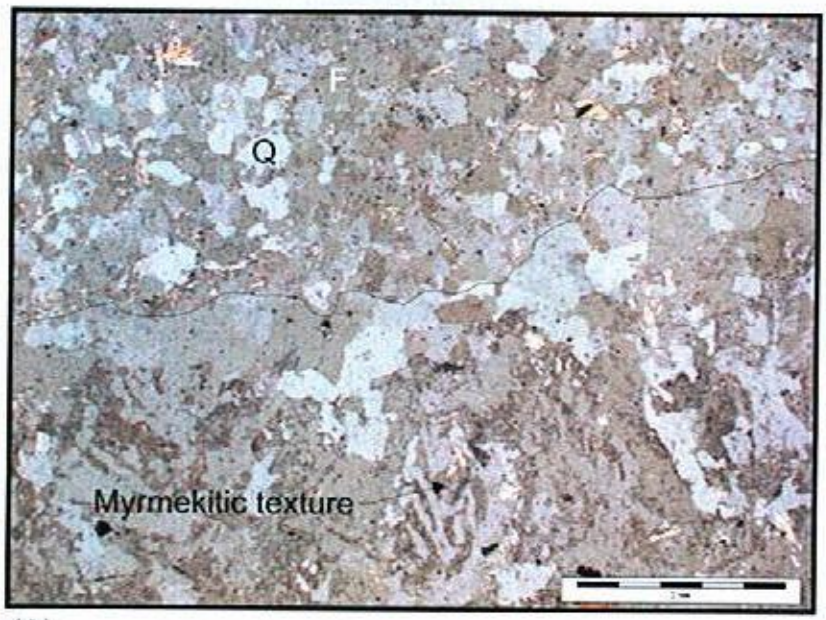

(A)

(B)

(C)

Plate 3.5 (A) Photomicrograph of an aplite 'vein' dyke (top of photo) composed of saccrahoid alkali feldspar and quartz. Minor hydrothermal sericite alteration. Myrmekitic texture developed along the margin of the dyke (E5.10). (B) Photograph of an aplite 'vein' dyke (E5.10). (C) Photograph of a greisen (E5.5). Scale bar is in cm

These dykes have been passively altered, resulting in radial (pseudo-acicular) sericite growth occurring throughout the dyke. This sericite alteration comprises approximately 10% of the dykes. These laths of sericite are typically 0.5 mm in length.

3.6 Magmatic-hydrothermal veins

Based on apparent cross cutting relationships, a broad vein and alteration paragenesis has been established. This is detailed in the following section

3.6.1 Quartz-layered textures

As previously stated quartz-layered textures are part of the family of magmatic hydrothermal transition textures. A quartz-layered texture was observed within the FBQ granodiorite. The observed texture was a poor example in comparison to those well documented in the literature (e.g. from Timbarra). The texture was first identified in drill core as a continuous 1cm thick feature, with apparent quartz growth in a single direction. The quartz-layered texture was substantiated microscopically from scanning cathodoluminescence (CL) images (Plate 3.6), acquired by David Steele using a Cameca SX100 electron microprobe at the Central Science Laboratory, University of Tasmania. The CL image illustrated a degree of internal complexity and demonstrated a potential growth origin. From the image it was determined that the growth orientation was to the top of the photo. Microscopy identified characteristic bipyramidal quartz crystals (indicative of β–quartz), with distinct apical terminations, and the occurrence of composite melt inclusions. Bipyramidal quartz is indicative of high temperature growth, and forms at temperatures above 573°C. Faint primary fluid inclusion trails define an inferred growth orientation/direction. Accessory minerals included acicular apatite (up to 100μm) and biotite laths (approximately 500μm). The presence of this texture provides evidence that the FBQ intrusion phase exsolved a volatile phase.

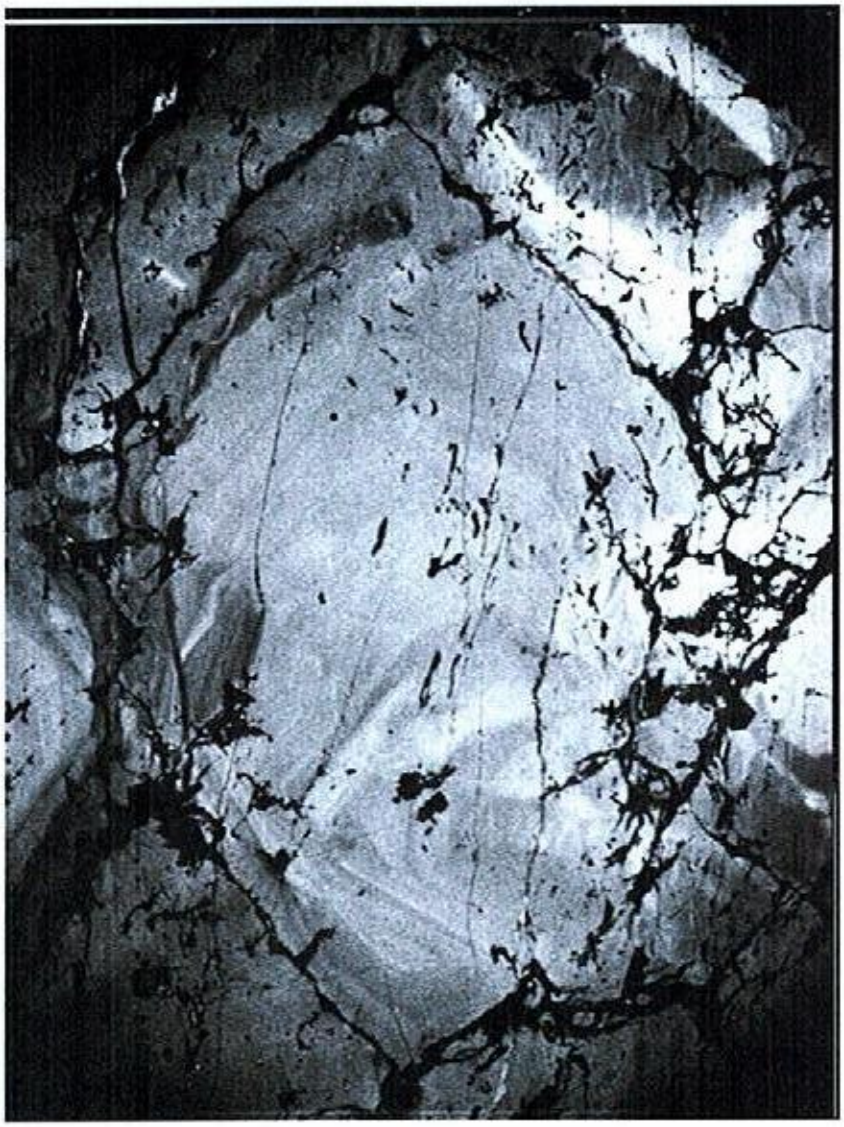

Plate 3.6 A scanning cathodoluminescence image of a bipyramidal quartz grain in a quartz layered texture (unidirectional solidification texture; ED6). The main crystal shape coincides with opaque filled diamond of cracks. Faint primary fluid inclusion trails distinguish internal growth zones. Note the weak internal complexity, especially developed in the lower right corner of the grain, suggestive of a growth point of origin. Inferred growth direction is up the page. The image is 1.25 mm wide.

3.6.2 Other textures

Small amounts of greisen were intersected down drill hole E005 (Appendix C) at the margins of the QF granodiorite (Plate 3.6 C). The greisen has an estimated composition of 70% muscovite, 20% quartz and 20% chlorite. Accessory minerals include apatite and an unidentifiable acicular mineral. The greisen is mineralised, containing approximately 1% arsenopyrite.

3.6.3 Alkali feldspar-quartz (± molybdenite ± pyrrhotite) veins

One of the earliest vein stages in the prospect are alkali feldspar-quartz veins (i.e. stage 1; Plate 3.7 A) that are variably mineralised with molybdenite and lesser pyrrhotite. These veins have been observed cross cutting all intrusive phases except the QF. Vein thickness varies from microveins approximately1 cm wide up to veins 10 cm thick. Vein densities are typically less than 5% of the rock, although in some drill core intersections these veins may make up to 20% of the rock.

The veins comprise alkali feldspar (~60%; ranging from crystals approximately 1 mm to 1 cm in length). The alkali feldspar occurs as subhedral crystals that are intergrown with subhedral to euhedral quartz. The alkali feldspar is generally more abundant than quartz; quartz is restricted to the margins of veins where it invariably occurs with sulphides. It is interpreted that the veins opened and were initially filled with quartz, but later feldspar precipitation prevailed.

Molybdenite typically occurs as blebs in trace amounts, and rarer dendritic growths making up ~10% of the vein. Molybdenite is restricted to quartz-rich fine-grained mosaic textures predominantly along the margins of veins, and lesser in the vein core. Pyrrhotite is less abundant than molybdenite, commonly occurring as fine grains in the vein core. Crosscutting relations are not well represented in drill core, but where seen these stage 1 veins are cut by all later vein stages.

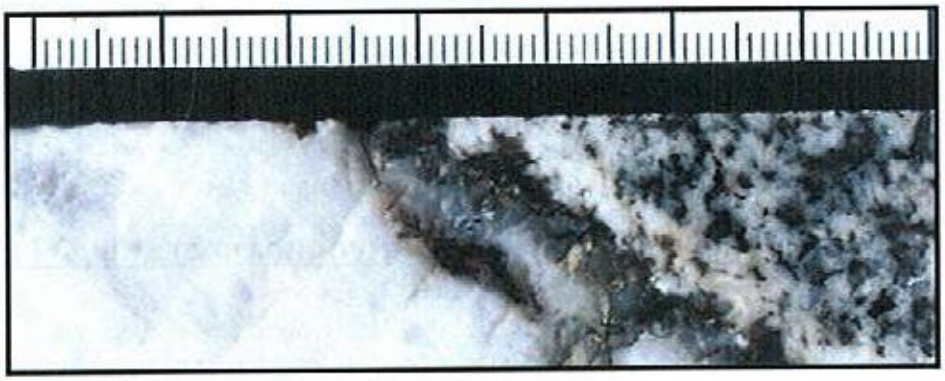

(A)

(B)

Plate 3.7 (A) Photograph of a typical alkali feldspar-quartz vein (± molybdenite ± Arsenopyrite ± pyrrhotite) with a feldspar- biotite vein selvage (E5.9) Scale bar represents 1cm intervals. (B) Photograph of typical gold-bearing quartz vein (+ arsenopyrite ± pyrrhotite ± pyrite). Assay results for this intersection are 0.4m at 14.4g/t Au. Hosted with in sericite and chlorite altered granodiorite (DDH E005 93m)

The veins are characterised by distinct alteration selvages composed of biotite, feldspar and lesser quartz. Biotite occurs as clusters of approximately 3mm long laths, forming a 0.5 cm selvage that rims the vein, and to a lesser extent extends into the margins of the vein. Bordering the biotite selvage is a 0.4 cm selvage of anhedral feldspar (unidentifiable) containing trace biotite laths (approximately 5% of the selvage). Adjoining the feldspar selvage is a minor subhedral quartz selvage.

3.6.4 Quartz (± arsenopyrite ± pyrrhotite ± pyrite ± gold)

Stage 2 veins (Plate 3.7 B) are very similar in appearance, occurrence and distribution to feldspar-quartz (± molybdenite ± pyrrhotite) veins. The common distinction between stage 1 and 2 veins is the absence of feldspar, more abundant sulphides and associated alteration selvage associated with stage 2 veins. The veins typically vary in size from 5 mm, up to 20 cm wide. Sulphide (arsenopyrite ± pyrrhotite ± pyrite) content seems to have no relationship to size of the vein. They typically make up less than 5% of the rock although rare densities of greater than 20% have been observed. Arsenopyrite, pyrrhotite and pyrite commonly occur as blebs predominantly along vein margins and/or as rare veinlets within the quartz veins, and typically make up <5% of these veins. The occurrence of gold is unclear, although it was not observed, assay results confirm its presence and concentration. It is assumed to be strongly correlated with arsenic from assay results. Rare amounts of chalcopyrite have been observed. Formation during a brittle deformation event is evident by contact morphology and the absence of ductile features. For example, vein boundaries are sharp and extent of the vein along strike. Most fluid inclusions have been destroyed in the major gold-bearing lodes probably due to post-depositional movement along these structures.

This vein stage is characterised by a moderately developed sericite and chlorite alteration halos. Plagioclase feldspars have been altered, with sericite altering the cores and or growth zones of phenocrysts. Chlorite is lesser developed and alters primary and secondary biotite and hornblendes. Adjacent to veins alteration is moderate and rarely texturally destructive. Further from veins alteration is less developed, however relationships are not well constrained as later veinlets and their associated alteration obscure the earlier formed alteration.

These veins appear to have predominated during gold deposition and most of the gold is hosted within them. A typical vein intersection possesses grades of 0.4 metres at 14.4 g/t gold (Plate 3.5 A). Although gold was not observed in the veins, its presence and concentration is known from assay results. It appears that elevated gold concentrations may be related to elevated arsenopyrite concentrations. For example, the 0.4 metres at 14.4 g/t intersected across the Enterprise vein that was 40 cm thick, but contained ~20% arsenopyrite. By comparison, intersections of 0.2 metres at 3.5 g/t gold in a section of Enterprise vein that was 20 cm's thick, mainly composed of buck quartz, had only veinlets of arsenopyrite. Assay results for drill hole E005 support this gold-arsenic relationship with elevated gold concentrations corresponding with elevated arsenic concentrations (Figure 3.4)

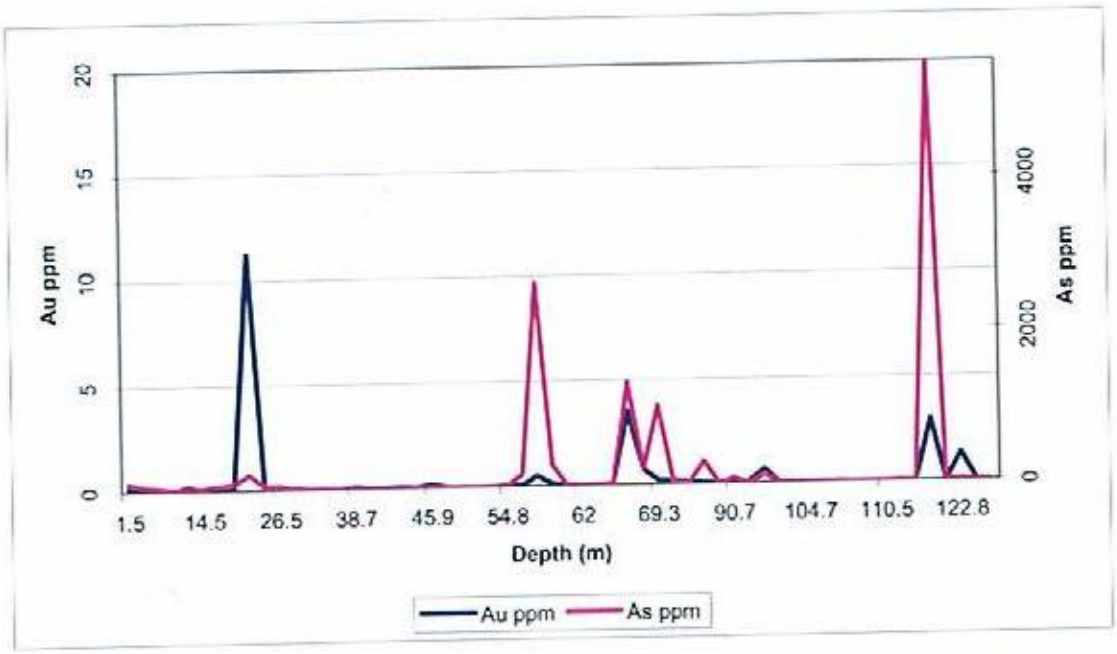

Figure 3.4 Plot down drill hole ED002 of assayed gold and arsenic grades. This plot shows an apparent correlation between gold and arsenic.

3.6.5 Quartz veinlets

Quartz veinlets commonly occur and cut all intrusive phases except the quartz-feldspar granodiorite. The veinlets are irregular in their morphology and are typically less than 1 mm in thickness. The composition of these is inferred to be quartz, as most veins are too small to identify (even under microscope magnification). These veins are characterised by narrow halos of intense pervasive sericite and chlorite alteration. These alteration halos vary in thickness, typically 5 mm either side of a vein. Rare occurrences have been observed of micro-vein frequencies of ~25% with veins forming stockworks. These veins commonly crosscut all other units except where no relationship has been identified, eg. Stage 2 quartz veins and narrow vein dykes.

3.7 Alteration assemblages

Three dominant alteration assemblages were observed at the Enterprise prospect:

(1) Secondary 'shredded' biotite and phlogopite replacing primary biotite and hornblende phenocrysts is texturally destructive. This appears to be in part related to the first vein stage (feldspar-quartz veins). It may also predate this vein stage, as it is the most widespread occurring in places distal to these veins.

(2) Sericite-quartz (less than 200 μm grain size) replacing plagioclase and alkali feldspar phenocrysts and usually preserves original textures. This assemblage is equally as abundant as the first; its intensity varies from intense texturally destructive to passive texturally preserving, according to proximity to veins and other units. This assemblage is associated with stage 2 veins: quartz (± arsenopyrite ± pyrrhotite ± pyrite ± gold) and stage 3 veins: quartz veinlets.

(3) Last and least developed, chlorite alteration has replaced primary phenocrysts and earlier formed secondary Fe-Mg minerals (biotite and hornblende).

3.8 Igneous and alteration petrology of the Potoroo Prospect

Geochemical soil sampling initially discovered the Potoroo prospect, which was not exposed by historical workers. This was followed up by trenching and RC drilling that delineated a prospective target for mineralisation. More recent diamond drilling (2004) has further exposed the resource potential. Potoroo is one of the most recent and thus least exposed gold occurrences in the Lisle/Golconda area. Although the mineralisation at the Potoroo prospect isn't as well represented as the Enterprise, attempts will be made to characterise it.

The granodiorite has an estimated average composition of 60% feldspar, 30% quartz and 10% biotite. Accessory minerals include hornblende, apatite, zircon and magnetite. Magnetite occurs interstitial to crystal phases and has been observed to coat grain boundaries. The rock has a porphyritic texture, with ~10% phenocrysts of plagioclase. Plagioclase feldspars show well developed oscillary zoning, with sericite alteration most common along these zones. Sericite alteration, to a lesser extent, is developed in a 'cross hatched' arrangement. Feldspars are typically 5mm in size, however, rare phenocrysts up to 1cm have been observed. Approximately 2 to 3% of the biotite component has been altered to chlorite. Secondary 'shredded' biotite is common occurring in clumps or 'clots' with chloride and sulphides. Arsenopyrite is the predominant sulphide observed. It occurs as interstitial microscopic aggregates commonly occurring with biotite and/or chlorite. Based on observations at the Enterprise, gold is likely to be associated with arsenopyrite. Accessory sulphides include pyrite and to a lesser extent chalcopyrite.

Quartz veins containing arsenopyrite, pyrite and chalcopyrite cut the Potoroo granodiorite. Alteration associated with the veins is difficult to interpret due to poor drill core recovery. However, it is probably related to the pervasive alteration observed in the granodiorite.

3.9 Summary

The Enterprise prospect is host to three main petrographically distinct intrusive phases. Although cross cutting relations are limited and/or obscured, an apparent paragenetic sequence of first feldspar-biotite quartz, followed by feldspar-hornblende-biotite and feldspar quartz granodiorite is suggested. The relationship between the intrusives and mineralised stage 2 veins is not well understood. Primary pyrrhotite has been observed in the FBQ granodiorite, suggesting a potential magmatic origin for at least some of the mineralisation. More than one intrusive event potentially denotes multiple mineralising events (volatile exsolution) assuming that metals were sourced from the intrusions. At least 4 distinctive magmatic-hydrothermal vein stages are present coupled with discrete alteration assemblages.

Evidence for a magmatic-hydrothermal transition is in the form of distinguishing textures and intrusive units. Magmatic-hydrothermal transition textures, including quartz-layered textures, aplite 'vein' dykes and greisens are all evident at the Enterprise prospect, in particular within the FBQ. These textures provide evidence that individual magma batches exsolved volatile phases. If in significant amounts this volatile phase may have been able to transport large amounts of metals, caused extensive hydrothermal alteration and potentially mineralisation. A fundamental feature of intrusion-related gold deposits is the fact that metals are sourced from felsic intrusion. The relationship of a volatile phase to mineralising fluids at Enterprise is unclear; however, the forthcoming fluid inclusion study will attempt to establish any relationships (see chapter.5)

Gold is primarily associated with one vein stage: quartz (± arsenopyrite ± pyrrhotite ± pyrite ± gold), which is primarily hosted in the FBQ granodiorite, and hence postdates it, or developed by exsolution of fluids from it at deeper structural levels. Gold mineralisation occurs in quartz veins that are associated with the most extensive alteration assemblage, sericite and lesser chlorite. These veins are characterised by variable amounts of arsenopyrite, pyrrhotite, pyrite and trace chalcopyrite. Visual relationships between apparent arsenopyrite proportions in quartz veins and assayed gold values (Figure 3.4) suggest a correlation. Increasing visual sulphide percentage

in veins appears to correspond with increasing gold grades. Hypothetically, gold is likely to be present as microscopic grains within arsenopyrite or incorporated within its crystal lattice, but this should be tested with micro-analysis. The observation raises the possibility that higher arsenic zones in soils should be priority targets in exploration at Enterprise. This also suggests a potential depositional mechanism for gold, sulphide deposition, a known catalyst for gold deposition.

4 Intrusion Chemistry

4.1 Introduction

The chemistry of intrusions can be used to attempt to evaluate the ore-element associations of intrusion-related ore deposits (Blevin, 2004). An intrusions composition, relative oxidation state and fractionation characteristics can all be studied using whole-rock chemistry. The Devonian granitoids of Tasmania are associated with a diverse range of ore-deposits, e.g., the oxidised S-type granites of the northwest are associated with tin and tungsten (± gold, silver, lead and zinc), and reduced granitoids of the northeast have high background gold (Solomon and Groves, 1994). This chapter will compare analyses from the Enterprise and Potoroo prospects to existing datasets of the Scottsdale Batholith and known gold-bearing granitoid suites from eastern Australia. A considerable database of major and trace element compositions is available for the Blue Tier and Eddystone Batholiths, and to a lesser extent for the Scottsdale Batholith (McClenaghan, 1984). Data from 91 samples collected throughout the Scottsdale Batholith were sourced from Mineral Resources Tasmania (written communication McClenaghan, 2004). This data represents the most up-to-date records and covers most rock types from the Scottsdale Batholith.

The timing of volatile exsolution with respect to the progress of fractional crystallisation is very important (Blevin, 2004). Exsolution of a volatile phase early rather than late may result in a different ratio of compatible to incompatible ore elements being exsolved, as their concentrations change as a factor of fractional crystallisation. Therefore fractional crystallisation will have an effect on the amounts of ore elements being exsolved, thus, the potential to form an ore deposit. It has been shown (Blevin and Chappell, 1992) that those suites characterised by a classic petrographic and compositional behaviour, consistent with the processes of fractional crystallisation, are also those suites most commonly associated with significant mineralisation

4.2 Methods

15 samples from the Enterprise and 1 from the Potoroo prospect (for a total of 16) were analysed at the University of Tasmania using a Phillips PW 1480 X-Ray fluorescence spectrometer (Appendix E). Samples were prepared by crushing 1 to 2 kg pieces of drill core in a jaw crusher to reduce the particle size to less than 1cm. Samples were pulverised using a chrome still mill for approximately one minute to produce pulps. Contamination associated with a chrome steel mill includes: Fe (up to 0.15%), Cr (up to 150 ppm) and traces of Mn, Si, C and V. Silica sand cleaners were used between samples to minimise the risk of contamination.

Of these 16 samples, 5 of them, and a standard sample, were analysed for ferrous iron (FeO) using titration methods at Amdels commercial laboratory in South Australia (Appendix F). The standard sample submitted for ferrous iron returned a result of 2.00% FeO with expected results of between 1.80 and 2.08% FeO therefore an estimated error of ±0.20% was applied to these particular results

Representative sample material was collected from drill core that represents the dominant intrusive units, as described in Chapter 3. Samples were selected that appeared to be the least altered in the field and distal from extensive veining. However, the samples location within a mineralised site meant that some samples were in fact altered. Major and selected trace elements and are detailed in Table 4.1.

CAPTION FOR NEXT PAGE

Table 4.1 Whole rock geochemical data for granodiorite and 'vein' dyke samples from the Enterprise and Potoroo prospects. Major (wt %) and trace (ppm) elements determined by XRF, Fe_2O_3 and FeO determined by titration.

Sample ID	ED2.3	ED2.4	ED2.12	ED2.13	E5.1	E5.2	E5.4	E5.7	E5.10	E5.12	E5.131	ED6.1	ED6.11a	ED6.14	PD1.1	ED6.11b
Lithology	AVD*	FHB	FBQ	QF*	FBQ	QF*	QF*	VD	AVD*	QF*	FBQ	FHB	FHB	FHB	FBQ[P]	PVD*
SiO_2 wt %	77.85	65.99	66.60	76.61	66.84	77.88	79.20	58.95	78.96	76.97	63.43	65.76	67.69	58.58	65.12	71.69
TiO_2	0.02	0.49	0.46	0.04	0.48	0.07	0.09	0.70	0.03	0.12	0.54	0.49	0.43	1.04	0.54	0.49
Al_2O_3	12.00	16.06	15.61	12.47	15.90	11.81	12.41	15.85	10.70	12.21	16.52	15.98	15.26	15.66	16.35	12.85
Fe_2O_3			-0.11		0.06	-0.07								0.27	1.80	
FeO			4.10		3.60	0.60								7.40	2.40	
FeO*	0.54	4.29	4.00	0.59	3.65	0.54	0.68	5.49	0.74	0.82	4.61	4.15	3.50	7.60	4.02	3.54
MnO	0.01	0.08	0.06	0.01	0.06	0.01	0.03	0.10	0.02	0.01	0.04	0.08	0.06	0.14	0.05	0.06
MgO	0.15	2.13	1.82	0.17	2.16	0.29	0.26	3.82	0.16	0.42	2.07	2.25	1.95	3.59	2.35	2.52
CaO	0.86	4.27	3.58	0.96	3.79	1.03	0.45	5.99	1.93	1.88	4.50	4.33	3.90	5.19	2.39	2.34
Na_2O	3.47	4.28	4.14	3.66	3.94	3.30	4.40	4.28	4.07	4.23	4.04	4.13	4.11	3.67	3.63	3.58
K_2O	4.48	1.53	1.69	4.66	1.52	3.63	1.47	1.15	1.64	1.63	1.55	1.60	1.48	1.93	1.77	2.15
P_2O_5	0.01	0.16	0.14	0.01	0.14	0.02	0.02	0.25	0.01	0.04	0.18	0.14	0.13	0.35	0.15	0.11
Loss inc. S-	0.77	0.58	1.59	0.74	1.11	1.10	1.02	2.39	1.71	1.50	1.60	0.61	0.73	1.12	2.85	0.92
Total	100.22	100.34	100.13	100.00	99.99	99.74	100.09	99.58	100.04	99.93	99.59	99.99	99.83	99.71	99.66	100.02
S	0.10	0.04	0.33	0.05	0.07	0.01	0.05	0.34	0.05	0.08	0.82	0.01	0.10	0.71	1.64	0.04
Mo ppm	1	<1	65	66	24	4	23	2	3	51	1	1	97	25	<1	71
Sb	<2	<2	<2	<2	<2	<2	<2	<2	<2	<2	<2	<2	<2	<2	<2	<2
Sn	<1.5	<1.5	<1.5	<1.5	<1.5	<1.5	<1.5	3	2	<1.5	2	<1.5	<1.5	<1.5	2	<1.5
Nb	3	9	8	4	8	5	3	8	5	4	7	9	8	13	8	11
Zr	50	112	104	55	102	80	54	121	88	64	109	105	100	180	120	116
Sr	109	460	423	58	472	148	151	781	150	222	527	443	414	499	397	263
Ba	456	601	553	660	498	700	574	518	256	629	417	553	533	677	381	481
Sc	<2	12	11	<2	12	<2	<2	17	2	3	14	12	11	18	13	11
V	3	98	86	3	93	10	12	156	6	22	104	99	83	198	107	88
Y	4	13	12	7	9	10	7	15	7	8	15	13	11	21	14	12
U	6	4	4	5	2	9	6	3	16	6	2	3	4	3	2	3
Rb	70	54	66	62	69	61	43	57	40	41	70	49	50	82	94	83
Th	18	10	9	15	8	23	21	8	23	19	6	8	7	4	6	9
Pb	14	9	7	20	6	14	9	5	10	7	6	7	6	7	8	7
As	4	<3	<3	<3	<3	<3	80	<3	<3	<3	<3	<3	<3	<3	5	<3
Bi	<2	<2	<2	<2	<2	<2	<2	<2	<2	<2	<2	<2	<2	<2	<2	<2
Zn	4	69	57	5	45	17	9	54	4	10	38	58	47	102	36	43
Cu	21	12	65	8	14	4	6	47	13	19	135	6	25	202	64	9
Ni	5	16	11	5	18	4	4	47	9	4	10	18	15	22	17	21
W	<2	<2	16	<2	5	<2	3	87	<2	4	163	<2	<2	3	<2	<2

Abbreviations: AVD = Aplite 'vein' dyke, FBQ = Feldspar-biotite-quartz granodiorite, FBQ[P] = Feldspar-biotite-quartz granodiorite from the Potoroo prospect, FeO* = total Fe, FHB = Feldspar-hornblende-biotite granodiorite, PVD = porphyritic 'vein' dyke, QF = quartz feldspar granodiorite,
* denotes hydrothermally altered sample.

4.3 Scottsdale Batholith

Whole-rock geochemical data has been used to assess internal variations in chemistry of the Scottsdale Batholith (McClenaghan, 1984). The Scottsdale Batholith is made up of a number of separate plutons including the Diddleum, Upper Blessington, Porcupine Creek, Russels Road, Hogarth Road, Tombstone Creek and Mt Stronach. Broadly, the Scottsdale Batholith is divided into two distinct rock associations divided by a screen of Mathinna Group sediments (Figure 2.1). Granodiorite occurs in the west, and biotite adamellite, alkali feldspar and granodiorite to the east. The western granodiorite suite is called the Diddleum Pluton. Scatter plots after McClenaghan (1984), show two broad linear trends that are particularly evident in the case of Ba and Zr, and to a lesser extent CaO and MgO, when plotted against SiO_2 (Figures 4.1, 4.2) a standard analytical practice for unaltered granitic rocks. McClenaghan (1984) recognised the flatter slopes for Ba and Zr versus SiO_2, to consist of data from granodiorites, whereas the other steeper trend consists of data from adamellites and alkali-feldspar granites. The granodiorite trend contains data from both sides of the Mathinna Group screen. Granodiorites from west of the Mathinna Group screen typically have SiO_2 values less than 65 wt % and granodiorites from east of the Mathinna beds screen typically have SiO_2 values greater than 65 wt %. From this, McClenaghan (1984) demonstrated that the Scottsdale Batholith is composed of two chemical suites, the granodiorite suite predominantly in the west, and the adamellite and alkali-feldspar suite to the east.

Chemically the granodiorites from the Enterprise and Potoroo prospects form part of the western granodiorite suite of the Scottsdale Batholith as expected from their physical location (Figure 2.2). Samples of the host granodiorites from the Enterprise and Potoroo prospects analysed by this project have SiO_2 values ranging from 58.58 to 79.20 wt %. Values between 58.58 and 67.89, are similar to the overall suite range indicated by McClenaghan (1984). My initial interpretation of the SiO_2 values greater than 70 wt % was addition of quartz through alteration because they exceed all values collected previously. The samples with SiO_2 values greater than 70 wt % include aplite 'vein' dykes, narrow 'vein' dykes and QF.

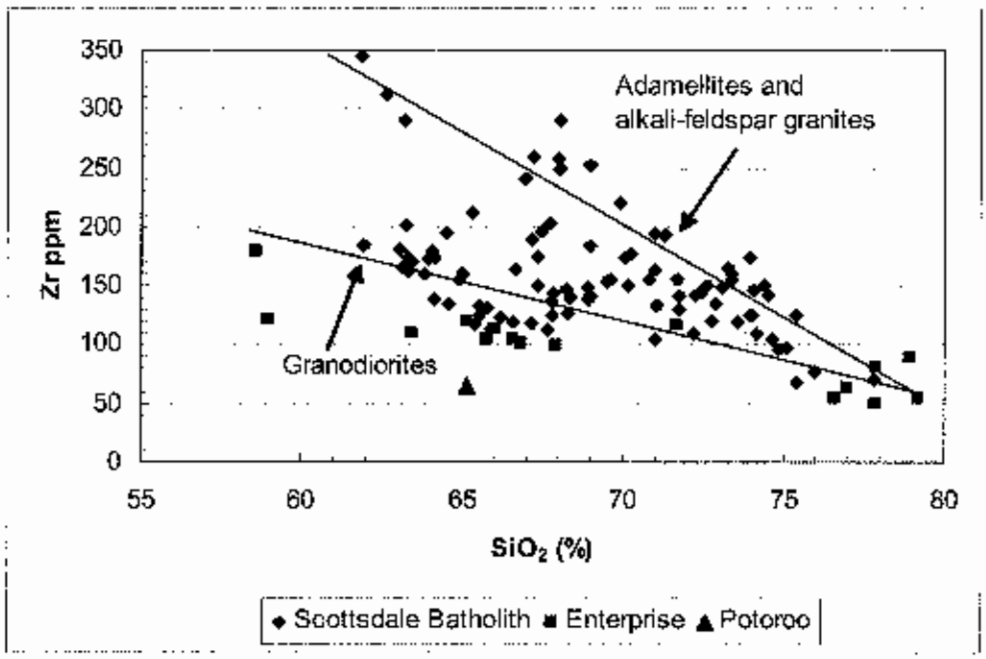

Figure 4.1 Zr versus SiO_2 for the Scottsdale Batholith including the Enterprise and Potoroo prospects. Note the two trends for the two different suites as defined by McClenaghan (1984).

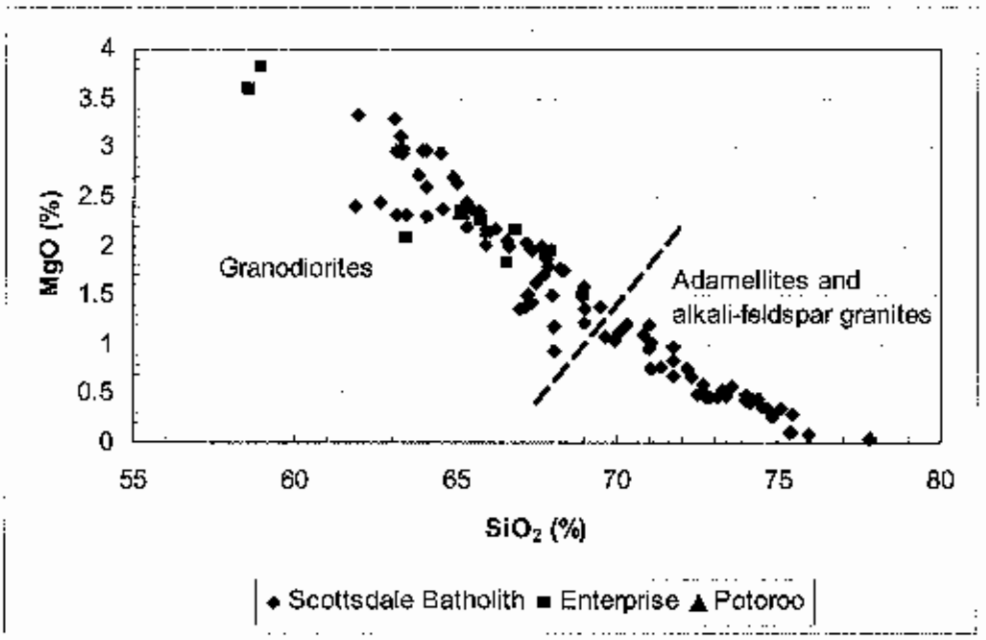

Figure 4.2 MgO versus SiO_2 for the Scottsdale Batholith including the Enterprise and Potoroo prospects. The plot shows the positions of the two different suites as defined by McClenaghan (1984).

Although only a small sample size, the data from the Enterprise and Potoroo prospects consistently plots across the 65 wt % SiO_2 boundary, a value that approximately reflects the spatial boundary between granodiorites either side of the Mathinna Group screen. This could support an argument for the Lisle/Golconda granodiorites (including the Enterprise and Potoroo prospects) constituting a separate body, distinct from other plutons in the Scottsdale Batholith. The name 'Lisle Pluton' was suggested by Roach (1994) for granodioritic rocks that outcrop at Lisle, Golconda, Lone Star and Panama on the basis of petrological, geochemical and petrophysical characteristics. In the following section, data review will further evaluate this theory.

4.4 Classification

Classification based on composition is important as a guide to the abundance of elements and volatiles in intrusions and their behaviour during the fractionation processes. The intrusions that comprise the Scottsdale Batholith have all been classified as I-type (McClenaghan, 1984), being intrusions with an igneous source. Characteristics that define I-type intrusions include: hornblende and biotite as the mafic minerals, high concentrations of calcium, low potassium to sodium ratio (K_2O/Na_2O), typically less than 1, low molecular $Al_2O_3/ (Na_2O + K_2O + CaO)$, and a low initial $^{87}Sr/^{86}Sr$ ratio (Chappell and White, 1974).

Samples from the Enterprise and Potoroo prospect, as with the rest of the Scottsdale Batholith are broadly classified as I-type intrusions on the basis of these criteria. While major element data from the Enterprise and Potoroo prospects appear to plot similarly to data from the Scottsdale Batholith, some of the data diverges markedly (Figure 4.4 and 4.5). Data below 70 wt % SiO_2 broadly plots along side the Scottsdale Batholith, data greater than 70 wt % SiO_2 does not. This is probably also reflecting the affects of alteration as previously indicated. However, those data points that appear to be least altered (less than 70 wt % SiO_2) plot within the sodic and peraluminous fields (Figure 4.3, 4.4)

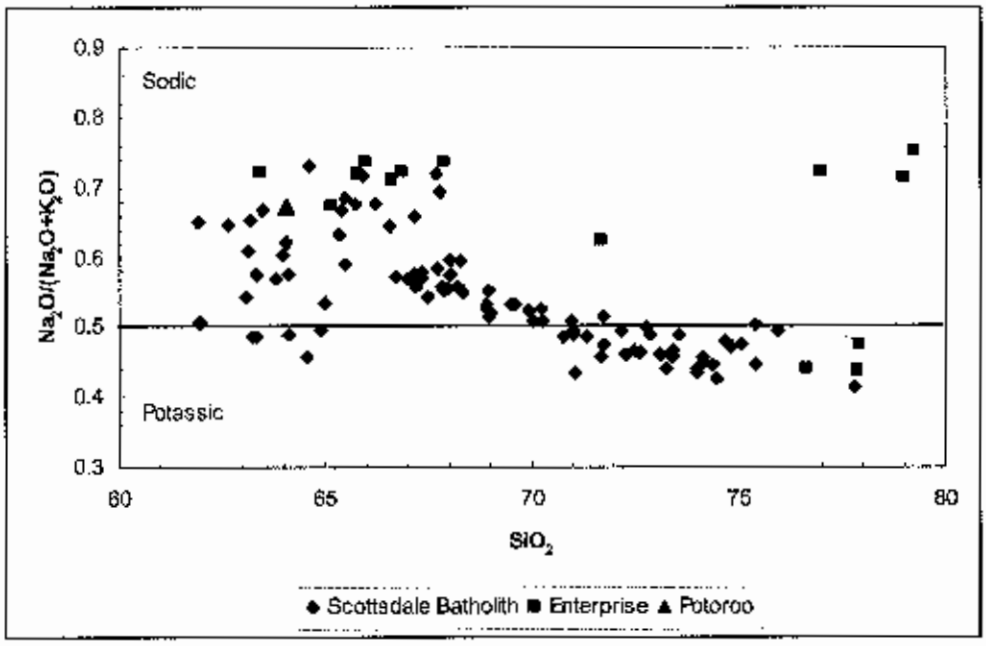

Figure 4.3 Sodic versus potassic plot for the Scottsdale Batholith including the Enterprise and Potoroo prospects (Ferris and Schwarz, 2004).

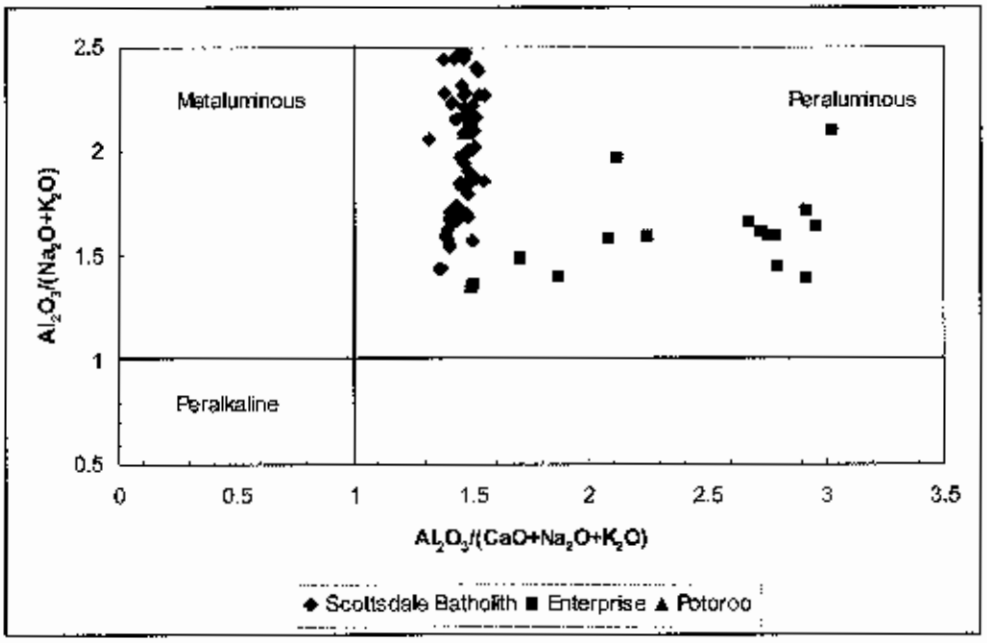

Figure 4.4 Meta-peraluminous plot for the Scottsdale Batholith including the Enterprise and Potoroo prospects (Ferris and Schwarz, 2004).

4.5 Oxidation State

Oxidation state of magmas plays a major role in controlling the compatible or incompatible nature of many ore elements. Oxidation state is largely inherited from the magma source region, although the effects of wall-rock interaction can be locally important. Oxidation state can be measured through a number of means, including: whole rock Fe_2O_3/FeO ratio; mineral assemblages (magnetite and titanite versus pyrrhotite stable mineral assemblages); mineral chemistry (Fe^{3+} in biotite and ilmenite, Mn in apatite); mineral colours (eg. pink potassium feldspar in oxidised rocks, foxy-red biotite in reduced rocks); and through magnetitic susceptibility (Blevin, 2004).

The ratio of Fe_2O_3 to FeO provides a measure of the oxidation state of the magma and increases with increasing oxidation. FeO was analysed for 5 samples from the Enterprise and Potoroo prospects, and was used to calculate the ratio of Fe_2O_3 to FeO. Two samples produced negative Fe_2O_3 concentrations; this was attributed to analytical error associated with using two methods for obtaining total Fe as Fe_2O_3 and FeO. Negative values were interpreted to represent an absence of Fe_2O_3 (i.e. all Fe occurring as FeO) and were converted to zero, or 100% reduced. The results produced three Fe_2O_3 to FeO ratios of 0.02, 0.03 and 0.75. The value from the Potoroo prospect (0.75) is comparably higher than those ratios determined from the Enterprise prospect intrusive rocks. Given that the Fe_2O_3 to FeO ratios for the Scottsdale Batholith range from 0.01 to 1.00, with an average of 0.27, the results from the Enterprise and Potoroo prospects lie within this range. Roach (1994) attributed higher Fe_2O_3 to FeO ratios for samples in the Lisle area to the presence of magnetite rather than ilmenite as an accessory phase. Down drill hole magnetic susceptibility of the granodiorites from the Enterprise and Potoroo prospects averaged 0.51 x 10^{-3} SI units, consistent with the 'non-magnetic ' granodiorite described by Roach (1994).

An oxidation parameter (ΔOx) developed by Blevin (2004) based on Fe_2O_3/FeO and FeO* can be used to classify oxidation state:

$$\Delta Ox = \log_{10} (Fe_2O_3/FeO) + 0.3 + 0.03*FeO*$$

Where $FeO^* = (0.9*Fe_2O_3) + FeO$, and Fe_2O_3, FeO and FeO^* are in weight percent.

Five oxidation classes are recognised (Figure 4.6): very strongly, strongly and moderately oxidised, and moderate and strongly reduced. The four samples from the Enterprise prospects all gave results within the strongly reduced field (-1.40 to 0.30; Figure 4.5). The single data point from the Potoroo prospect plotted in the strongly oxidised field. An average ΔOx value for the Scottsdale Batholith of -0.27 was calculated, which plots in the moderately reduced oxidation field. By using this measure of oxidation state, granodiorites from the Enterprise prospects were estimated to be strongly reduced. This conforms to observation of a reduced mineralogy (Chapter 3) including presence of anomalous molybdenum (incompatible in oxidised melts), foxy-red biotite (phlogopite), and pyrrhotite (Blevin, 2004).

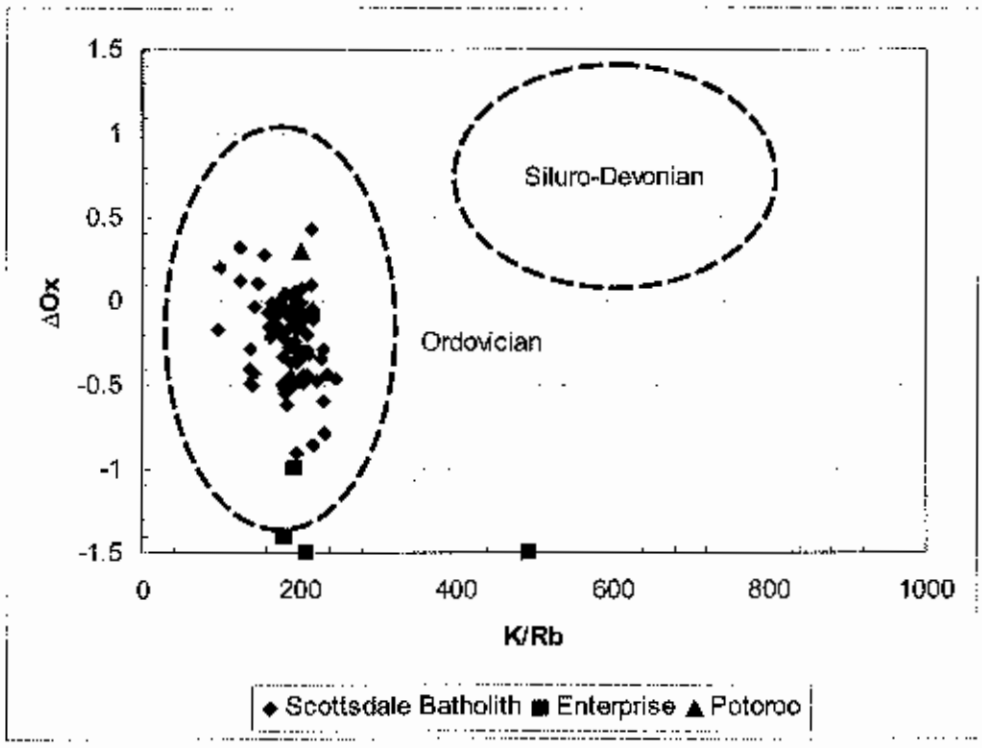

Figure 4.5 K/Rb ratio versus relative oxidation state (ΔOx) for the Scottsdale Batholith including the Enterprise and Potoroo prospects. Plot shows the approximate positions of Ordovician and Siluro-Devonian granitoids from the Lachlan Fold Belt (Blevin, 2004).

The Potoroo prospect is characterised by a mineral assemblage of arsenopyrite, pyrite and trace chalcopyrite. Potoroo produced a $\log(Fe_2O_3/FeO)$ value of -0.13, almost identical to that of the Stanthorpe Leucomonzogranite, the host of the Timbarra deposit (-0.02; Mustard, 2001). Both the Potoroo prospect and Timbrrra deposit are hosts to disseminated gold mineralisation in granodiorite.

However, one explanation for Potoroo plotting in the strongly oxidised field may be that very felsic granites usually have exaggerated Fe_2O_3/FeO ratios and are susceptible to alteration effects, and other methods need to be employed to determine oxidation state (Blevin and Chappell, 1992). Contamination by the Mathinna Group sedimentary rocks may also have had a localised effect (Mathinna Group intersected in Potoroo prospect drill core), and/or subsolidus reactions caused by magmatic phases. However, the oxidation state of the local Mathinna Group was not determined.

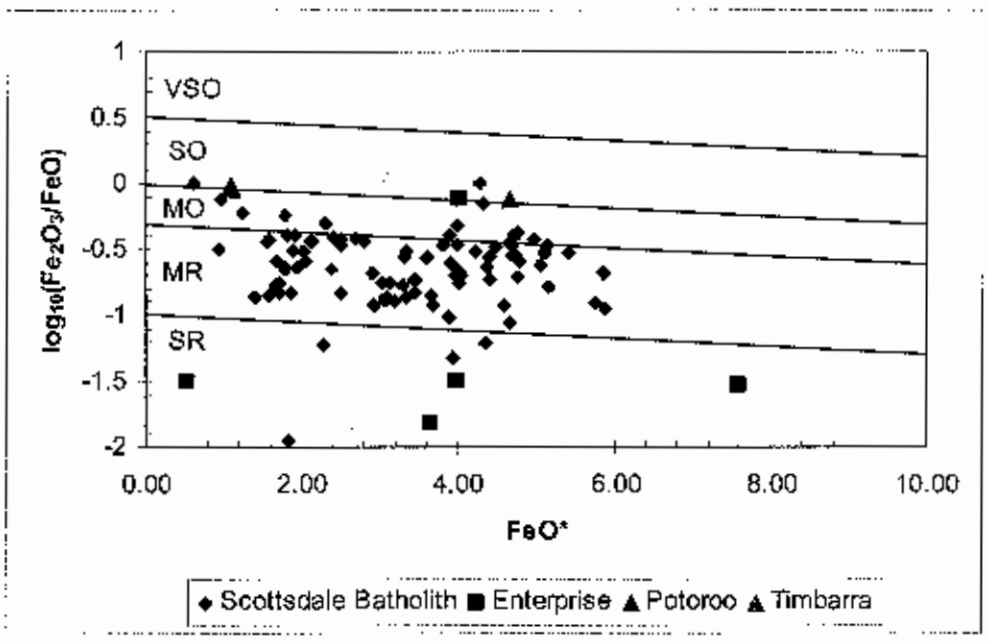

Figure 4.6 Fe_2O_3/FeO versus FeO for the Scottsdale Batholith including the Enterprise and Potoroo prospect. Also shown is the Stanthorpe Leucomonzogranite, host to the Timbarra deposit, NSW (Mustard, 2001). Abbreviations: VSO = Very strongly oxidised, SO = strongly oxidised, MO = moderately oxidised, MR = moderately reduced, SR = strongly reduced (Blevin, 2004).

4.6 Fractionation

The degree and type of fractionation is important in determining both the potential for mineralisation and the type of mineralisation that a granite suite is associated with (Blevin, 2004). Fractional crystallisation can preferentially change the abundance of elements in a granite suite by removing compatible elements and concentrating incompatible ones. Fractional crystallisation can be measured by using compatible/incompatible element ratios (e.g. Rb/Sr ratio), and the behaviour of selected trace elements that indicate the incoming or outgoing of crystal phases (e.g. variations in Ti, Mg, Ca, Ba, Zr, Y etc). Suites that show classic petrographic and compositional behaviour consistent with the processes of fractional crystallisation are also those suites most commonly associated with significant mineralisation (Blevin, 2004). The presence of porphyritic rocks at the Enterprise and Potoroo prospects may suggest that fractional crystallisation has occurred at least to some degree, and could also explain the large variation in SiO_2 values across the whole Scottsdale Batholith.

Globally, individual granite suites show distinctive trends when elements are plotted on variation diagrams against SiO_2 wt % or total Fe (as FeO*) (Blevin and Chappell, 1992), for example, Figure 4.7. Curved trends are characteristic of fractional crystallisation, whereas straight-line trends have been attributed to varying degrees of mixing between melt and the solid residual fraction (restite) carried up from the source. In the latter, fractional crystallisation may nevertheless occur in the more felsic members of suites that have eliminated their restite component. Figure 4.7 illustrates a subtle curved trend for the Scottsdale Batholith; the Enterprise and Potoroo prospect analyses show a discrete straight-line trend highly divergent the main trend. However, it is more likely that the low Rb values at SiO_2 values greater than 70 wt % are the result of alteration effects, causing the dilution of Rb by the addition of quartz (verbal communication Berry, Crawford and Roach, 2004). Therefore it is likely that the Enterprise and Potoroo prospect data would exhibit a similar trend to the Scottsdale Batholith on the basis of the remaining data, and represent altered versions of the most mafic compositions in the batholith. Blevin (1992) preferred Rb as an indicator of fractionation in the Lachlan Fold Belt, as concentrations above 250 ppm could be used to indicate significant K-feldspar

fractionation. Low SiO_2 samples (i.e. least altered) from the Enterprise prospect gave Rb concentrations of between 40 and 94 ppm. This narrow range of low concentrations is interpreted to indicate a low degree of fractionation.

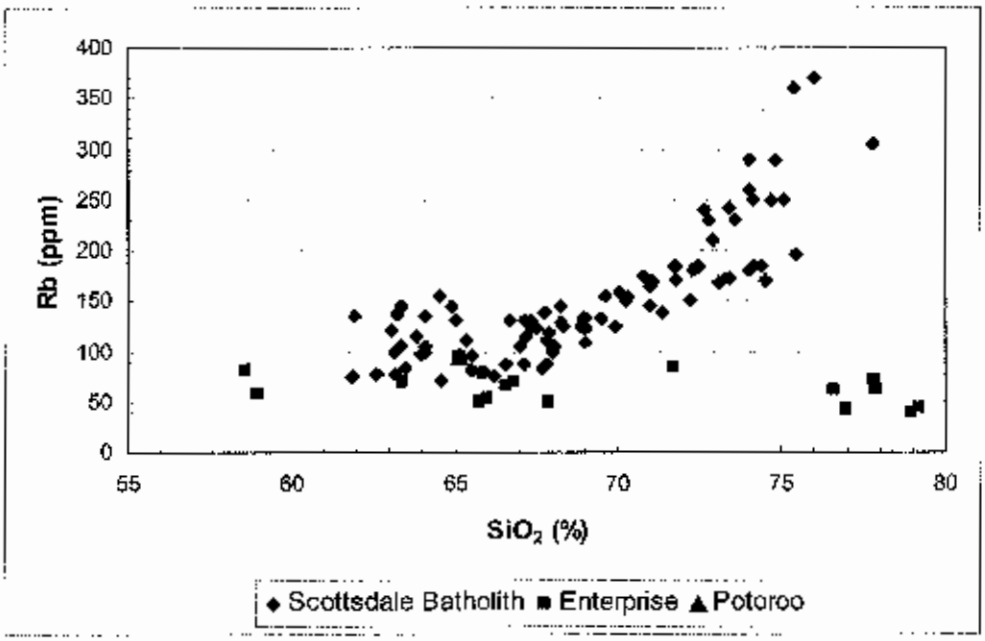

Figure 4.7 Rb versus SiO_2 for the Scottsdale Batholith including the Enterprise prospect and Potoroo prospects.

On K_2O versus Al_2O_3 and Sr versus Rb plots (Figures 4.8, 4.9), the Enterprise and Potoroo prospect granitoids are chemically distinct from those of the rest of the Scottsdale Batholith. The Enterprise and Potoroo granodiorites have low K_2O and high Al_2O_3 concentrations in comparison to the Scottsdale Batholith. The granodiorites also have comparatively high Sr and low Rb concentrations. Roach (1994) concluded on the basis of similar findings in the district that samples from the Lisle area were geochemically distinct and the least fractionated of the Tasmanian granitoids. Geochemical data for the Enterprise and Potoroo prospects support this theory that these granodiorites are chemically distinct and appear to be the least fractionated of the Scottsdale Batholith. This observation supports the theory that the granitoids in the Lisle/Golconda area are part of a separate body distinct from the Scottsdale Batholith.

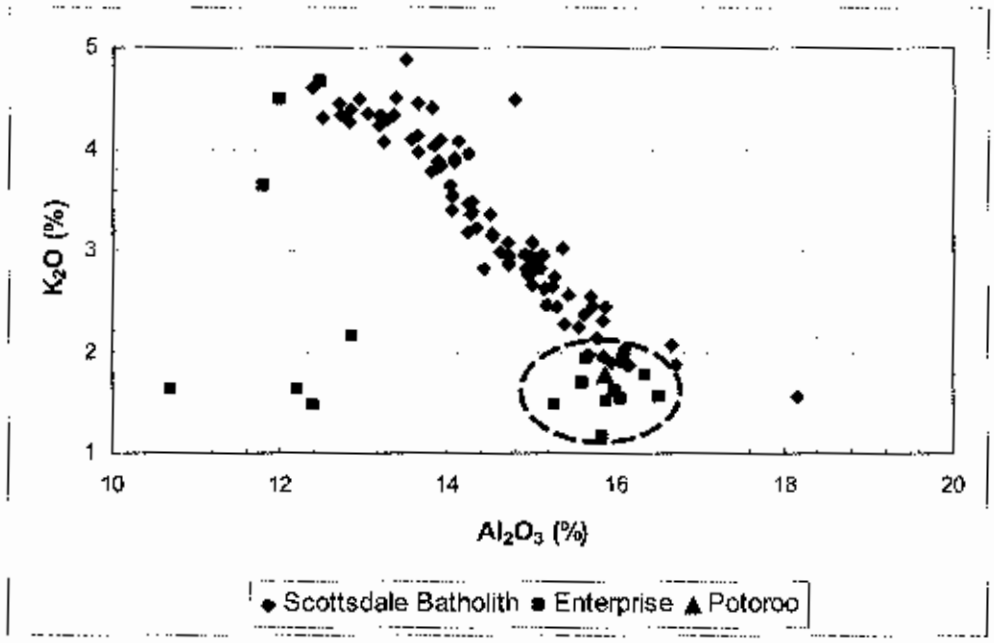

Figure 4.8 K_2O versus Al_2O_3 for the Scottsdale Batholith including the Enterprise and Potoroo prospects. Unaltered samples delineated by the circle.

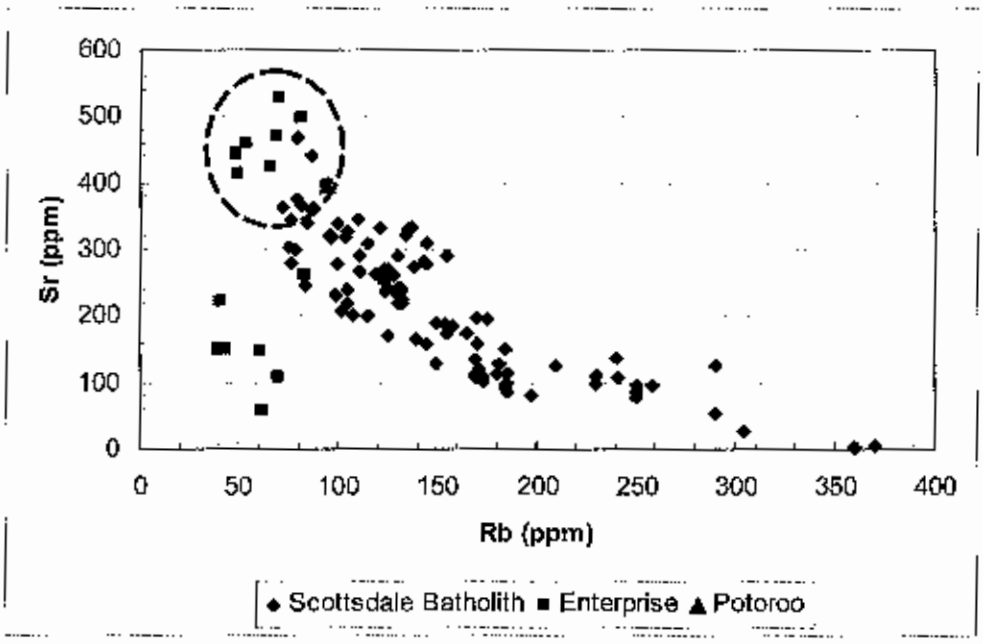

Figure 4.9 Sr versus Rb for the Scottsdale Batholith including the Enterprise and Potoroo prospects. Unaltered samples delineated by the circle.

Incompatible element ratios (e.g. Rb/Sr) can be used as monitors to trace evolution of the magma, while Fe_2O_3/FeO is a measure of relative oxidation state. Figure 4.9 summarises the distribution of rocks from the Scottsdale Batholith relative to analyses from elsewhere in eastern Australia (Blevin et al., 1996). Samples from the Enterprise Prospect appear to be slightly more reduced than the rest of the Scottsdale Batholith (as previously noted) and least fractionated in comparison to the rest of the batholith (Figure 4.10). The Potoroo prospect appears to be distinct from the Enterprise, it is more oxidised and fractionated, and plots closest to the ore-element associations defined by Blevin (1996). Only three samples from the Enterprise prospect were used in these analyses, more analyses would constrain the relationship between the Enterprise and Potoroo prospect granodiorites and the ore-element associations for eastern Australia. However, even with a small number of analyses they plot in a restricted area, therefore the values appear to be consistent.

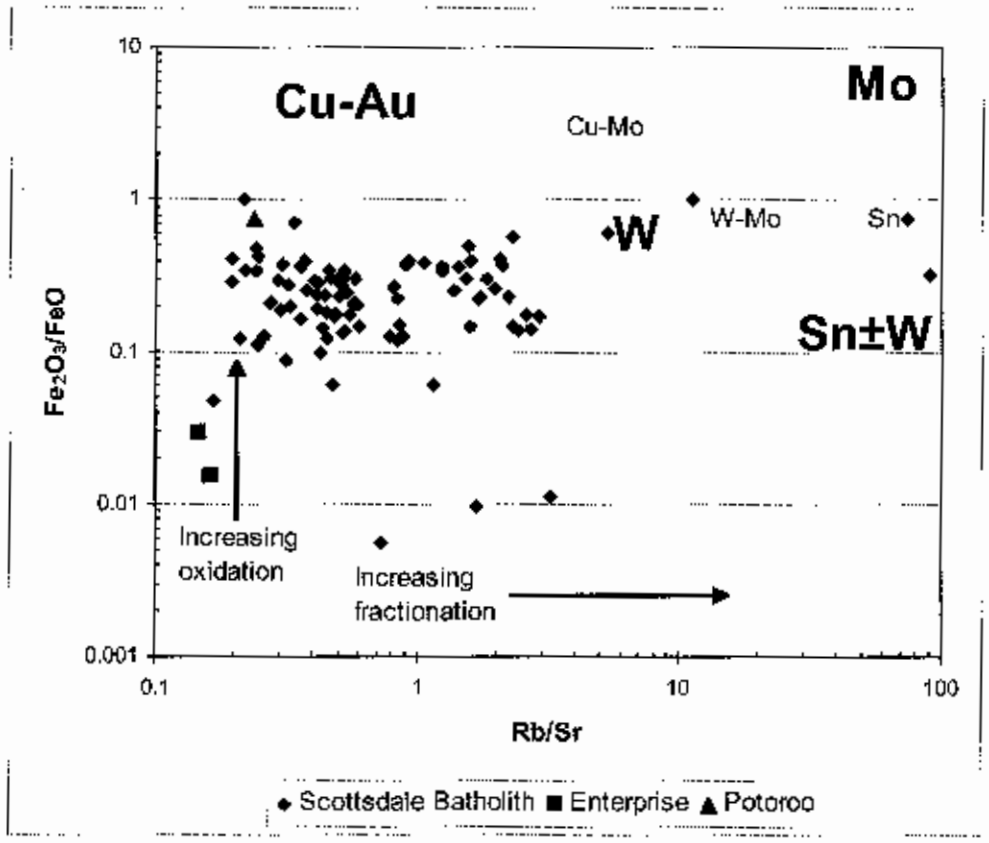

Figure 4.10 Fe_2O_3/FeO versus Rb/Sr for the Scottsdale Batholith including the Enterprise and Potoroo prospects. Plot shows the dominant ore element associations, based on granite analyses from eastern Australia (Blevin et al., 1996).

Geochemical data from the Scottsdale Batholith were plotted on graphs of $\log Fe_2O_3/FeO$ versus total FeO* (Figure 4.6) and Fe_2O_3/FeO versus Rb (Figure 4.11). Total FeO and Rb provide an indication of degree of fractionation while Fe_2O_3/FeO is a measure of oxidation. The gold bearing granitoid field is shown, determined from the Lachlan Fold Belt data of Blevin and Chappell (1992). Least altered samples from the Enterprise prospect plot outside the field, whereas the Potoroo prospect plots within the field (e.g. Figure 4.11). The Potoroo has an oxidation state comparable to the Timbarra deposit and thus, plots along side its host granodiorite (Figure 4.6). The samples from the rest of the Scottsdale Batholith are typically less oxidised than Potoroo and more oxidised than the Enterprise, but span a wide range of fractionation degrees. On the basis of the few analyses for ferrous iron, it appears the Potoroo prospect shows the best correlation with widely recognised gold bearing granitoids from the Lachlan Fold belt as defined by Blevin & Chappell (1996). Notably the Enterprise samples are far more reduced than the regional Scottsdale Batholith, supporting their status as reflecting a separate pluton. In contrast, this could also potentially be a factor of local wall-rock reduction effects, or reduction through high temperature alteration

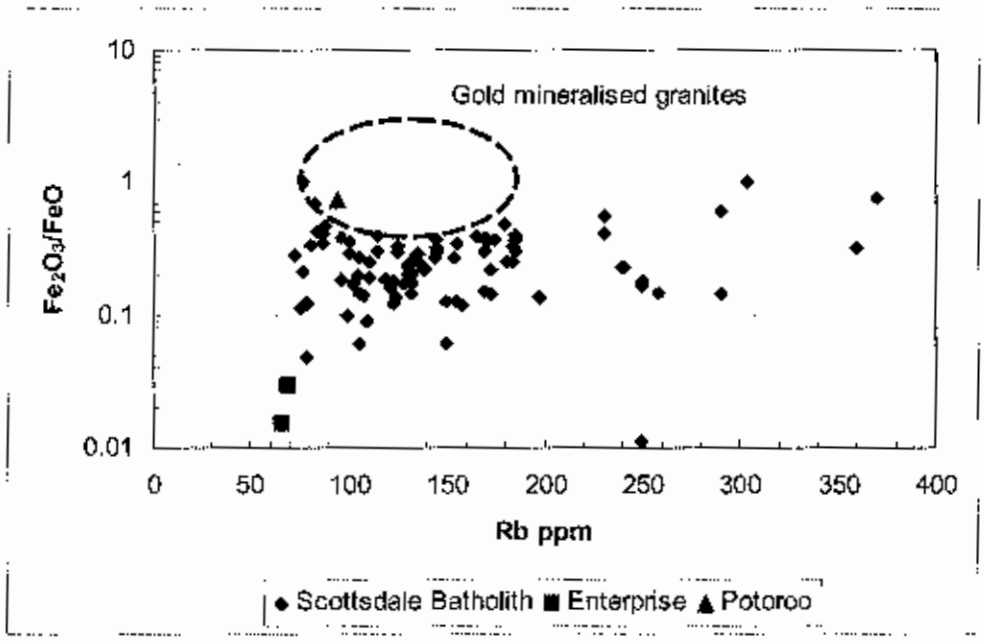

Figure 4.11 Fe_2O_3/FeO versus Rb for the Scottsdale Batholith including the Enterprise and Potoroo prospects. The sample from the Potoroo prospect plot within the field for gold bearing granitoids from the Lachlan Fold Belt (Blevin and Chappell, 1992). The Enterprise plots away from the field, and is distinct from the Scottsdale Batholith.

4.7 Trace elements

Specific elements cited in the literature as significant in intrusive-related gold systems are discussed here, e.g. As, Bi, Te, W, Mo, Sn and Pb. Trace element data from the Enterprise prospect (Table 4.1) has been plotted against the average abundance for granodiorite (Figure 4.12; Levinson, 1974) to assess any major divergence from average concentrations. In general many of the metals here show a 'spiky' enrichment that would not be consistent with typical intrusive rocks. Samples were selected to illustrate the variations in trace element concentrations (Figure 4.12), and included:

- ED2.4 = Unaltered feldspar-hornblende-biotite granodiorite
- E5.4 = Altered quartz-feldspar granodiorite
- E5.13 = Unaltered feldspar-biotite-quartz granodiorite
- ED6.14 = Unaltered feldspar-hornblende-biotite granodiorite

Average global granodiorite Mo is 1ppm (Levinson, 1974). Molybdenum at the Enterprise prospect has an erratic distribution across the samples (Table 4.1). A high concentration (71ppm) occurs in a porphyritic 'vein' dyke, interpreted to be a late feature that has components of the host granodiorite included within it. This may imply that the molybdenum in this 'vein' dyke was sourced from the intrusion and concentrated in the dyke. Other high concentrations (23-95ppm) occur in all the intrusive units in samples interpreted to have been altered to some extent. In contrast, unaltered samples (on the basis of SiO_2) had concentrations less than 5ppm. Therefore, an alteration process seems to be responsible for concentrating molybdenum. The erratic distribution in the granodiorites may be attributed to a primary magmatic effect and or later alteration.

Background global granodiorite As is 2ppm (Levinson, 1974). Most samples have arsenic concentrations below the detection limit (<3ppm). A single altered granodiorite (QF) sample has an arsenic value of 80ppm, as did the Potoroo granodiorite (5ppm).

Rb shows irregular concentrations across the samples, however, all are less than the average abundance for global granodiorite (120ppm; Levinson, 1974). Alteration e.g. addition of quartz and dilution of trace elements may account for these values.

Sample ED6.14 (Table 4.1) was interpreted to be unaltered very mafic parent material (personal communication Berry and Crawford, 2004). This sample also corresponds with the highest concentrations of copper and zinc observed in the analyses. This may be interpreted to imply that the parental magma has elevated concentrations of copper and zinc. Comparably high concentration of copper and tungsten were observed in sample E5.13, an unaltered feldspar-biotite-quartz granodiorite. This may also suggests that the intrusions were a source of at least some of the metals found at the Enterprise and Potoroo prospects.

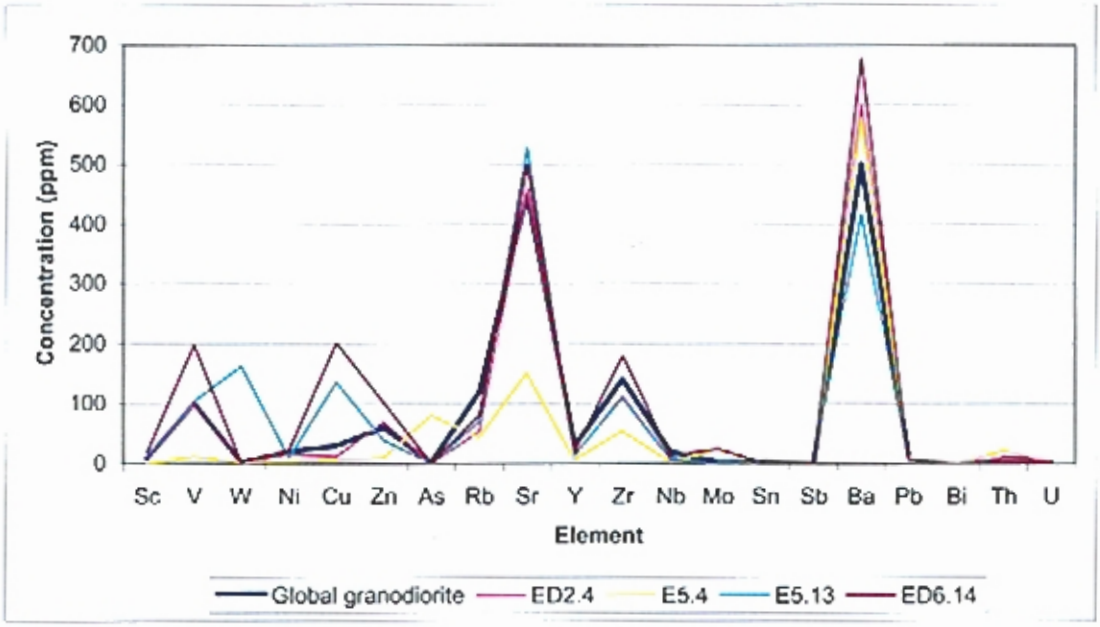

Figure 4.12 Selected trace element abundances for four samples from the Enterprise prospect plotted against the average abundance for global granodiorite (Levinson, 1974). Trace elements in order of atomic number from left to right.

4.8 Summary

The significant finding of this chapter is that the Enterprise and Potoroo prospects appear to be chemically distinct from the rest of the Scottsdale Batholith. Samples appear to be chemical end members when major and trace elements (Figures 4.8, 4.9) were plotted alongside analyses from the rest of the Scottsdale Batholith. Samples from the Enterprise prospect are distinctively more reduced and appear to be less fractionated than the rest of the Scottsdale Batholith with the lowest SiO2 and Sr contents of the whole Batholith (unaltered samples only), (Figure 4.10).

The parameters discussed: classification, oxidation state, and degree of fractionation; have been successfully used to study metallogeny of granitic rocks (Blevin, 2004). Each parameter is important when assessing a granitoids potential for mineralisation. Analyses from the Enterprise and Potoroo prospects were plotted against known gold bearing granitoids from eastern Australia. When plotted on graphs of Fe_2O_3/FeO against Rb, total FeO and Rb/Sr samples from the Enterprise prospect intrusives appear to plot outside these fields whereas the Potoroo prospect plots within. The reduced signature of the Enterprise prospect observed from the Fe_2O_3/FeO ratio and mineralogy (foxy-red biotite (phlogopite) and pyrrhotite) of the intrusions, indicate that a reduced state existed or was imposed during formation.

Trace element and some major element variations across the samples chosen appear to be the result of alteration effects. These effects were not recognised in the mineralogical analysis, and suggest that small-scale subtle silicification occurred at some point in the intrusion history, particularly affecting the host intrusions. The addition of quartz correlates with dilution in some elements (e.g. Rb and Sr), this suggests that these traces were immobile during quartz addition, though they are not 'classic' high field strength elements. Zr, however, showed the same features (Figure 4.1). In contrast, samples interpreted to be unaltered also appear to have Mo, Zn, Cu values much greater than the rest of the samples and for the average granodiorite abundance. If the Enterprise and Potoroo granodiorites boast low degrees of fractionation as previously suggested, variations in minor element abundances may be strongly controlled by alteration effects. Overall, the chemistry of these rocks is very distinctive, and this should be a very useful criterion for recognition of Au-associated intrusive in the area.

5 Fluid Characteristics and Pressure Determination

5.1 Introduction

Fluid inclusion analyses can provide useful information regarding fluid composition, temperature, pressure and the volatile evolution in hydrothermal systems. They can also assist discrimination of deposit types. At the Enterprise and Potoroo prospects, probable deposit models are reasonably confined to classic lode gold (metamorphic fluid) versus intrusive-related gold models. In addition to exploring the evolution of the local fluids a secondary aim is to use the fluid properties to help assign the mineralisation to one or other of the above models.

The evolution of fluid composition in intrusion-related gold deposits is influenced in part by depth, pressure, temperature conditions, and the effects that the behaviour of CO_2 will have on other volatiles in the melt (Baker, 2002). Intrusions that are emplaced in deeper environments appear to exsolve abundant CO_2, whereas shallower systems typically exsolve saline H_2O-rich fluids more readily. The fluids associated with intrusive-related deposits are interpreted to have a magmatic origin, although contamination from meteoric sources has also been suggested (e.g., Donlin Creek, SW Alaska; Goldfarb et al., 2004). Evidence for the passage of such fluids can locally be found in fluid inclusions trapped in veins and magmatic-hydrothermal transition textures.

In contrast, most mesothermal vein-hosted gold deposits are believed to have formed from fluids with temperatures between 200 and 400°C, low salinities (less than for seawater), and commonly unusually high carbon dioxide content, largely metamorphic in origin (Robert et al., 1995). Phase analysis has revealed the presence of coexisting immiscible carbonic and aqueous phases in mesothermal deposits. CO_2 is a common component of these fluids, and in carbon bearing lithologies the existence of carbonic phases such as methane and carbon dioxide is often interpreted as evidence for fluid interaction with carbonaceous wall rock. In addition, fluids derived from metamorphic sources are believed to contain carbon dioxide generated during prograde metamorphism.

This chapter will focus on fluid inclusions in samples taken at the Enterprise prospect by studying the characteristics of fluid inclusions from three important stages in the intrusive history: magmatic, magmatic-hydrothermal transition and hydrothermal. Petrographic observations, combined with a detailed microthermometric study of fluid inclusions found in quartz, is important to identifying any discrete fluid inclusion populations (and therefore magmatic-hydrothermal batches). Furthermore, observations of the fluid inclusions, make it possible to characterise the pressure and temperature conditions of the associated ore fluids. Finally the fluid features are compared to those of the deposit models discussed above.

5.2 Previous studies

In order to better understand the fluids present at the Enterprise prospect previous studies in the area were considered. Previous fluid inclusion studies on intrusion-related gold mineralisation are sparse. Mesothermal lode gold style deposits are the most common gold deposit type in northeast Tasmania and therefore most studied. A preliminary fluid inclusion study was carried out by Taheri and Bottrill (1994) on samples from 22 different gold prospects in northeast Tasmania. Two types of fluid inclusions were recognised: CO_2-bearing fluid inclusions (with variable amounts of CO_2 vapour ± H_2O component) and two phase (liquid + vapour) H_2O fluid inclusions. Total homogenisation (T_h) for CO_2-rich fluid inclusions ranged between 16.5° and 28.0°C, with H_2O-bearing CO_2-rich fluid inclusions having T_h between 245° to 355°C, with a significant population between 280° and 320°C. T_h for the H_2O-rich inclusions ranged between172° and 269°C. Based on CO_2 contents an estimated pressure of between 400 and 550 bars was determined. This fluid inclusion study identified a H_2O-CO_2-rich fluid, inferred to be metamorphic in origin, that boiled, causing gold precipitation. In addition, other mechanisms such as wall-rock interactions may have contributed, to further gold deposition.

The Tasmania Reef at Beaconsfield is the largest lode gold deposit in Tasmania and one of the more studied examples. The Tasmania Reef at Beaconsfield hosts two types of fluid inclusions (Jones, 2001): H_2O-rich, and CO_2-rich. CO_2-rich fluid inclusions are nearly pure CO_2, and have no detectable CH_4. Early gold-bearing

quartz hosts coexisting H_2O-rich and CO_2-rich fluid inclusions that suggest phase separations to be an important mechanism for gold deposition. Later quartz and sphalerite contain only H_2O-rich fluid inclusions. The fluid inclusion data indicate initial fluids with temperatures up to 274°C and low salinities mixed with later more saline fluids (11 to 21 eq. wt % NaCl), with temperatures up to 466°C. The high salinities identified at this site caused Jones to speculate that a magmatic fluid may have at least partially contributed to the deposit.

5.3 Methods

5.3.1 Fluid inclusions

A total of 130 quartz-hosted fluid inclusions from 7 approximately 150-μm-thick double polished sections were analysed during this study (sample numbers E5.0, E5.9, ED2.1, ED2.5 and ED6). These samples were selected to provide the most complete history, from magmatic, transitional, to hydrothermal dominated states, within the granodiorite at the Enterprise prospect. Of these, 5 samples were used in heating and freezing experiments, including: a quartz-layered texture; Stage 1 quartz-feldspar vein (molybdenite ± pyrrhotite); and a late stage barren quartz vein, all of which were from within the granodiorite. The main gold-bearing quartz veins (± sulphides) did not preserve good fluid inclusions and therefore were not used for heating and freezing experiments. This may be due to reactivation of faults that are parallel to the main gold-bearing veins.

Fluid inclusion microthermometry was performed by the author using a LINKAM MS600 heating/freezing stage (-196 to +600°C) mounted on an Olympus BX60 microscope at the Centre for Ore Deposit Research, University of Tasmania. All heating and freezing measurements were made at x 200 magnification. Temperatures represent homogenisation temperature prior to any pressure correction unless otherwise stated. Fluid inclusion data is documented in Appendix I.

5.3.2 Hornblende Geobarometry

Hornblendes from three granodiorite samples (ED2.2, ED2.12 and ED6.14) were analysed by David Steele using a Cameca SX100 electron microprobe at the Central Science Laboratory, University of Tasmania (Appendix H). Probe data was obtained using a 10μm beam at 15Kv positioned to acquire mineral chemistry from the core and rims of hornblende phenocrysts. The freshest primary magmatic hornblendes in equilibrium with a quartz, plagioclase, K-feldspar, biotite assemblage at the time of crystallisation were selected for analyses. Due to the nature of the rocks and their associated potassic alteration assemblage many of the hornblendes had weak biotite and chlorite alteration selvages along margins and in fractures. Best attempts were made to discard such hornblendes but due to the limited sample size, some analyses were conducted on altered hornblendes. Ron Berry and Russell Fulton helped to source relevant information from the literature for this technique.

5.3.3 Sulphur Isotopes

Gold bearing quartz veins from the Enterprise Prospect contain variable amounts of arsenopyrite, pyrrhotite and pyrite. Samples of each sulphide were selected for isotope analysis to represent a origin of sulphide and potentially the associated gold. Other samples included: molybdenite from quartz-feldspar veins and a pyrrhotite aggregate within the granodiorite. A total of 12 sulphides were extracted by hand drilling and analysed by Keith Harris and Christine Cook at the Central Science Laboratory, University of Tasmania. A combustion with cuprous oxides technique was used, and sample were quantitatively measured by a VG Sira 10 mass spectrometer.

5.4 Fluid inclusion classification

Fluid inclusions were classified as primary, pseudo-primary or secondary according to the Roedder (1984) definition. Primary inclusions form during the crystal growth of precipitated minerals from a fluid: the crystals show imperfections on their surfaces, which can be filled with surrounding fluid and sealed off during crystal growth. The trapping of fluids along growth discontinuities due to processes that disturb the crystal growth is the most common process in the formation of primary inclusions. The geometry of the entrapped inclusions varies depending on the style of entrapment. In contrast, secondary inclusions are trapped after crystal growth. Deformation in brittle and ductile environments causes very small cracks in crystals, which are then likely to fill with fluid present during or after deformation. Fluids are then trapped when the fracture heals. Pseudosecondary inclusions form along micro fractures during crystal growth. They form by the same mechanism as the secondary inclusions, but have the same significance as primary inclusions. They are commonly recognized by their occurrences on planes that are over grown by later hydrothermal phases.

Three main types and six subtypes of fluid inclusions were recognised based on phase relationships at room temperature (~20°C) and the above classification. The three main types of inclusions (Figure 5.1) consist of CO_2-bearing inclusions (*Type 1*), H_2O-rich inclusions (*Type 2*), and halite bearing H_2O-rich inclusions (*Type 3*). Photomicrographs of the fluid inclusion types are located in Plates 5.1 and 5.2.

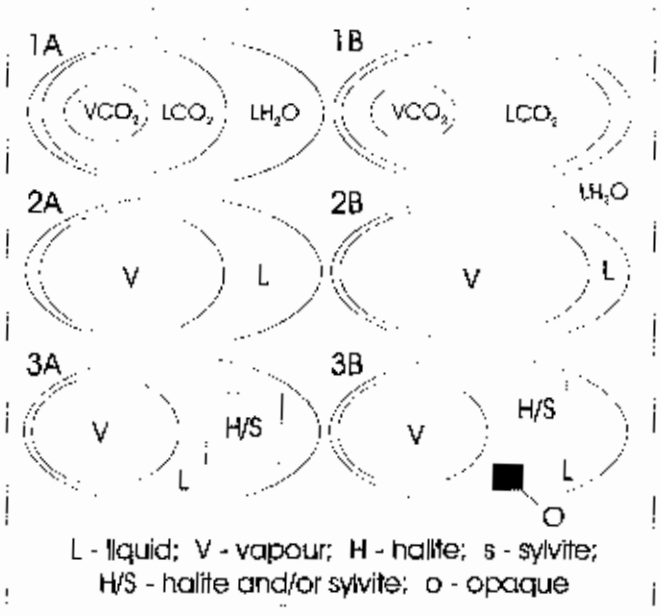

Figure 5.1 Schematic sketches of fluid inclusion types observed from the Enterprise prospect.

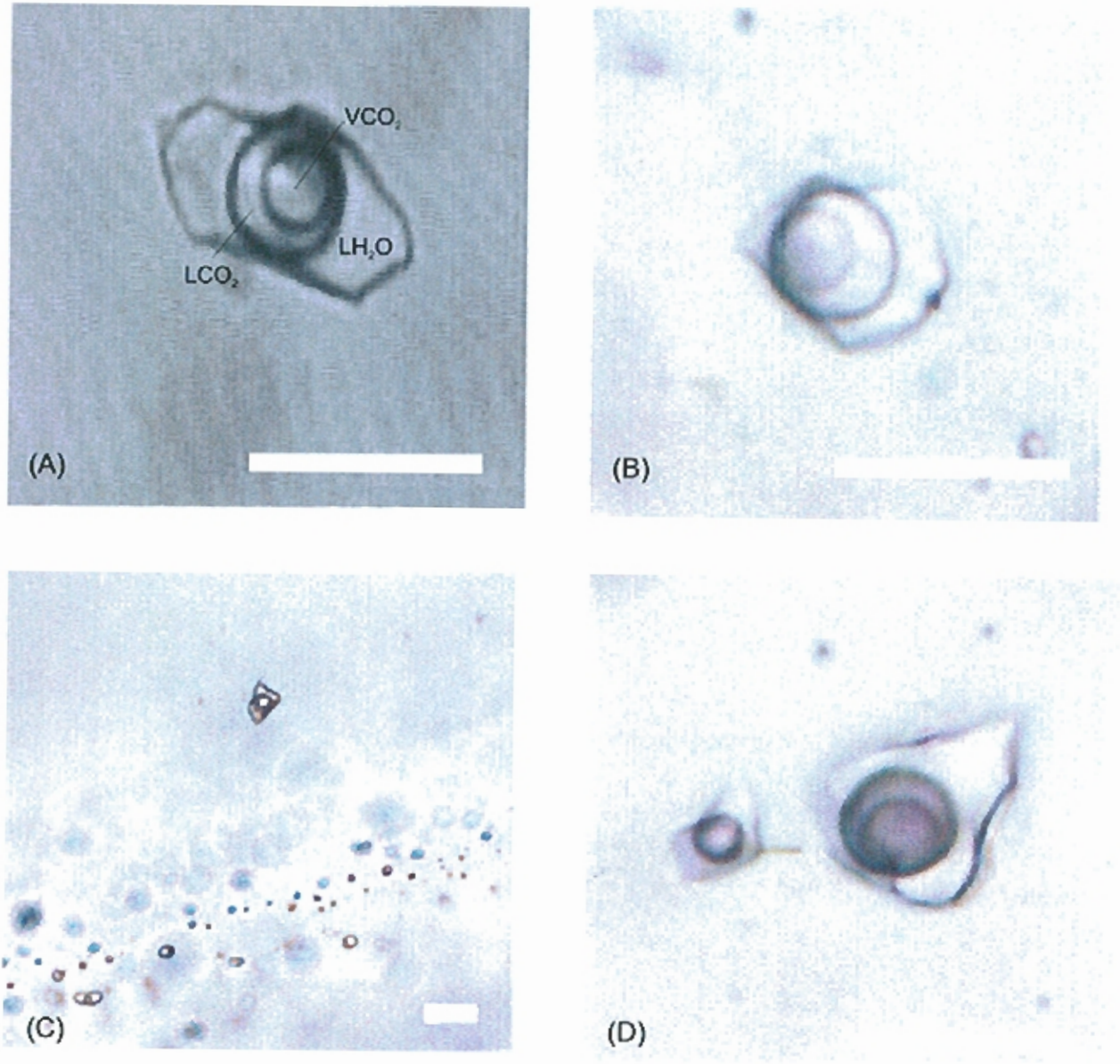

Plate 5.1 Type 1 fluid inclusions from a quartz-layered texture. (A) Type 1A 2-phase fluid inclusion with ~50% V+L CO_2 component. (B) Type 1B fluid inclusions with >50% V+L CO_2 component. (C) Isolated *Type 1* inclusion adjacent to a secondary inclusion trail. (D) Two *Type 1* fluid inclusions, showing the variation in size, from ~10μm to <5 μm. Scale bars are 10 μm.

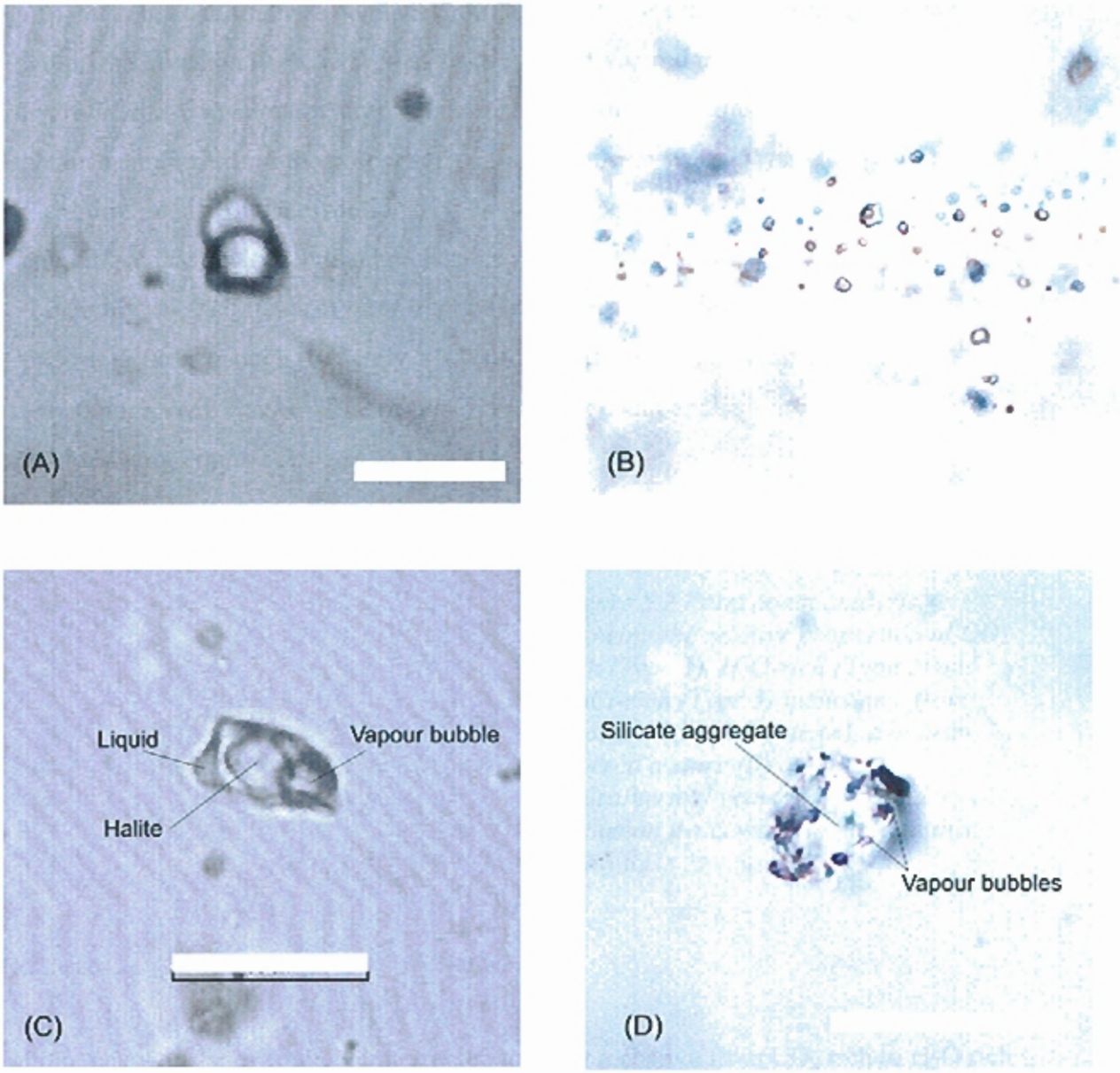

Plate 5.2 (A)*Type 2* V+L fluid inclusion from an isolated population in a quartz-layered texture. (B) A secondary fluid inclusion trail of *Type 2* inclusions. (C) A *Type 3* fluid inclusion with a distinctive halite salt phase. (D) A composite melt inclusion from a quartz-layered texture. Its vapour and silicate melt component are indicated. Scale bars are 10 μm.

A point count analysis was conducted on fluid inclusions in samples of quartz from within the intrusion itself, as well as from a quartz-layered texture (magmatic-hydrothermal transition texture) and various hydrothermal veins. The aim was to obtain a simple idea of the proportion of fluid inclusion types (*Types 1, 2 and 3*) at these three stages in the evolution of the intrusion complex. The method involved counting at least 200 individual inclusions from each of the 3 sample types. Randomly selected fields of view under 40x magnification were used and only fluid inclusions large enough (typically > ~3-4μm) to identify phase relations at room temperature were chosen. The results of the point count analysis are represented in the following Figure 5.2.

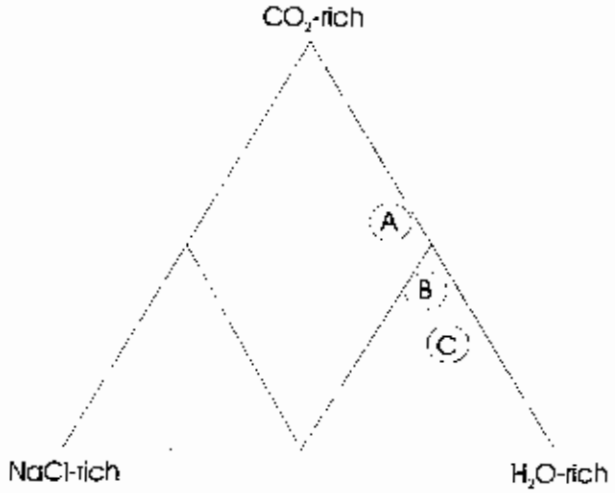

Figure 5.2 Point count analysis. Showing the relative proportion of CO_2 rich (Type 1), H_2O-rich (Type 2) and NaCl-rich (Type 3) inclusions, from quartz in granodiorite (A), a quartz-layered texture (B) and in hydrothermal veins (C). Secondary inclusion trails were not used in this analysis.

Point count analyses could be interpreted to show a change from CO_2 rich to H_2O rich types as the complex evolved from a magmatic to hydrothermal state. However, the data shows no definite trend, rather it illustrated the ratio of inclusion types at each of the three important stages in the evolution of an intrusion.

5.4.1 Type 1: Vapour CO_2 + Liquid CO_2 + Liquid H_2O inclusions

Type 1 inclusions are interpreted to be primary, occurring as isolated inclusions or grouped in three-dimensional arrays. To a lesser extent these inclusions have been observed in small trails occurring along possible healed fractures and or growth zones and these were therefore interpreted to be pseudosecondary. *Type 1* inclusions typically range from 4 to 10μm in size (Plate 5.1 D) At ambient temperatures, inclusions containing both CO_2 and H_2O commonly contain three phases: liquid and gaseous CO_2 and liquid H_2O (Roedder, 1984). *Type 1* inclusions are three phase inclusions at room temperature (~20°C). *Type 1* inclusions are further divided into two subtypes: *Type 1A* that contain a smaller CO_2 bubble (vapour and/or liquid) than aqueous fluid (~>50% of the inclusion volume by visual estimate); *Type 1B* contained a larger CO_2 bubble than the aqueous liquid (~<50% of the inclusion volume by visual estimate).

Type 1 inclusions are characterised by variable CO_2 contents, which reflects the range in homogenisation of the CO_2 vapour phase (T_{hCO2}) (Figure 5.3). Homogenisation of the CO_2 vapour phase has a distinct bimodal distribution, interpreted to define the two subgroups of *Type 1 (1A and 1B)*. It could also be argued that this bimodal distribution for T_{hCO2} appears to correlate with the bimodal distribution for total homogenisation temperatures (T_h) in Figure 5.4. T_{hCO2} ranges between 14° and 29°C with a mean of 22.5°C and a significant peak at 27°C. Homogenisation was by critical behaviour (fading of the meniscus) rather than to the liquid phase (bubble point) or vapour phase (dew point).

The range of T_h was from 290° to 450°C with a mean of 362°C and a significant peak at 380°C. All measured samples homogenised to the liquid phase. T_h for *Type 1* inclusions in Figure 5.4 exhibits a slightly skewed to symmetrical distribution.

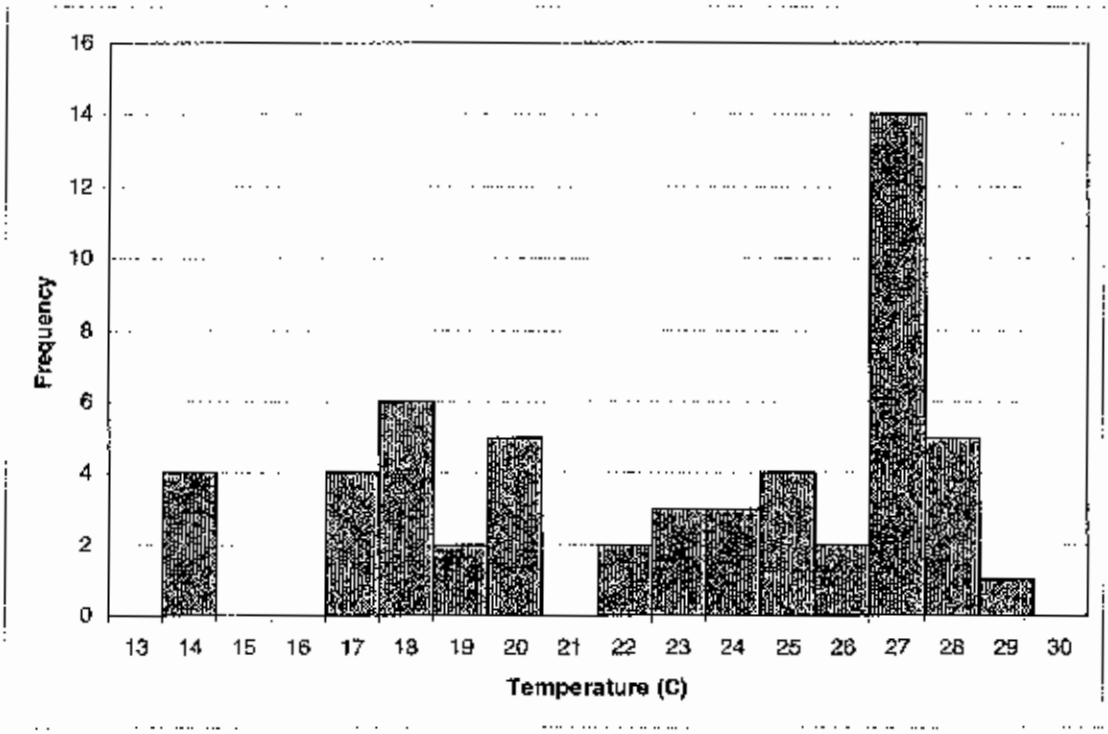

Figure 5.3 Microthermometric data for homogenisation of the carbonic phase of type 1 inclusions within quartz from a quartz-layered texture and quartz-feldspar vein. Population size is 55 measurements.

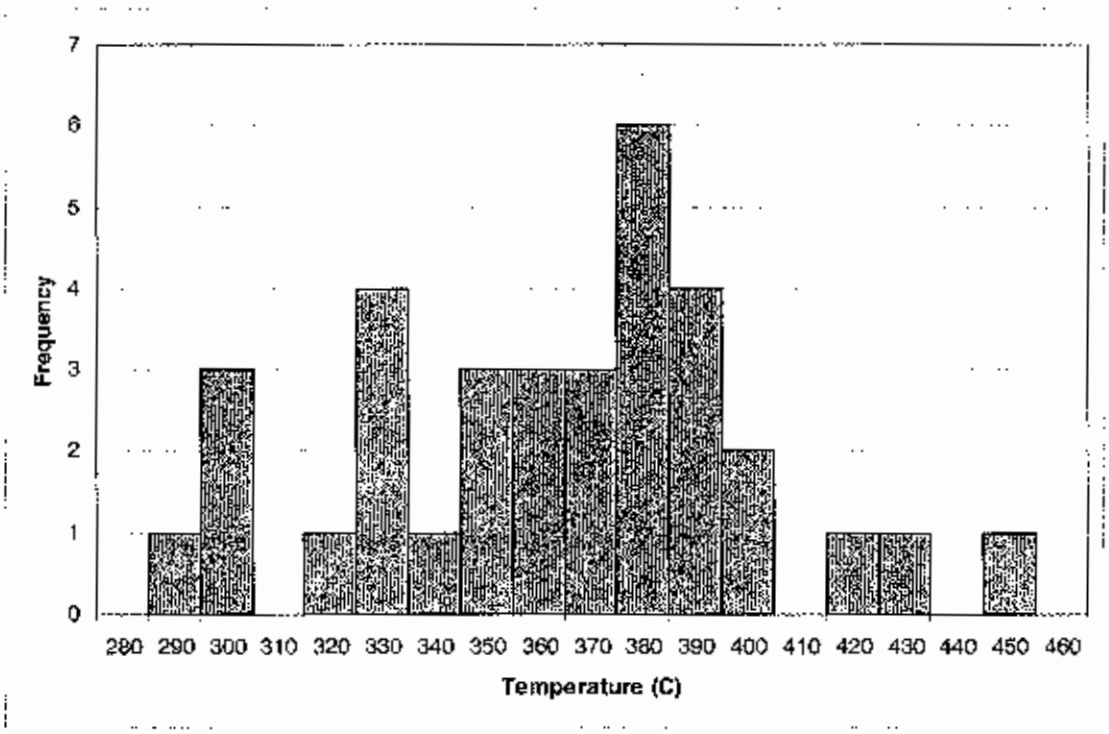

Figure 5.4 Microthermometric data for total homogenisation of type 1 inclusions within quartz from a quartz-layered texture and quartz-feldspar vein. Population size is 34 measurements.

5.4.2 Type 2: Vapour + liquid inclusions

Type 2 fluid inclusions are the predominant inclusion type in the majority of samples. *Type 2* commonly occur in trails and are interpreted to be secondary inclusions. To a lesser extent *Type 2* inclusions vary widely in size, with inclusions ~5µm most common. Microthermometric analyses divided *Type 2* inclusions into those existing in isolated groups in three-dimensional arrays (primary) and those in secondary trails. *Type 2* inclusions occur as isolated groups in three-dimensional arrays and at times coexisting with *Type 1*, therefore interpreted to be primary in origin. *Type 2* inclusions frequently occur along healed fractures that have been observed to traverse across grain boundaries, which make it uncertain if these inclusions are secondary or pseudosecondary. *Type 2* are two phase liquid and vapour (L+V) and can also be subdivided into two types: 2A containing a smaller vapour bubble than aqueous liquid (over 50 percent of inclusion volume by visual estimation); type 2B which contain a larger vapour bubble than the aqueous liquid (up to 50 percent of inclusion volume by visual estimation). Unidentified daughter crystals have been observed in *Type 2* inclusions, characterised by their yellow colour and small short 'stubby' morphology. A second unidentifiable solid phase was observed and interpreted to be biotite or rutile due to its opaque colour and elongate bladed habit.

Type 2 inclusions in isolated groups homogenised over temperatures between 290° and 420°C, with a mean of 368°C and a significant peak at 400°C (Figure 5.5). *Type 2* inclusions in isolated groups could be interpreted to show a skewed distribution with a significant population between 380° and 400°C. These results correlate well with those of *Type 1* inclusions, confirming that *Type 2* inclusions are largely primary.

Type 2 inclusions in trails homogenised over a wider range of temperatures between 160° to 370°C with a mean of 273°C and a significant peak at 300°C (Figure 5.6). Lower homogenisation temperatures compared with *Type 2A* unequivocally distinguishes the two types and supports their subdivision. Homogenisation temperatures for *Type 2* inclusions in trails display at least 3 prominent populations: 160° to 180°C, 270° to 310°C and 330° to 350°C. Multiple populations are interpreted to represent multiple generations evident from crosscutting relations in section.

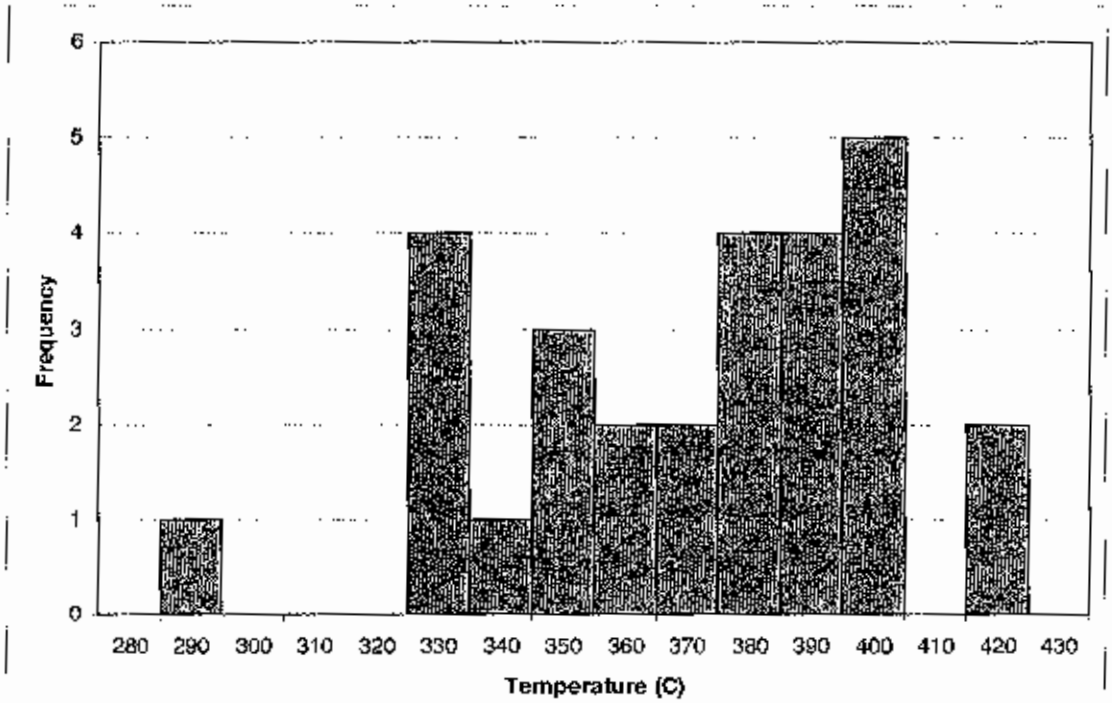

Figure 5.5 Microthermometric data for total homogenisation of type 2 fluid inclusions occurring in isolated groups within quartz from a quartz-layered texture and quartz-feldspar vein. Population size is 28 measurements.

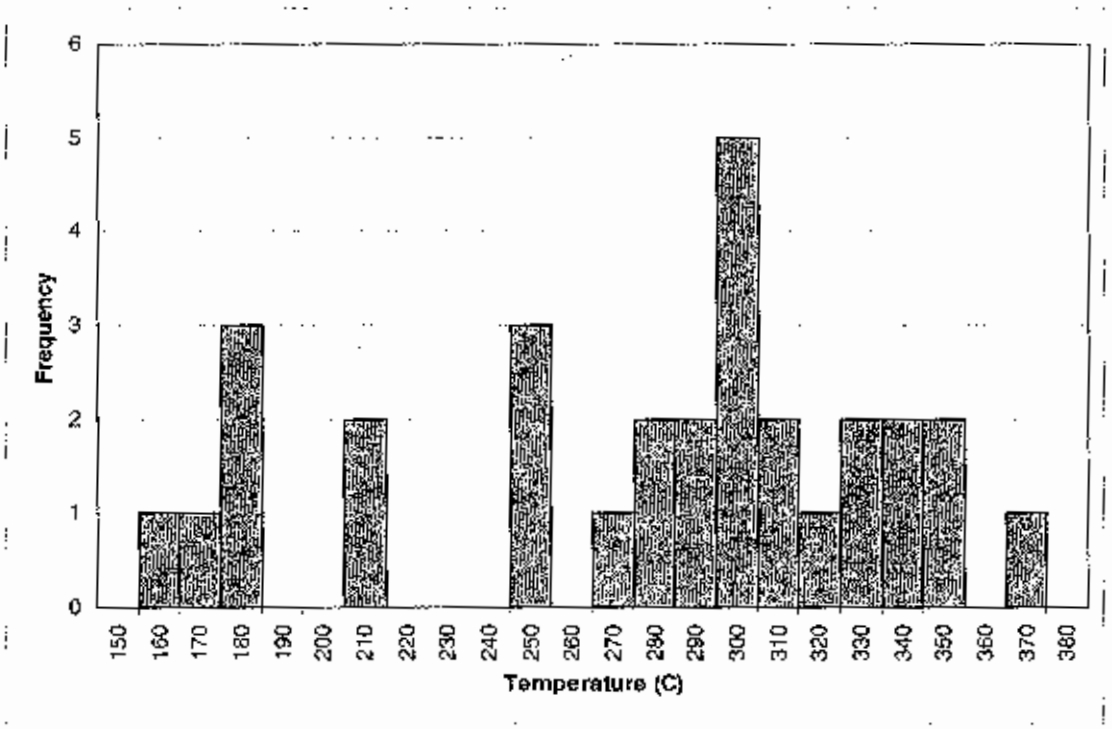

Figure 5.6 Microthermometric data for total homogenisation of type 2 fluid inclusions occurring in trails within quartz from a quartz-layered texture and quartz-feldspar vein. Population size is 30 measurements.

5.4.3 Type 3: Vapour + liquid + salt (± opaque) inclusions

Type 3 fluid inclusions are the least abundant type and are exceedingly rare in all samples. *Type 3* can also be subdivided into two types: *Type 3A* are typical three phase inclusions consisting of a liquid, vapour bubble and salt crystal (L + V + S), 3B is a four phase inclusion similar to *Type 3A*, but contains an additional opaque daughter crystal (L + V +S + opaque). *Type 3A* is more abundant than *Type 3B*; *Type 3B* is very rare and subsequently poorly represented and documented in the samples, only a single inclusion was found with this composition. Halite is the predominant salt phase and was identified by its cubic habit. However, some of the identified salts did not display a cubic habit, they possessed an elongate shape with a yellowish colour and were interpreted to be sylvite. *Type 3* inclusions were typically between 5 and 10μm in size.

Heating of *Type 3* inclusions yielded poor results. In initial experiments, the inclusions decrepitated before any vapour or salt phase homogenised. Temperatures of decrepitation ranged between 220° and 300°C. Initial interpretations were that these inclusions had a high internal pressure. Therefore, thicker sections (approximately 200μm) were prepared. Subsequent experiments were performed at a slower rate (5° to 10°C per minute). Experiments were conducted on a single salt bearing fluid inclusion (Figure 5.7). This inclusion yielded a similar result to previous attempts, although decrepitation temperature was higher, at 420°C. Temperatures of first salt dissolution were observed: S1 80°C, S2 150°C and S3 340°C. S1, with its cubic habit, was interpreted to be halite. S2 was interpreted to be sylvite due to its elongate habit; it was the only solid phase noted to disappear at 353°C. It was concluded that on the basis of decrepitation before salt disappearance combined, with a boiling-like assemblage (i.e. coexisting with *Type 2* inclusions), that these were leaked inclusions.

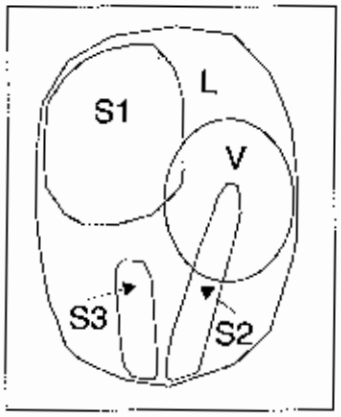

Figure 5.7 Sketch of a Type 3 fluid inclusion from a quartz-layered texture. Sketch illustrates the presence of 3 salt phases: S1, S2, S3, a vapour phase (V) and a liquid phase (L). The inclusion is approximately 10μm wide observed at room temperature (~20 °C).

5.5 Salinity and Density

PvTx (by LINKAM) software modelling for fluid inclusions (Version 2.1) was used to generate density and salinity (wt % NaCl equiv) estimations for each of the fluid inclusion types. The software automatically calculates salinity and density using a number of variables including: type, origin, shape, size, fill, temperature of eutectic, temperature of last ice melt (Tm_{ice}), homogenisation of the aqueous phase or Th_{CO2}, homogenisation phase, $Tm_{clathrate}$ and T_h. Salinity variations for *Type 1* inclusions were obtained from a sample population of 53 measurements, results ranged from 0 to 14 wt % NaCl equiv, with an average of 4.7 wt % NaCl equiv. Salinity variations for *Type 2* inclusions in isolated groups from a sample population of 17 measurements, ranged from 0.8 to 11.7 wt % NaCl equiv, and had an average of 7.2 wt % NaCl equiv. Salinity variations from *Type 2* inclusions in secondary trails from a sample population of 17 measurements ranged from 2.5 to 12.2 wt % NaCl equiv, with an average of 9.1 wt % NaCl equiv. Due to the lack of data obtained from *Type 3* inclusions the software was unable to determine a salinity and density. On the basis of halite as the predominant salt bearing phase, the salinity must exceed 26.5 wt % NaCl equiv (halite saturation solubility).

Density estimates for each fluid inclusion population were also calculated. *Type 1* inclusions produced density estimates ranging from 0.15 and 0.86 g/cm^3 with an average of 0.70 g/cm^3. *Type 2* interpreted to be primary in isolated groups produced densities between 0.30 and 1.05 g/cm^3 and an average of 0.63 g/cm^3, whereas those *Type 2* inclusions interpreted to be secondary ranged from 0.61 to 0.95 g/cm^3 and averaged 0.81 g/cm^3.

5.6 Melt Inclusions

Melt inclusions were observed in samples from within the granite, and from within a quartz-layered texture. The melt inclusions are composed of a vapour phase and a silicate aggregate/melt phase when observed at room temperature (~20°C) (Plate 5.2 D). Melt inclusions were extremely rare, and consequently did not provide a comprehensive view of the melt history.

A single melt inclusion from a quartz-layered texture was used in some preliminary microthermometry experiments. Little or no response was observed when heated using a LINKHAM high temperature heating stage to ~650°C at a rate of 50°C per minute. At 650°C it was noted that vapour bubbles had possibly began to relocate and the silicate aggregates may have began melting, however this was uncertain. The same inclusion when heated in a furnace to 650°C for an extended period of time (>8hrs), unfortunately showed no change in phase relations. The lack of response to heating resulted in melt inclusion microthermometry to be abandoned, but 650° likely represents a minimum constraint on the formation temperature of this quartz.

5.7 Geobarometry

5.7.1 Introduction

Determination of the emplacement pressures and, subsequently, emplacement depths of granitic rocks, is vital in understanding the emplacement history of an intrusive complex. It is also important in interpreting conditions of ore deposition and formation of intrusion-related gold where the deposit-magma link is proven. CO_2-rich fluid inclusions occurring in magmatic textures provide an excellent means of obtaining reliable pressure and subsequent depth of emplacement estimates. A second geobarometric method was tested in this study, hornblende geobarometry. The aim was to obtain robust estimates of emplacement pressure of observed lithologies.

5.7.2 Fluid inclusion barometry

In most fluid inclusion work, the composition of the inclusions is unknown or is imprecisely known from volume measurements. *Type I* inclusions contain three phases: liquid and gaseous CO_2 and liquid H_2O. The phases are essentially pure (relative to each other), so by measuring the volumes of the three phases at a known temperature and using the density data for CO_2 and H_2O, Roedder (1984), was able to calculate the mole percent CO_2 (and thus H_2O) in the inclusion. The CO_2 solubility diagram (Figure 5.6; Roedder, 1984) provides an empirical model for estimating pressure from the mole percent/volume percent (at 25°C) of liquid-vapour CO_2 and temperature of homogenisation of inclusions containing both CO_2 and H_2O.

Type I inclusions, when primary and occurring in quartz-layered textures, are inferred to represent a fluid trapped during the final stages of crystallisation and emplacement of the host intrusion. The mole percent CO_2 content for *Type I* inclusions is estimated to range from 25 to 66 mole percent CO_2 based on visual observations coupled with the inset from Figure 5.8 of two-dimensional appearances for cylindrical inclusions. *Type I* inclusions have a T_h ranging from 290° to 450°C as previously stated. According to the CO_2 solubility diagram, combined with the above parameters, an approximate pressure of formation from 400 to 1000 bars is suggested.

1000 bars of hydrostatic pressure equates to a depth of approximately 4 km for a granitic rock, as 1 km of granitic rock exerts a lithostatic pressure of 264 bars (Figure 5.9). 400 bars of hydrostatic pressure also equates to an approximate depth of 4 km, as 1km of water exerts a hydrostatic pressure of 98 bars per kilometre of depth. Therefore if the intrusion was emplaced at 1000 bars it would reflect of depth of ~ 3.79 km.

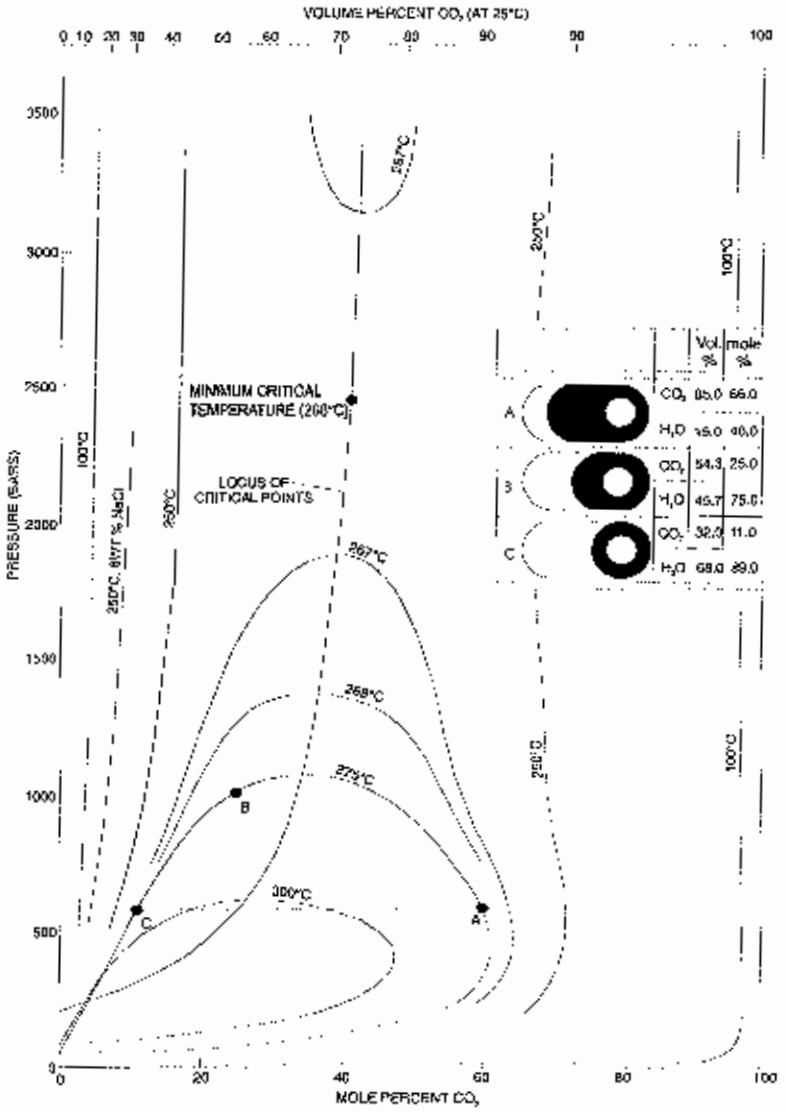

Figure 5.8 P-X plot of isotherms showing compositions of coexisting phases in the system H2O-CO2, using data of Todheide and Franck (1963) and Greenwood and Barnes (1966). The upper abscissa of CO2 liquid, CO2 vapour, and H2O liquid of 0.71, 0.24 and 1.0 g/cm3, respectively (Newitt et al. (1956); Keenan et al. (1969)). The inset shows the two-dimensional appearance at the stated conditions for three cylindrical inclusions having compositions as given (liquid CO2 shaded), which are also shown on the diagram. The 250°C isotherm of a 6 wt % NaCl solution from Takenouchi and Kennedy (1965) is shown for comparison. After Roedder (1984).

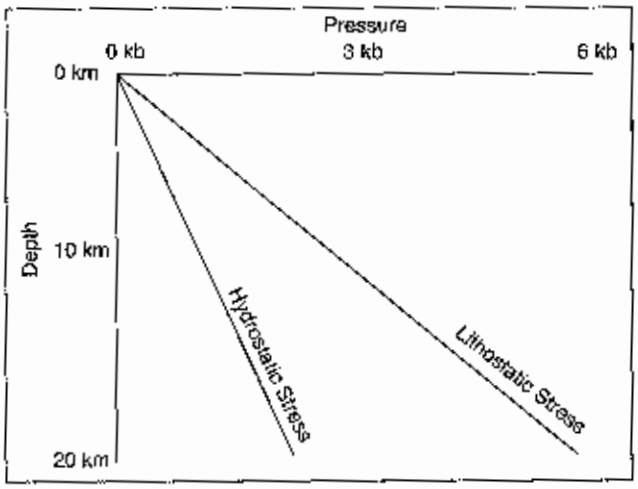

Figure 5.9 Plot of Pressure (kbar) against depth (km). Showing the positions of lithostatic and hydrostatic stress conditions.

Most CO_2-bearing fluid inclusions contain an aqueous salt solution rather than pure H_2O. When NaCl is added to the CO_2-H_2O system, the critical solubility of CO_2 at a given temperature and pressure decreases, and the miscibility gap is widened. For example, Roedder (1984) illustrated this using a 10 mole % CO_2 inclusion that had a T_h of 250°C, trapped as a homogeneous fluid. Figure 5.8 shows that it would have had a minimum pressure of trapping of 750 bars, assuming that the inclusion consists of pure CO_2 and H_2O. However, if the H_2O phase contained 6 wt % NaCl equiv, the minimum trapping pressure would have been ~2500 bars, determined by extrapolating the 250°C, 6 wt % NaCl isotherm of Takenouchi and Kennedy (1965) to higher pressure.

Type 1 fluid inclusions salinity estimations ranged from 0 to 14 eq wt % NaCl equiv, with an average of 4.7 eq wt % NaCl equiv. Pressure estimations using Figure 5.8 assume a pure CO_2 and H_2O solution. Therefore the pressures calculated using this model represent minimum constraints on pressure of emplacement. As the *Type 1* fluid inclusions have been shown to have a NaCl component, true values must have been greater than those estimated.

5.7.3 Hornblende geobarometry

Fluid inclusion barometry based on CO_2-rich inclusions, as illustrated above, is an accurate method of obtaining minimum emplacement pressure estimates. Another method that has been widely used as a barometer since the early 1980's is hornblende geobarometry. The hornblende barometer correlates the aluminium content of magmatic hornblende linearly with the crystallising pressure of an intrusion. By adopting this method, it was aimed to compare the results with the more 'reliable' fluid inclusion pressure estimations and other hornblende based data sets from northeast Tasmanian granitoids (Goscombe et al., 1994; Patison, 1999; Varne and Fulton, 1994). The use of two methods for obtaining a pressure estimate will better constrain a set of results and test the validity of aluminium in hornblende as an effective geobarometer.

The application of aluminium-in-hornblende to barometry has been the subject of debate since Hammarstrom and Zen (1986) showed that the aluminium content of hornblende coexisting with quartz, plagioclase, K-feldspar, biotite, titanite, Fe-Ti oxides, supercritical fluid, and melt could be used to calculate the pressure at which the assemblage equilibrated.

To calculate pressures from the aluminium content, four best-fit equations were used, as documented in the literature. They represent best-fit equations for real world and experimentally derived data for the relationship between aluminium content in hornblende and pressure. The equations are as follows:

1. P (± 3 kbar) = $-3.92 + 5.03Al^{tot}$, $r^2 = 0.80$: Hammarstrom and Zen (1986);
2. P (± 1 kbar) = $-4.76 + 5.64Al^{tot}$, $r^2 = 0.97$: Hollister et al. (1987);
3. P (± 0.5 kbar) = $-3.46 + 4.23Altot$, r2 = 0.99: Johnson and Rutherford (1989);
4. P (± 0.6 kbar) = $-3.01 + 4.76Al^{tot}$, $r^2 = 0.99$: Schmidt (1992).

The results are summarised in Table 5.1. Each equation was used to calculate pressure (bars) for all the hornblende data points. Data for each equation and for each data point were averaged to remove any anomalous inconsistency. The most recent calibration for aluminium-in-hornblende by Schmidt (1992) also has the smallest associated error (± 600 bars). The results obtained using this calibration (Equation 4) show the closest correlation with the numbers obtained from the fluid inclusion barometry. Fluid inclusions produced pressure estimates from 400 and 1000 bars, and the aluminium-in-hornblende geobarometer between -100 and 920 bars. However, equation 4 was considered to be the most valid and yielded results averaging 920 bars, on the basis of arguments put by Schmidt (1992).

The relationship between aluminium content of magmatic hornblendes and pressure is clearly shown in the literature (Ague, 1997; Hammarstrom and Zen, 1986; Hollister et al., 1987; Johnson and Rutherford, 1989; Schmidt, 1992). However, its application to natural geologic settings remains controversial. Ague, J (1997) outlined four important questions and made attempts to address them. They include the effects of equilibration in supercritical fluid and melt; effects from temperature variations, effects from magma bulk composition, fluid composition, mineralogy and oxygen fugacity; pressure sensitive chemical reactions that control hornblende chemistry in granitic rocks. A better understanding of the impact of these variables on hornblende geobarometry would improve its application to natural geologic settings. Due to these unknown effects data obtained using this method must be treated with caution, but the similarity of results by methods at this site does correlate the validly of the technique. Moreover, it provides evidence supporting a magmatic connection between Type 1 fluid inclusions and magmatic exsolution processes, since the inclusions have similar pressures to the magmas at the time of crystallisation.

Table 5.1 Results of aluminium-in-hornblende geobarometry (kbars)

Sample #	Hole	Depth (m)	Location	Al^{tot}	Equation 1	Equation 2	Equation 3	Equation 4	Average
ED2.2	ED002	44	CORE	2.28	7.55	8.10	6.19	7.85	7.42
ED2.2	ED002	44	RIM	1.45	3.37	3.41	2.67	3.89	3.33
ED2.2	ED002	44	CORE	0.59	-0.95	-1.43	-0.96	-0.20	-0.88
ED2.2	ED002	44	RIM	0.79	0.04	-0.32	-0.13	0.74	0.08
ED2.12	ED002	97.2	CORE	0.60	-0.89	-1.36	-0.91	-0.14	-0.83
ED2.12	ED002	97.2	RIM	0.57	-1.06	-1.56	-1.06	-0.31	-1.00
ED2.12	ED002	97.2	CORE	0.65	-0.66	-1.11	-0.72	0.07	-0.60
ED2.12	ED002	97.2	CORE	0.69	-0.44	-0.86	-0.54	0.28	-0.39
ED6.14	ED006	103.7	CORE	0.94	0.80	0.54	0.51	1.46	0.83
ED6.14	ED006	103.7	CORE	0.40	-1.89	-2.49	-1.76	-1.09	-1.81
ED6.14	ED006	103.7	CORE	0.47	-1.56	-2.11	-1.47	-0.77	-1.48
ED6.14	ED006	103.7	CORE	0.49	-1.48	-2.02	-1.41	-0.70	-1.40
				Average	0.24	-0.10	0.03	0.92	0.27

5.8 Sulphur Isotopes

5.8.1 Introduction

Stable isotopes have become an important tool for studying ore deposits. They provide key data on the sources of sulphur in hydrothermal ore deposits, and can discriminate: magmatic sulphur, marine sulphate, and sedimentary sulphide sources. Sulphur in magmatic systems may be released into a fluid phase or sulphide melt via magmatic exsolution, or crystallised as magmatic sulphide or sulphates. The source of magmatic sulphur in hydrothermal ore deposits may therefore be from the original magma or by leaching of other sources. In this study, sulphur isotopes were undertaken to determine whether sedimentary sulphur may have contributed to the mineralisation, which would assist discrimination of magmatic and metamorphic models. Sedimentary sulphur in northeast Tasmania and Palaeozoic Victoria is generally in the range 10-30‰ (personal communication Davidson, 2004), but no data was collected as part of this study. In sulphide-dominated melts, little fractionation occurs between the melt, crystals, and fluid phases under reduced conditions; all typically have $\delta^{34}S$ values in the range of -2 to +2 per mil (‰) (Campbell and Larson, 1998). Under oxidising conditions, the $\delta^{34}S$ exsolved magmatic fluid may range up to +5 ‰ (Ohmoto, 1972).

5.8.2 Results

The results for $\delta^{34}S$ (Table 5.2) ranged from -0.3 to 2.4 ‰ with a mean of 1.1 ‰ (Figure 5.10). Pyrite values are slightly more positive within this group.

Table 5.2 Results of sulphur isotope analysis.

Sample ID	Drill Hole	Depth (m)	Mineral	$\delta^{34}S$ (wrt CDT) permil
S1	E005	85	molybdenite	0.17
S2	E005	85	molybdenite	0.83
S3	E005	93.8	arsenopyrite	-0.36
S4	E005	93.8	arsenopyrite	0.28
S5	E005	111.5	pyrrhotite	0.44
S6	E005	111.5	pyrrhotite	1.78
S7	E005	141.5	pyrite	2.25
S8	E005	145	pyrite	2.43
S9	E005	145	arsenopyrite	2.07
S10	E005	147	molybdenite	1.40
S11	ED006	94	pyrrhotite	0.93
S12	ED002	77.4	pyrrhotite	1.31

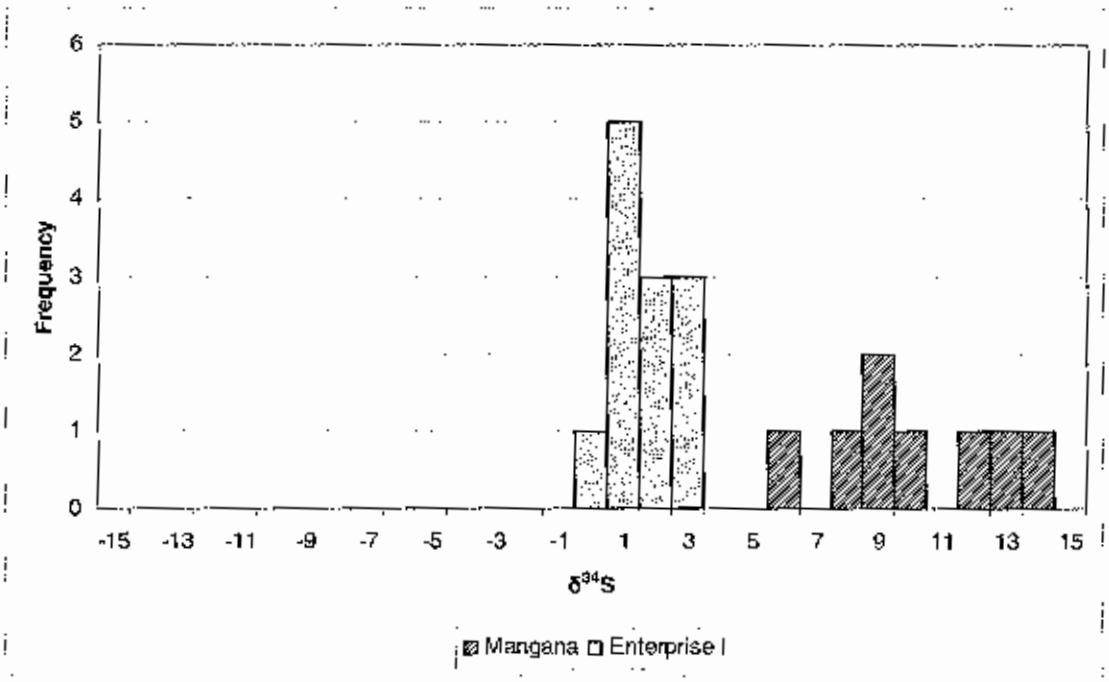

Figure 5.10 Frequency histogram of sulphur isotope values from the Enterprise prospect compared to those from Mangana (Manzi, 1995).

5.9 Discussion and Summary

5.9.1 Fluid features of northeast Tasmanian gold systems

A widespread fluid inclusion study has been conducted on lode-gold style mineralisation in northeast Tasmania (Taheri and Bottrill, 1994). Two types of fluid inclusions were recognised; CO_2-rich and H_2O-rich. Inclusions yielded T_h temperatures of less than 355°C, on average much cooler than those identified at the Enterprise prospect (up to 450°C). CO_2–rich inclusions from their study produced pressure estimations of 400-550 bars, comparably lower than those estimated at the Enterprise, of up to 1000 bars.

T_h temperatures higher than those measured by Taher and Bottrill (1994) have been observed at the Tasmania Reef, Beaconsfield. CO_2-rich fluid inclusions with T_h temperatures up to 466°C have been identified with salinities between 11 and 21 wt % NaCl equiv (Jones, 2001). *Type 1* CO_2-rich fluid inclusions from the Enterprise prospect with comparable T_h temperatures have salinities with an average of 4.7 wt % NaCl equiv, substantially lower than those from Beaconsfield.

On the basis of the fluid physiochemical characteristics, the Enterprise prospect appears to be distinct from the widespread mesothermal lode-gold style mineralisation in northeast Tasmania.

5.9.2 Fluid features of intrusive related gold systems

Intrusion-related gold deposits as documented in the literature show that intrusions emplaced in deeper environments (i.e. primitive high temperature) appear to exsolve abundant CO_2, whereas shallower (more evolved lower temperature) systems typically exsolve saline H_2O-rich fluids more readily. The point count analyses (Figure 5.2) could be interpreted to suggest this change occurred at the Enterprise prospect, from CO_2-rich to H_2O-rich inclusions as the system evolves from magmatic through magmatic-hydrothermal transition to the hydrothermal stages. Salinity estimations from fluid inclusions at the Enterprise prospect indicate later secondary

inclusions (*Type 2* in trails) having higher salinities (average 9.1 equiv wt % NaCl) than earlier primary inclusions (*Type 1* and *Type 2* in isolated populations; average 4.7 and 7.2 wt % NaCl equiv). Homogenisation temperatures also indicate an evolving fluid. Early primary inclusions exhibit higher T_h temperatures (290°-450°C) than later secondary inclusion (160°-370°C).

The initial volatile content of most biotite and hornblende-bearing felsic magmas is ~2-7% H_2O (Burnham, 1979), but because most of the crystals forming from the magma have only trace volatile constituents in their structure (e.g. F, Cl, OH^-, CO_2 etc.), the volatile concentration of the residual melt increases as crystallisation continues (Roedder, 1992). Pressure-depth constraints play an important role in determining whether or not a magmatic fluid will exsolve. This is because at deep crustal levels, H_2O is typically incorporated in to hydrous magmatic minerals and is not released as a separate volatile phase

Pressures estimated from CO_2-rich fluid inclusions and aluminium-in-hornblende geobarometry ranged from 400 to 1000 bars. The pressures estimated from CO_2-rich fluid inclusions can be interpreted to represent both lithostatic and hydrostatic pressure conditions at similar depths. Therefore, the fluid inclusions may represent fluid trapped during periods when the intrusion carapace was under greater pressure, solidifying. At times when the pressure was reduced potentially through fracturing, a fluid was released. This process could have resulted in significant cooling and/or wall-rock interaction, a key mechanism for ore precipitation in many deposit types, including porphyry Cu-Au and lode gold (Cooke et al., 1998; Yeats and Vanderhor, 1998). Therefore, a possible key process related to ore deposition may be a temperature and pressure reduction associated with the rise of an intrusion and to a lesser extent fracturing of the carapace.

The intrusion-related gold deposit model, as documented in the literature, proposes an entirely magmatic origin for the ore fluids and their associated components that form spatially associated gold deposits (Thompson and Newberry, 2000). The presence of *Type 1* CO_2-rich inclusions at all stages in the evolution of the Enterprise intrusion is similar to observations of intrusion-related gold deposits, and supports a similar fluid being responsible for their formation. Homogenisation temperatures for *Type 1*

inclusions range between 290 and 450°C. The initial postulation was that these are indicative of magmatic fluids (similar to those found in porphyry Cu-Au deposits), too hot to be from most other sources (Cooke et al., 1998).

5.9.3 Sulphur isotope evidence for origin

The results for sulphides from the Enterprise prospect sit within the known range for magmatic sulphur. The only sulphide phase interpreted to be a primary magmatic aggregate from in the granodiorite was pyrrhotite and yielded a $\delta^{34}S$ of 0.44 ‰, also indicating a magmatic source. An alternative is that magmatic $\delta^{34}S$ components were derived by fluid circulation through magmatic wall rock.

Sulphur isotope values for pyrite associated with mineralisation from Mangana (Figure 2.2) range from 5.3 to 13.6‰ with a mean of 9.5‰ (Manzi, 1995). The spread of this data (Figure 5.10) was attributed to different mineralisation events and/or a combination of sulphur sources. Sulphur isotopes values from the Beaconsfield and Lefroy deposits (Figure 2.2), range from 7 to 11.1 and 12.1 to 12.7 (Russell and Van Moort, 1992). The sulphur from these deposits has been interpreted to derive from the mixing or fractionation of Devonian seawater or connate fluids derived from seawater (Russell and Van Moort, 1992). The narrow range of values for Lefroy was interpreted to represent a single sulphur source. In contrast the spread of values for Mangana and Beaconsfield was interpreted to represent mixing of multiple sulphur sources.

Porphyry copper deposits most likely have a magmatic source of sulphur, with $\delta^{34}S$ values for sulphides falling in the narrow range of –3 to +1 ‰, close to the accepted mantle range (Rollinson, 1993). Intrusion-related gold deposits such as the Shotgun deposit produced $\delta^{34}S$ values of between –5.5 to –5 ‰ (Rombach and Newberry, 2001), and the Clear Creek deposit –2.9 to +0.4 ‰ (Marsh et al., 2003). My results are noted to be consistent with intrusion-related gold deposits in southwest and interior Alaska, where an igneous source for the sulphur has been concluded.

6 Origin of the Enterprise/Potoroo gold mineralisation

6.1 Synopsis and Discussion

Gold in the Lisle/Golconda area was first discovered in the early 1870's. Much of the gold was recovered from historical alluvial workings, with little known about its source. The Enterprise and Potoroo prospects are two occurrences in the area, and gold at both is hosted predominantly in, and immediately adjacent to, granitic intrusions. The intimate link between the distribution of hypogene gold and the intrusions implies that the granitoids may be the gold source. Several important features (e.g. host intrusions, physiochemical characteristics of the fluids, depth of emplacement and distribution/style of alteration and mineralisation) make the Enterprise and Potoroo prospects very similar to well characterised intrusion-related gold deposits as outlined in Table 1.1.

6.1.1 Detailed comparisons with known intrusion-related gold systems

Depth of magma emplacement has been shown to have a systematic effect on mineralisation style in intrusion-related gold deposits (Baker, 2002). Deposits in shallow crustal settings (<5 km) include sheeted veinlets associated with stocks, sills, dykes and volcanic domes (e.g., Korri Kollo, Brewery Creek, Donlin Creek and Shotgun deposits) and include systems with stock-works similar to those in porphyry-type settings, and to epithermal-like veins and breccias. Deeper systems (>5km) have characteristics of mesothermal environment deposits, in that the host pluton contains sheeted veins, flat lenses, greisen-style and disseminated gold (e.g., Fort Knox, Pogo, Salvae and Timbarra). Depth of emplacement also has a systematic effect on the physiochemical nature of the ore-fluids, i.e. intrusions that are emplaced in deeper environments appear to exsolve abundant CO_2 (e.g. Timbarra), whereas shallower systems typically exsolve saline H_2O-rich fluids more readily (e.g. Korri Kollo, Bolivia) (Baker, 2002).

Pressure of emplacement calculations using both CO_2-rich fluid inclusions, and aluminium-in-hornblende barometry, estimated pressures of up to 1000 bars or 4 km for the Enterprise intrusion. In contrast, aluminium-in-hornblende geobarometry for the western margin of the Scottsdale Batholith ranged from 1300 to 2400 bars or between approximately 5 and 9 km (Varne and Fulton, 1994). Thus, the intrusives in the Lisle/Golconda area were potentially emplaced at comparatively shallower crustal levels than the Scottsdale Batholith, implying relative uplift of the western margin compared to more peripheral western granites, syn- or post- the Devonian intrusion episode (Figure 6.1). At Enterprise, mineralisation is hosted within sub vertical sheeted veins in a granodiorite intrusive, typical of deep intrusion-related deposits (Table 1.1). Sub-vertical zones of mineralised quartz veins occur in some of the best documented examples of intrusion-related gold style deposits. The pressure and depth constraints from the Enterprise prospect are comparable with similar examples of these at Donlin Creek, Dublin Gulch and Kidston. Donlin Creek is characterised by near-vertical veins/veinlets in rhyolite sills/dykes, Dublin Gulch by near-vertical sheeted veins in granodiorite and Kidston by breccia and sheeted veins in a rhyolite porphyry stock (Table 1.1). The fluid inclusions at the Enterprise prospect associated with but not within gold bearing quartz, are CO_2-rich, having T_h temperatures up to 450°C and with salinities less than 14 wt % NaCl equiv. These characteristics are comparable to those from Dublin Gulch, Fort Knox and Timbarra, i.e. the deeper described intrusive-related deposits (Baker, 2002).

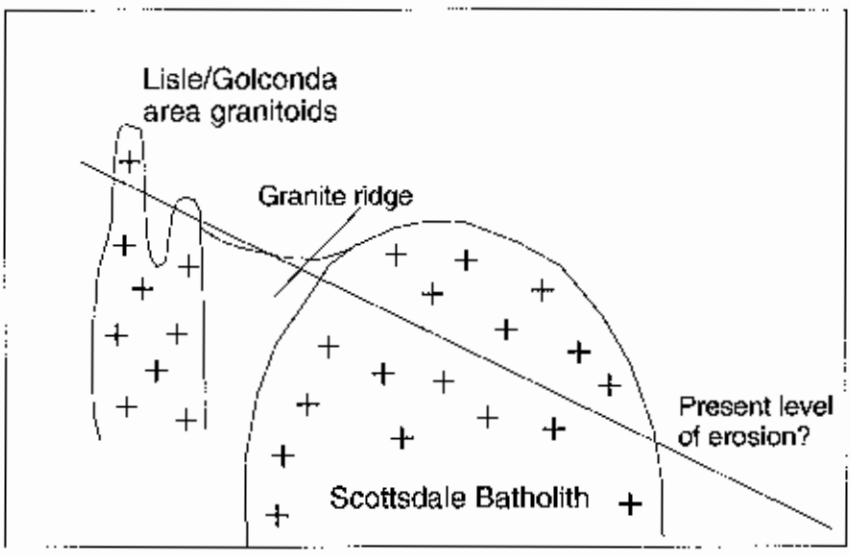

Figure 6.1 Schematic illustration of the Lisle/Golconda area granitoids with respect to the main Scottsdale Batholith plutons.

Fluid physiochemistry and pressure estimates were not made for the Potoroo prospect. However, two examples from the literature, Brewery Creek and Timbarra, possess a deposit style comparable to the Potoroo prospect (Table 1.1). Potoroo consists of disseminated mineralisation in pervasively altered granodiorite that is cut by minor sulphide-bearing quartz veins. Brewery creek comprises disseminated ore and veinlets in monzonite sills whereas Timbarra consists of disseminated ore in granodiorite (Baker, 2002). Based on fluid inclusion investigations, Brewery Creek has been estimated to have formed at pressures of approximately 500 bars or 2 km (slightly shallower than Enterprise) from immiscible brine (NaCl eq wt % > 40). In contrast, Timbarra formed at approximately 2000 bars or 7 km from fluids very similar to that of the Enterprise prospect. Pressure, depth, and volatile content may have been factors in controlling the two mineralisation styles present at the Potoroo and Enterprise prospects. Pressure estimations and a fluid inclusion study at Potoroo would better constrain the affects of emplacement depth on mineralisation style in the Lisle/Golconda area.

6.1.2 Comparison to known gold-associated granites

The name 'Lisle Pluton' was suggested by Roach (1994) for granodioritic rocks that outcrop at Lisle, Golconda, Lone Star and Panama on the basis of distinctive petrological, geochemical and petrophysical characteristics. The presumption that the intrusives in the Lisle/Golconda area form part of a separate body to the Scottsdale Batholith is supported by findings from this project. Evidence includes the distinctively shallower pressure/depth estimations for the Enterprise intrusives compared to the Scottsdale Batholith, distinctive geochemistry, and the physical location (Figure 6.1).

Oxidation state of magmas plays a major role in controlling the compatible or incompatible nature of many ore elements (Blevin and Chappell, 1992). Intrusion-related gold deposits are characterised by an association with reduced granitic intrusions and by their reduced sulphide mineralogy (Lang and Baker, 2001). The ratio of Fe_2O_3 to FeO, coupled with mineralogy, was used to evaluate the oxidation state of the Enterprise and Potoroo host granodiorites. However, localised alteration

affects (e.g. from Mathinna Group sedimentary rocks or another source), may also have had an effect. The Enterprise mineralisation is characterised by a reduced ore and alteration mineralogy consisting of molybdenite, phlogopite and pyrrhotite. This supported by a low Fe_2O_3 to FeO ratio that plots in the strongly reduced oxidation field. Potoroo is characterised by a mineral assemblage of arsenopyrite, pyrite and lesser chalcopyrite. Potoroo has a much higher Fe_2O_3 to FeO ratio, which plots at the moderately to strongly oxidised boundary. Mineralogy and the Fe_2O_3/FeO ratio indicate that the oxidation state during the mineralising event was higher, however, the reason behind this is not understood. On the basis of oxidation state, the Enterprise and Potoroo prospects are distinct. This is evidence that oxidation states varied between adjacent mineralised sites in the area. Potoroo plots closest to the field of known gold mineralised granitoid suites (e.g. the Timbarra host granodiorite).

Fractional crystallisation has been shown to concentrate gold so long as gold behaves incompatibly (Cygan and Candela, 1995). Discoveries of gold in silicate-melt inclusions from primarily the most fractionated stages of the Timbarra deposit granodiorite, support a model of incompatible enrichment of gold in late stage granitic melts (Mustard et al., 2004). Geochemistry from the Enterprise and Potoroo prospect has shown the host granodiorites to be the least fractionated of the Scottsdale Batholith. This was also shown by Roach (1994) on similar rocks from the Lisle/Golconda area. If fractionation of the magma was a principle mechanism for gold concentration at Enterprise and Potoroo, it may have not been sufficient enough to concentrate enough gold to form a large tonnage and/or grade deposit (e.g. Timbarra).

A poor example of a quartz-layered texture (in comparison to those documented in the literature; Shannon et al., 1982a) was identified in the FBQ from the Enterprise prospect. Its occurrence, combined with the presence of aplites and extensive alteration, may suggest that magmatic volatiles were exsolved during the evolution of the Enterprise pluton from levels deeper than currently exposed. The discovery of further magmatic-hydrothermal transition textures would better constrain the extent of volatile exsolution and help target intrusion-related gold deposits. The melt and fluid inclusion relationships at Timbarra are consistent with entrapment of late stage melt with an associated high magmatic volatile content (Mustard, 2003a). Candela and

Blevin (1995) suggested for high temperature magmatic hydrothermal mineral deposits to develop in, or near, the apical regions of a pluton (including intrusion-related gold systems such as Timbarra), large quantities of the magmatic volatile phase need to be channelled to the apical region. This in turn must occur before significant cooling crystallisation occurs to prevent dilution of the aqueous phase, and to ensure that important ore forming elements are not trapped in the crystallising phases. They also illustrated that early establishment of connectivity fluid pathways within melts is favoured by higher initial water concentrations and lower confining pressures.

Mineralisation style and fluid physiochemistry (fluid inclusions and sulphur isotopes) suggest an intrusive source for the Au at the Enterprise and potentially the Potoroo prospect. If an intrusive was the source of Au, an intrusion at a deeper level than currently exposed, may account for gold in veins at the current level and cryptic Na and Si alteration. Na and Si alteration was evident in the intrusions chemistry, however, this was not accounted for by any petrographic textural feature. Potentially this alteration may have occurred post intrusion emplacement and pre gold mineralisation, suggesting a later intrusive phase at depth exsolving fluids. If this is the case, gold sourced from a deeper intrusion, it is likely that Timbarra-style disseminated Au is occurring deeper within this pluton. Disseminated mineralisation could occur if any Au was deposited prior to brittle failure of the crystallising granodiorite and emplacement of the observed veins.

6.2 Conceptual model

The release of magmatic fluids during fractionation is widely accepted as the primary mechanism that initiates ore deposition in porphyry deposits. In porphyry deposits this process is dramatic, commonly producing multiple sets of multi-directional quartz veins. A similar process is postulated for intrusion-related gold deposits, however, the result is usually more passive, resulting in sheeted or poorly developed stock works, with little evidence for multiple events (Thompson and Newberry, 2000). Features from the Enterprise and Potoroo prospects, combined with observations reported in the literature, have been used to construct an interpretative model for the genesis of this style of mineralisation on the margin of the Scottsdale Batholith (Figure 6.2), which is discussed here in a combination of text and figures.

A number of changes in fluid conditions are argued to cause gold deposition. Four potential mechanisms responsible for gold deposition at the Enterprise prospect include, pressure reduction (decompression), cooling, boiling and/or sulphide deposition. Pressure estimates ranging from 400 to 1000 bars can be interpreted to suggest decompression. Such a range can be inferred to represent both lithostatic and hydrostatic stress regimes at similar depths. Early primary inclusions exhibit higher T_h temperatures (290°-450°C) than later secondary inclusion (160°-370°C). This is suggestive of cooling over time and also supports decompression. The presence of coexisting liquid rich (*Type 2A*) and vapour rich (*Type 2B*) fluid inclusion in hydrothermal veins is indicative of boiling. The strong correlation between gold and arsenic/arsenopyrite indicated from mineralogy and assay results suggest that the deposition of arsenopyrite may have been a catalyst for gold deposition.

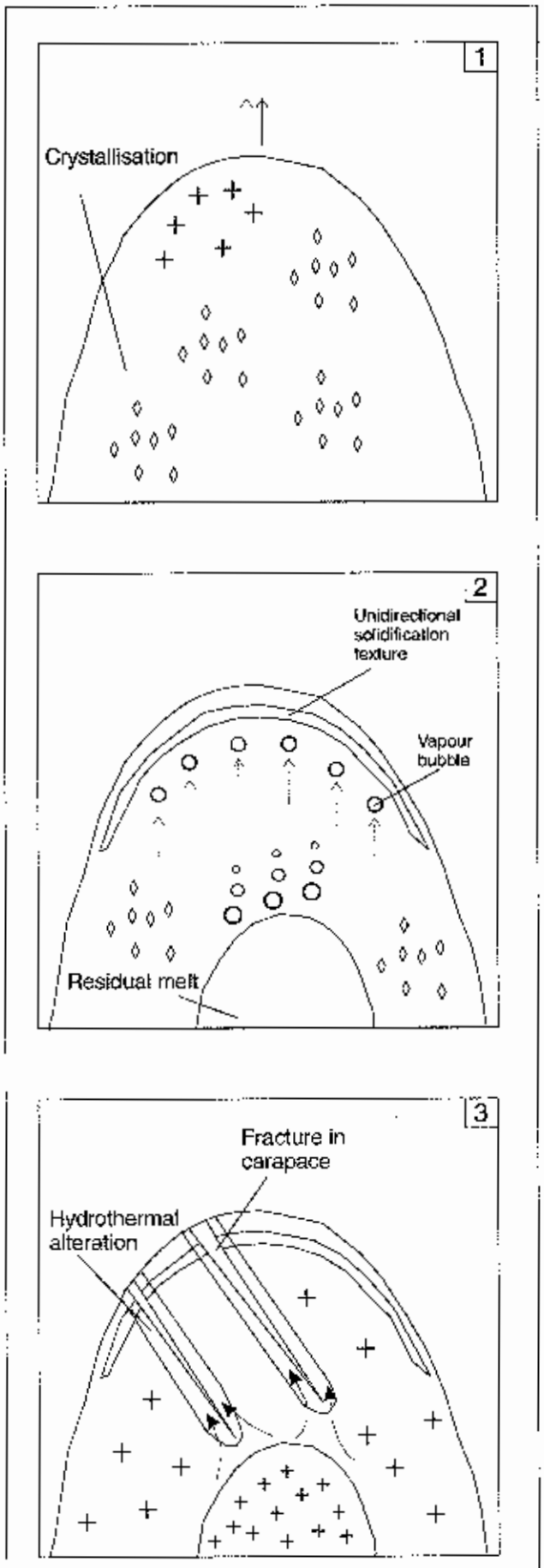

Figure 6.2 Interpretive model for the genesis of mineralisation at the Enterprise and Potoroo prospects.

Stage 1, Magmatic: involves the rise of a magma body in the crust. As the magma rose it cooled and began to crystallise.

Stage 2, Magmatic-hydrothermal transition: A volatile phase separated (volatile exsolution) from deeper parts of the magma (residual melt?). The volatile phase rose buoyantly and accumulated at the carapace of the intrusion. This volatile phase is preserved in textures such as miarolitic cavities high temperature silicification, interconnected miarolitic textures, unidirectional solidification textures, pegmatite's and aplitic vein-dykes.

Stage 3, Hydrothermal: Further cooling of the intrusion at deeper levels resulting in volatile exsolution, and brittle fracturing of the carapace. The volatile phase was released and resultant fluid flow leads to the formation of intrusion- and/or wall rock-hosted brittle quartz veins and shear zones with sericite alteration. Au deposited by decompression, cooling and/or boiling.

6.3 Major findings of this thesis

- A detailed igneous and alteration petrology exemplified the inhomogeneous nature of the host intrusion. Three intrusive phases were recognised along with a series of 'vein' dykes and veins.

- A distinct vein stage associated with gold mineralisation was investigated. A relationship between gold and arsenic was made based on mineral proportions and assay results from the veins.

- Magmatic-hydrothermal transition textures were recognised: a quartz layered texture, aplite vein dykes, greisen and myrmekites. These textures suggest that the host granodiorites exsolved a volatile phase. However, gold was likely sourced from exsolution at deeper structural levels, based on the highly discordant and straight vein margins.

- The Enterprise and Potoroo granodiorites are geochemically distinct from the Scottsdale Batholith based on a major and trace element characteristics, supporting the findings made by Roach (1994) on rocks from the same area.

- Granodiorites and/or their altered equivalents from the Enterprise prospect, appear to be less evolved (fractionated) and more reduced, than gold bearing granitoid suites from eastern Australia. Granodiorites from the Potoroo prospect are slightly more evolved and oxidised than the Enterprise, and are comparable to gold bearing granitoid suites from eastern Australia (e.g. Timbarra). The extent to which these oxidation states reflect magmatic character over high temperature magmatically induced alteration was not established.

- A detailed fluid inclusion study of pre- and post-Au veins identified three inclusion types: CO_2-rich, H_2O-rich and salt bearing. Primary CO_2-rich and H_2O-rich inclusions with total homogenisation temperatures from 290° to 450°C were identified in all the stages of the intrusion, from magmatic, through the magmatic-hydrothermal transition and hydrothermal. This supports a common fluid type present throughout the evolution of the intrusive.

- Two geobarometry methods were used: liquid-vapour CO_2 fluid inclusions and aluminium-in-hornblende. These methods were used to estimate a pressure of intrusion emplacement of up to 1000 bars, or approximately 4km (assuming lithostatic conditions).

- Sulphur isotopes from the Enterprise prospect were consistent with a magmatic source for sulphur. Sulphur isotope values from the Enterprise formed a distinctive lighter population ($\delta^{34}S$ of -0.6 to 2.43‰) when compared to values from lode gold style deposits hosted in sedimentary rock from northeast Tasmania (e.g. Beaconsfield and Mangana; $\delta^{34}S$ of 7 to 11.1‰ and 5.3 to 13.6‰). A wider range of heavier values for Beaconsfield and Mangana was attributed to mixing of multiple sulphur sources including external sedimentary sulphur by other authors (Russell and Van Moort, 1992). The narrow range of lighter isotope values for the Enterprise prospect was attributed to an origin from one sulphur source.

6.4 Exploration

The following points may assist better exploration for intrusive-related gold deposits in the greater Lisle/Golconda area:

- Geochemical surveys should focus on the key pathfinder elements, Au and As, in addition to those documented in the literature, however, it is not clear if As halos the gold zones, and this is important to determine for exploration. Bi, Te and to a lesser extent W, Mo, Sn and Pb are all known to be enriched in intrusion-related gold deposits, and should be included in future analytical work. Au has been illustrated to correlate best with As.

- The following magmatic-hydrothermal features were observed in the intrusives associated with Au veins: unidirectional solidification textures, myrmekitic, textures, greisen and 'vein' dykes. These textures all require development of exsolution of a volatile phase during magma crystallisation.

- The following alteration is spatially associated with gold quartz veining: moderate to intense sericite ± chlorite alteration. The presence of pyrrhotite is suggestive of a reduced fluid, with a component that may have been deposited as haloes around veins. Magnetic susceptibility has shown to detect pyrrhotite haloes around gold-bearing veins at small scales. The use of magnetic methods may be useful in defining these zones.

- In general, intrusion-related gold plutons are members of suites that are highly fractionated and reduced. However, Au mineralised suites from eastern Australia are predominantly associated with highly fractionated oxidised suites (e.g. Cadia, NSW). The evidence at Enterprise is that the host intrusions are the least fractionated and most primitive in the Scottsdale Batholith. If these magmas follow the principles seen in other intrusion-related plutons, than there may be more fractionated source phases at depth in the Lisle/Golconda area. However, empirically, gold in the Lisle/Golconda area is associated with the most mafic intrusives.

- Intrusions with low concentrations of Rb and K, high Sr and SiO2 delineate the most prospective units in the Scottsdale Batholith, and these features appear t related to cryptic Si-Na alteration sourced from deeper levels in the Enterprise pluton.

- Better understanding of the structural environment of magma emplacement is a potential key to predictive exploration along the margin of the Scottsdale Batholith. The EW granite ridge extending from the main Scottsdale Batholith toward the Enterprise area (Figure 2.1) is very anomalous in the area.

- The EW nature of dilation, evidenced by the regional EW granite ridge, may be repeated at a deposit scale, and suggests that some NS drill holes should be undertaken to explore for veins at EW orientation in the Enterprise pluton.

- If an underlying magma sourced the gold into veins at the Enterprise mine level, this magma may still contain some disseminated mineralisation at depth, i.e. Timbarra-style gold.

- The pressures currently available suggest the Scottsdale Batholith is greatly uplifted compared to the Enterprise area. This needs verification. Assuming greater amounts of erosion along the granite ridge to the east (Figure 6.1), then similar systems may be exposed here at a level appropriate for mining. In contrast, systems developed to the west may provide views to even higher crustal levels. Therefore, the whole granite ridge is worthy of exploration, on the principle that different volatile contents lead to emplacement of magmas at different levels.

References

Ague, JJ 1997, 'Thermodynamic calculation of emplacement pressures for batholithic rocks, California; implications for the aluminium-in-hornblende barometer', *Geology*, vol. 25, pp. 563-6.

Baker, EM & Andrew, AS 1991, 'Geologic, fluid inclusion, and stable isotope studies of the gold-bearing breccia pipe at Kidston, Queensland, Australia', *Economic Geology*, vol. 86, pp. 810-30.

Baker, T 2002, 'Emplacement depth and carbon dioxide-rich fluid inclusions in intrusion-related gold deposits', *Economic Geology and the Bulletin of the Society of Economic Geologists*, vol. 97, no. 5, pp. 1111-7.

Banks, MR 1962, 'The Geology of Tasmania - The Silurian and Devonian systems', *Journal of the Geological Society of Australia*, vol. 9, pp. 177-88.

Banks, MR & Smith, EA 1968, 'A graptolite from the Mathinna Beds, north eastern Tasmania', *Australian Journal of Science*, vol. 31, pp. 118-9.

Bierlein, FP, Foster, DA, Gray, DR & Davidson, GJ 2004, 'Timing of Orogenic Gold mineralisation in Northeast Tasmania - Implications for the Tectonic and Metallogenic Evolution of Palaeozoic SE Australia', *in press*.

Black, LP 2001, 'SHRIMP U-Pb dating. A. Crystallisation ages of Tasmanian granites, and their significance.' pp. The Geological Framework of Tasmania; Symposium Abstracts AGSO & MRT Conference, Hobart, Australia, June 13-4, 2001: 14.

--- 2004, 'New constraints on age and correlation of Tasmanian Proterozoic successions from SHRIMP U-Pb detrital zircon dating.' *Geological Society of Australia Abstacts 73*, p. 55.

Blevin, PL 2004, 'Redox and Compositional Parameters for Interpreting the Granitoid Metallogeny of Eastern Australia: Implications for Gold-rich Ore Systems', *Resource Geology*, vol. 54, pp. 241-52.

Blevin, PL & Chappell, BW 1992, 'The role of magma sources, oxidation states and fractionation in determination the granite metallogeny of eastern Australia', *Transactions of the Royal Society of Edinburgh: Earth Sciences*, vol. 83, pp. 305-16.

Blevin, PL, Chappell, BW & Charlotte, MA 1996, 'Intrusive metallogenic provinces in eastern Australia based on granite source and composition', *Transactions of the Royal Society of Edinburgh: Earth Sciences*, vol. 87, pp. 281-90.

Boiron, MC, Barakat, A, Cathelineau, M, Durisova, J & Moravcek, P 1995, 'Microfissural ore fluid migration: The example of a granodiorite-hosted gold deposit (Mokrsko, Bohemia)', in J Pasava, B Kribek & K Zak (eds), *Mineral deposits: From their origin to their environmental impacts, A.A. Balkema, Rotterdam Brookfield, Prague, 1995, Proceedings*, 3rd Biennial SGA Meeting, pp. 97-100.

Bottrill, RS, Huston, DL, Taheri, J & Zaw, K 1992, 'Gold in Tasmania', *Bulletin of the Geological Survey of Tasmania*, vol. 70, pp. 24-56.

Broadbent, G 1982, 'Pipers River EL 53/80. Geological report for year ending 17 December 1982. CRA Exploration Pty Ltd', *Unpublished Mineral Resources Tasmania Report*.

Burnham, CW 1979, 'Magmas and hydrothermal fluids', in HL Barnes (ed.), *Geochemistry of hydrothermal ore deposits 2nd ed*, New York, pp. 71-136.

Campbell, AR & Larson, PB 1998, 'Introduction to stable isotope applications in hydrothermal systems', *Reviews in Economic Geology*, vol. 10, pp. 173-93.
Candela, PA & Blevin, PL 1995, 'Do some miarolitic granites preserve evidence of magmatic volatile phase permeability?' *Economic Geology and the Bulletin of the Society of Economic Geologists*, vol. 90, pp. 2310-6.
Chappell, BW & White, AJR 1974, 'Two contrasting granite types', *Pacific Geology*, vol. 8, pp. 173-4.
Chappell, BW, White, AJR & Hine, R 1988, 'Granite provinces and basement terranes in the Lachlan fold belt, southeastern Australia', *Australian Journal of Earth Sciences*, vol. 35, no. 4, pp. 505-21.
Cocker, JP 1982, 'Rb-Sr geochronology and Sr isotopic composition of Devonian granitoids, eastern Tasmania.' *Journal of the Geological Society of Australia*, vol. 29, pp. 139-58.
Cole, A, Wilkinson, JJ, Halls, C & Screnko, TJ 2000, 'Geological characteristics, tectonic setting, and preliminary interpretations of the Jilau cold-quartz vein deposit, Tajikistan', *Mineralium Deposita*, vol. 35, pp. 600-18.
Cooke, DR, Heithersay, PS, Wolfe, R & Calderon, AL 1998, 'Australian and western Pacific porphyry Cu-Au deposits', *Journal of Australian Geology and Geophysics*, vol. 17, pp. 97-104.
Coroneus, C 1993, 'A poor mans diggings: An Archaeological Survey of the Lisle-Denison Goldfields, NE Tasmania. Part 2: Results of the historical and archaeological research.' *Report prepared for the Forestry Commission Hobart and the Queen Victoria Museum and Art Gallery, Launceston.*
Cromer, WC 1987, 'EL 32/85, Lisle-Golconda Annual Report, Year 2. Argyle Minerals NL', *Unpublished Mineral Resources Tasmania Report.*
Cygan, GL & Candela, PA 1995, 'Preliminary study of gold partitioning among pyrrhotite, pyrite, magnetite, and chalcopyrite in gold-saturated chloride solutions at 600 to 700°C, 140 MPa (1400 bars)', in JFH Thompson (ed.), *Magmas, fluids, and ore deposits.*, Min Assoc Can Short Coarse Scr, vol. 23, pp. 129-37.
Dickens, G 1991, 'The Lisle Goldfield - A Brief History', *Unpublished report to the Department of Mines. 1991/17.*
Diment, R 1996, 'Brewery Creek gold deposit, in Yukon exploration and geology: Field work report for 1995, Whitehorse, Yukon, Indian, and Northern Affairs Canada', *Exploration and Geological Services Division*, pp. 89-97.
Dunne, KPE 1995, 'Brewery Creek: Preliminary fluid inclusion study: Unpublished consultant report to Yukon Geology Program and Vicery Mining Pty., Vancouver B.C., Vicerory Mining Pty., 6p'.
Ebert, S, Miller, L, Petsel, S, Dodd, S & Kowalczyk, P 2000, 'Geology, mineralisation, and exploration at the Donlin Creek project, southwest Alaska', in TL Tucker & MT Smith (eds), *The Tintina gold belt: Concepts, exploration, and discoveries*, British Columbia and Yukon Chamber of Mines, Cordilleran Roundup 2000, pp. 99-114.
Ferris, GM & Schwarz, M 2004, 'Definition of the Tunkillia Suite, western Gawler Craton', *Quarterly Earth Resources Journal of Primary Industries and Resources South Australia*, vol. 34.
Gee, RD & Groves, DI 1971, 'Structural features and mode of emplacement of part of the Blue Tier Batholith in northeastern Tasmania', *Journal of the Geological Society of Australia*, vol. 18, pp. 14-56.

Goldfarb, RJ, Ayuso, R, Miller, ML, Ebert, S, Marsh, EE, Petsel, SA, Miller, LD, Bradley, D, Johnson, C & McClelland, W 2004, 'The Late Cretaceous Donlin Creek gold deposit, Southwestern Alaska; controls on epizonal ore formation', *Economic Geology and the Bulletin of the Society of Economic Geologists*, vol. 99, pp. 643-71.

Goscombe, BD, Findlay, RF, McClenaghan, MP & Everard, JL 1994, 'Multi-scale kinking in northeast Tasmania: crustal shortening at shallow crustal levels', *Journal of Structural Geology*, vol. 16, pp. 1077-92.

Greenwood, HJ & Barnes 1966, 'Binary mixtures of volatile compounds', in SP Clark (ed.), *Handbook of Physical Constants*, Geol. Soc. Am. Mem., vol. 97 revised ed., pp. 385-400.

Groves, DI, Cocker, JP & Jennings, DJ 1977, 'The Blue Tier Batholith', *Bulletin of the Geological Survey of Tasmania*, vol. 55.

Hammarstrom, JM & Zen, Ea 1986, 'Aluminium in hornblende; an empirical igneous geobarometer', *American Mineralogist*, vol. 71, pp. 1297-313.

Harris, M 1980, 'Gold mineralisation at the Salavae gold prospect Northwest Spain.' *Trans Inst Mining Metall, Appl Earth Sci*, vol. B89:B1-B4.

Higgins, NC, Solomon, M & Varne, R 1985, 'The genesis of the Blue Tier Batholith, northeastern Tasmania, Australia', *Lithos*, vol. 18, no. 2, pp. 129-49.

Hippertt, JF & Valarelli, JV 1998, 'Myrmekite: constraints on the available models and a new hypothesis for its formation', *Eur. J. Mineral.*, vol. 10, pp. 317-31.

Hollister, LS, Grissom, GC, Peters, EK, Stowell, HH & Sisson, VB 1987, 'Confirmation of the empirical correlation of Al in hornblende with pressure of solidification of calc-alkaline plutons', *Am. Mineral*, vol. 72, pp. 231-9.

Johnson, MC & Rutherford, MJ 1989, 'Experimental calibration of the aluminium-in-hornblende geobarometer with application to Long Valley caldera (California) volcanic rocks', *Geology*, vol. 17, pp. 837-41.

Jones, B 2001, 'Genesis of the Tasmania Reef, Beaconsfield', Honours thesis, University of Tasmania (unpubl.).

Keele, RA, Taheri, J & Bottrill, RS 1993, 'Structure and mineralisation in the Devonian-aged Mathinna-Alberton gold lineament', in University of Tasmania, Department of Geology.

Keenan, JH, Keyes, FG, Hill, PG & Moore, JG 1969, 'Steam tables; Thermodynamic Properties of Water, Including Vapour, Liquid and Solid Phases', *Wiley & Sons, New York, NY*, p. 162.

Lang, JR & Baker, T 2001, 'Intrusion-related gold systems; the present level of understanding', *Mineralium Deposita*, vol. 36, no. 6, pp. 477-89.

Leaman, DE & Richardson, RG 1989, 'Production of a residual gravity map for Tasmania and some implications', *Exploration Geophysics*, vol. 20, pp. 181-4.

Leaman, DE, Richardson, RG & Shirley, JE 1980, 'Tasmania - The gravity field and its interpretation', *Tasmanian Department of Mines Report 1980/36*.

Levinson, AA 1974, 'Introduction to Exploration Geochemistry', *Applied Publishing Calgary*.

Lowenstern, JB & Sinclair, WD 1996, 'Exsolved magmatic fluid and its role in the formation of comb-layered quartz at the Cretaceous Logtung W-Mo deposit, Yukon Territory, Canada', *Transactions of the Royal Society of Edinburgh: Earth Sciences*, vol. 87, pp. 291-303.

Mackenzie, DE, Black, LP & Sun, S-s 1988, 'Origin of alkali-feldspar granites; an example from the Poimena Granite, northeastern Tasmania, Australia', *Geochimica et Cosmochimica Acta*, vol. 52, no. 10, pp. 2507-24.

Maloof, TL, Baker, T & Thompson, JFH 2001, 'The Dublin Gulch intrusion-hosted gold deposit, Tombstone plutonic suite, Yukon Territory, Canada', *Mineralium Deposita*, vol. 36, no. 6, pp. 583-93.

Manzi, B 1995, 'The Devonian Mangana gold vein system and its Mathinna Group host rocks, northeast Tasmania', University of Tasmania (unpubl.).

Marmo, V 1971, *Granite Petrology and the Granite Problem*, Developments in Petrology 2, Elsevier Publishing Company, Amsterdam.

Marsh, EE, Goldfarb, RJ, Hart, CJR & Johnson, CA 2003, 'Geology and geochemistry of the Clear Creek intrusion-related gold occurrences, Tintina gold province, Yukon, Canada', *Canadian Journal of Earth Sciences = Revue Canadienne des Sciences de la Terre*, vol. 40, no. 5, pp. 681-99.

McClenaghan, MP 1984, 'Granitoids of northeastern Tasmania', *BMR Journal of Australian Geology and Geophysics*, vol. 9, no. 4, pp. 303-12.

---- 1989, 'Mid-Palaeozoic Granitoids', in CF Burret & EL Martin (eds), *The Geology and Mineral Resources of Tasmania*, Geological Society of Australia Special Publication 15, pp. 253-70.

McClenaghan, MP & Williams, PR 1982, 'Distribution and characterisation of granitoid intrusions in the Blue Tier area', *Pap. geol. surv. Tasm.*, vol. 4.

McClenaghan, MP & Higgins, NC 1993, 'The age and intrusive relationships of granitoids of the Blue Tier Batholith, NE Tasmania', *Mineral Resources Tasmania Report 1993/33.*

McCoy, DT, Newberry, RJ, Layer, PW, DiMarchi, JJ, Bakke, A, Masterman, JS & Minehane, DL 1997, 'Plutonic related gold deposits of interior Alaska.' in RJ Goldfarb & LD Miller (eds), *Ore deposits of Alaska*, Soc Econ Geol News, vol. 9.

Mustard, R 2001, 'Granite-hosted gold mineralization at Timbarra, northern New South Wales, Australia', *Mineralium Deposita*, vol. 36, no. 6, pp. 542-62.

---- 2003a, 'The magmatic-hydrothermal transition at Timbarra: Implications for the genesis of intrusion-related gold deposits.' in DGEe al (ed.), *Mineral Exploration Sustainable Development*, Millpress, Rotterdam, Netherlands, 2003, vol. 1, pp. 355-8.

---- 2003b, 'Carbon dioxide bearing melt inclusions within a gold-mineralized felsic granite', in DGEe al (ed.), *Mineral Exploration Sustainable Development*, Millpress, Rotterdam, Netherlands, 2003, vol. 1, pp. 351-4.

Mustard, R & Ulrich, T 2004, 'A melt-inclusion study on the behaviour of gold and other metals (Sn, W, Mo, Bi, As, Cu, and Sb) during fractional crystallisation of a felsic magma', in *Dynamic Earth: Past, Present and Future*, Geological Society of Australia, vol. Abstacts 73, p. 103.

Mustard, R, Ulrich, T & Mernagh, T 2004, 'The partitioning of gold and other metals between coexisting silicate melt and CO_2-rich low-salinity aqueous fluid at the magmatic-hydrothermal transition', in *Dynamic Earth: Past, Present and Future*, Geologicial Society of Australia, vol. Abstracts 73, p. 104.

Newitt, DM, Pai, MU & Kuloor, NR 1956, 'Carbon dioxide', in F Din (ed.), *Thermodynamic Functions of Gases*, Butterworths, London, vol. 1, pp. 102-34.

Ohmoto, H 1972, 'Systematics of sulphur and carbon isotopes in hydrothermal ore deposits', *Economic Geology*, vol. 67, pp. 551-78.

Patison, NL 1999, 'Geology of the Cashes Gorge/ Ralphs Fall Area, NE Tasmania', Hons thesis, University of Tasmania, Hobart (unpubl.).

Patison, NL, Berry, RF, Davidson, GJ, Taylor, BP, Bottrill, RS, Manzi, B, Ryba, J & Shepherd, RE 2001, 'Regional metamorphism of the Mathinna Group, Northeast Tasmania', *Australian Journal of Earth Sciences*, vol. 48, no. 2, pp. 281-92.

Petersen, EU & Fitzmayer, JR 1998, 'The alunite-sericite association: A new type of epithermal precious metal deposits', *Geological Society of America Program with Abstracts*, vol. 30, p. A127.

Phillips, ER 1974, 'Myrmekite - one hundred years later', *Lithos*, vol. 7, pp. 181-94.

Powell, CM & Baillie, PW 1992, 'Tectonic affinity of the Mathinna Group in the Lachlan Fold Belt', *Tectonophysics*, vol. 214, pp. 193-209.

Powell, CM, Baillie, PW, Conaghan, PJ & Turner, NJ 1993, 'The mid-Palaeozoic turbiditic Mathinna Group, Northeast Tasmania', *Australian Journal of Earth Sciences*, vol. 40, no. 2, pp. 169-96.

Reed, AR 2001, 'Pre-Tabberabberan deformation in eastern Tasmania: a southern extension of the Benambran Orogeny', *Australian Journal of Earth Sciences*, vol. 48, pp. 785-96.

---- 2002, 'Formation of lode-style gold mineralisation during Tabberabberan wrench faulting at Lefroy, eastern Tasmania', *Australian Journal of Earth Sciences*, vol. 49, no. 5, pp. 879-90.

Rickards, RB, Davidson, GJ & Banks, MR 1993, 'Silurian (Ludlow) graptolites from Golden Ridge, northeast Tasmania', *Association of Australian Palaeontologists Memoir*, vol. 15, pp. 125-35.

Roach, MJ 1994, 'The regional geophysical setting of gold mineralisation in northeast Tasmania', PhD thesis, University of Tasmania, Hobart (unpubl.).

Robert, F, Boullier, AM & Firdaous, K 1995, 'Gold-quartz veins in metamorphic terrains and their bearing on the role of fluids in faulting', *Journal of Geophysical Research*, vol. 100.

Roedder, E 1984, 'Fluid inclusions', in PH Ribbe (ed.), *Reviews in Mineralogy*, Mineralogical Society of America, vol. 12, p. 646.

---- 1992, 'Fluid inclusion evidence for immiscibility in magmatic differentiation', in RJ Bodnar & ETC Spooner (eds), *Geochimica et Cosmochimica Acta*, Pergamon, Oxford, vol. 56, pp. 5-20.

Rollinson, HR 1993, *Using geochemical data : evaluation, presentation, interpretation*, Longman geochemistry series, Longman Scientific, Burnt Mill, Harlow, Essex, England.

Rombach, CS & Newberry, RJ 2001, 'Shotgun Deposit; granite porphyry-hosted gold-arsenic mineralization in Southwestern Alaska, USA', *Mineralium Deposita*, vol. 36, no. 6, pp. 607-21.

Russell, DW & Van Moort, JC 1992, 'Mineralogy and stable isotope geochemistry of the Beaconsfield, Salisbury and Lefroy goldfields', *Bull. geol. Surv. Tasm.*, vol. 70, pp. 208-26.

Schmidt, MW 1992, 'Amphibole composition in tonalite as a function of pressure: an experimental calibration of the Al-in-hornblende barometer', *Contributions to Mineralogy and Petrology*, vol. 110, pp. 304-10.

Shannon, JR, Walker, BM, Carten, RB & Geraghty, EP 1982a, 'Unidirectional solidification textures and their significance in determining relative ages of intrusions at the Henderson Mine, Colorado', *Geology*, vol. 10, no. 6, pp. 293-7.

---- 1982b, 'Unidirectional solidification textures and their significance in determining relative ages of intrusions at the Henderson Mine, Colorado', *Geology*, vol. 10, pp. 293-7.

Smith, M, Thompson, JFH, Bressler, J, Layer, PW, Mortensen, JK, Abe, I & Takaoka, H 1999, 'Geology of the Liese Zone, Pogo property, east-central Alaska', *SEG Newsletter no. 38.*

Solomon, M & Groves, DI 1994, *The geology and origin of Australia's mineral deposits*, Oxford monographs on geology and geophysics, Oxford University Press Inc, NY.

Spiridinov, EM 1996, 'Granite rocks and gold mineralisation of North Kazahkstan', in V Shatov, R Seltmann, A Kremenetsky, B Lehmann, V Popov & P Ermolov (eds), *Granite related ore deposits of central Kazahkstan and adjacent areas*, Glagol Publishing House, St Petersburg, pp. 197-217.

Streckeisen, AL 1973, 'Plutonic rocks: Classification and nomenclature recommended by the IUGS Subcommission on the Systematics of Igneous Rocks', *Geotimes*, vol. 18, pp. 26-30.

Taheri, J & Bottrill, R 1994, *A study of the nature and origin of gold mineralisation, Mangana-Forester area, Northeast Tasmania*, Mineral Resources Tasmania Report.

Takenouchi, S & Kennedy, GC 1965, 'The solubility of carbon dioxide in nacl solutions at high temperatures and pressures', *American Journal of Science*, vol. 263, no. 5, pp. 445-54.

Taylor, BP 1992, 'Structural traverse across the Mathinna Group, northeastern Tasmania', BSc(Hons) thesis, University of Tasmania, Hobart (unpubl.).

Thompson, JFH & Newberry, RJ 2000, 'Gold deposits related to reduced granitic intrusions', *Reviews in Economic Geology*, vol. 13, pp. 377-400.

Todheide, K & Franck, EU 1963, 'Two-phase range and the critical curve in the system carbon dioxide-water up to 3500 bars', *Z. Physik. Chem. (Frankfurt)*, vol. 37, pp. 387-401.

Turner, NJ 1980, 'Composite geological profile across Tasmania', *Tasmanian Department of Mines Report 1980/38.*

Twelvetrees, WH 1909, 'The Lisle Goldfield', *Bull. geol. Surv. Tasm.*, vol. 4.

Varne, R & Fulton, R 1994, 'Contentious speculations about the role of Devonian granodiorites and the influence of Tabberabberan tectonism in Tasmania-North Victoria Land (Antarctica) correlations', in Geological Society of Australia, Tasmania Division.

Williams, E 1959, 'The sedimentary structures of the upper Scamander sequence and their significance', *Papers and Proceedings of the Royal Society of Tasmania*, vol. 93, pp. 29-32.

Yeats, CJ & Vanderhor, F 1998, 'Archean lode-gold deposits', *Journal of Australian Geology and Geophysics*, vol. 17, pp. 253-8.

Appendices

Appendix A

Literature Review

Features of Intrusion-Related Gold Deposits and their applications to exploration

Features of Intrusion-Related Gold Deposits and their applications to exploration

Nicholas J. Fitzpatrick BSc

UNIVERSITY
OF TASMANIA

A literature review submitted as partial fulfilment
of a Bachelor of Science with Honours

CODES SRC
Centre for Ore Deposit Research

1. Introduction

A new class of magmatic-hydrothermal gold deposits has recently been defined in the literature. These deposits are primarily hosted within or in the immediate wall rocks to intrusions. In the past this deposit style has had a number of names given by a variety of authors, including Porphyry Gold (Hollister 1992), Fort Knox-style Gold (Bakke 1995), Intrinsic Gold (Newberry, McCoy & Brew 1995), Plutonic Gold (McCoy et al. 1997), Granitoid Gold (Goldfarb et al. 2000) and Intrusion-related Gold (Lang & Baker 2001; Lang et al. 2000; Sillitoe 1991; Thompson et al. 1999). More recently, the term 'Intrusion-related gold' has become the most widely used and accepted although it was first used by Sillitoe (1991). This deposit class is economically significant with a large number of deposits containing a gold resource of greater than 100 tonnes. Although the deposits themselves have been known and mined for sometime the characteristic features of this class of deposits have only surfaced in the last ~5 years. Intrusion-related gold mineralisation possesses features common to other deposit classes, namely 'porphyry copper- gold, 'orogenic lode gold' and 'reduced tin-tungsten rich' magmatic hydrothermal systems. These deposits are globally widespread, with several of the most documented examples deriving from the Tintina gold belt in the Yukon (Canada) and Alaska (USA).

In the past, intrusion-related gold deposits have been referred to as 'porphyry-related gold deposits' (Bakke 1995; Hollister 1992) however, recognition that these are separate types with common features has led to an improved understanding. They share similarities in generative processes such as formation from magmatic fluids that commonly underwent separation of an immiscible phase, and in complexity of deposit types and their zoning patterns (Lang et al. 2000). In contrast to classic porphyry-related deposits, intrusion-related gold systems are characterised by CO_2 rich fluids, a metal assemblage characterised by Au, Bi, As, and Te (with lesser W, Mo, Sn, Pb and Sb), low sulphide volumes and small volumes of hydrothermal fluid. Intrusion-related systems are also characterised by a close association with reduced intrusions and restricted alteration, compared to the kilometre-scale alteration associated with porphyries.

The 'orogenic lode gold' or 'mesothermal' style deposits also have similar features to intrusion-related gold systems. Common features shared between the two deposit classes include dominance of CO_2 rich fluids, and a similar metal assemblage (e.g. Au, As, Te ± W, Mo and Sb). The two deposit styles have differing alteration assemblages; intrusion-related gold deposits are typically fracture controlled and have rarer pervasive alteration that can include felspathic, sericitic, silicic, greisen, calc-silicate, and/or advanced argillic types; orogenic lode gold deposits have halos of strong sericite-ankeritic carbonate alteration, and alkali feldspar alteration is generally moderately developed or absent (Lang & Baker 2001).

Intrusion-related gold deposits also possess similarities to reduced tin-tungsten rich magmatic hydrothermal systems (Thompson & Newberry 2000). Their similarities include the reduced composition of the intrusion, the presence of CO_2-rich fluids, similar tectonic setting, and similar depths of formation (<~8km). The main differences are that intrusion-related gold deposits have lesser amounts of fluid, less alteration, intrusions are not as consistently peraluminous, greater lateral extent and diversity of deposit styles (Lang & Baker 2001).

Although intrusion-related gold deposits do possess similar features to other more conventional deposit classes their differences as depicted in the literature do warrant a separate classification. The new classification class, 'intrusion related gold', has led to improved understanding of common features through additional studies, with the benefits including advancements in developing a more comprehensive exploration model.

2. Geological features of major examples

The best documented examples of intrusion-related gold style deposits are from the Tintina Gold Belt in the Yukon (Canada) and Alaska (USA); they include Fort Knox, Donlin Creek, Pogo, Dublin Gulch, True North and Brewery Creek. Other examples include Mokrsko (Czech Republic), Vasilkovskoe (Kazakstan), Salave (Spain), Korri Kollo (Bolivia) and from Australia, Kidston and Timbarra.

It is agreed upon in the literature (Goldfarb et al. 2000; Hollister 1992; Lang & Baker 2001; Lang et al. 2000; Lang et al. 1997; McCoy et al. 1997; Newberry 2000; Newberry et al. 1988; Newberry, McCoy & Brew 1995; Sillitoe 1991; Thompson et al. 1999) that there are several features common among intrusion-related gold deposits/provinces:

1. A spatial and temporal association with predominantly metaluminous, subalkalic intrusions of felsic to intermediate composition that span the boundary between ilmenite and magnetite series.
2. A metal assemblage characterised by Au, Bi, As, and Te and to a lesser extent W, Mo, Sn, Pb and Sb.
3. A reduced sulphide mineral assemblage commonly including pyrrhotite, pyrite, arsenopyrite, and loellingite.
4. Low sulphide mineral volume (typically less than 5 vol% of veins).
5. Comparatively (e.g. to porphyry style) restricted zones of predominantly fracture controlled hydrothermal alteration.
6. CO_2-rich hydrothermal fluids.
7. Formation within a continent, well inboard of inferred or recognised convergent plate boundaries.

The characteristics of intrusion-related gold deposits with resources >0.5 million ounces are summarised in Table 1 (Baker, T. 2002). The deposits are listed in order of depth (km) of formation. Depth of formation is an important factor controlling a number of features, in particular fluid composition and deposit style.

Depth of magma emplacement has a systematic effect on mineralisation style (Figure 1). The deposits exhibit a range of characteristics that vary over a wide range of emplacement depths (<1 to >7 km) and pressures (<0.5 kbar to >2 kbar) (Baker, T. 2002). Deposits in shallow crustal settings (~<5 km) are associated with sheeted veinlets, stocks, sills, dykes and volcanic domes (e.g. Korri Kollo, Brewley Creek, Donlin Creek and Shotgun deposits) and include systems with epithermal-like veins to breccia and stockworks similar to porphyry type settings. Deeper systems (~>5km) have characteristics of mesothermal environment deposits, and are hosted by plutons containing sheeted veins, flat lenses, greisen and disseminated gold (eg Fort Knox, Pogo, Salvae and Timbarra).

Data on gold-bismuth correlation from the Fairbanks district indicates the Fort Knox deposit to have the strongest and highest correlation (McCoy et al. 2002) which in relation to other deposits in the district is the deepest emplaced, contains the most early high temperatures sheeted and/or stockwork veins and has the least shear hosted gold ore in surrounding schist. This observation is in agreement with the fact that gold and bismuth have paired mineralogy at high temperatures and are thus best correlated in deep and/or intrusion proximal deposits.

As previously stated, intrusion-related gold mineralisation has a 'spatial and temporal' relationship with its associated intrusion. Intrusion-related gold deposits have a range of hosts. They range from entirely intrusion-hosted, such as Fort Knox (Bakke 1995) and Dublin Gulch (Lang et al. 2000), to systems hosted by both intrusions and wall rocks, such as Mokrsko (Moraveck 1995), Salvae (Harris, M. 1980) and Vasilkovskoe (Spiridinov 1996), to deposits primarily hosted by country rocks, such as Brewery Creek (Diment & Craig 1998), True North (Harris, R. & Gorton 1998), and Pogo (Smith et al. 1999). According to Mustard (2001), Timbarra (Australia) lies at the 'intrusion-hosted end of this continuum, and is similar to most other intrusion-hosted deposits, which are genetically associated only with particular phases of composite intrusive bodies'. For example the Timbarra deposit is predominantly associated with coarser-grained intrusive units within the interior of the pluton.

TABLE 1. Characteristics of Intrusion-Related Gold Deposits with Resources >0.5 M oz (after Baker, 2002)

Deposit	Size (Mt)	Grade(g/t Au)	Host Intrusion	Deposit Style	Metal suite	Au/Bi r[2]	Ore minerals	Alteration	Fluids (T=°C, S= wt%NaCl equiv)	(kbar)/ Depth (km)	References
Korri Kollo, Bolivia	64	2.3	Dacite domes, I?	Sheeted veinlets	Ag, As, Sb, Sn, Bi, Cu, Zn, Pb, W	?	Py, Apy, Ccp, Gal, Bim, Sbn, Sph	Argillic	Early H_2O-NaCl brine S = 8-45, T >300; later H_2O-NaCl S =5-15, T =200-350	<0.5/0.4-0.8	Peterson and Fitzmeyer (1998)
Brewery Creek, Yukon	13.3	1.4	Monzonite sills, I>M	Disseminated and veinlets	As, Sb, (Hg)	Abs	Py, Po, Apy, Sbn	Qtz, Ser, Carb, Clay	Immiscible H_2O-NaCl brine S > 40, vapour (CO_2) S < 3, T >450; later H_2O-CO_2-NaCl, S < 10, T <250	~0.5/~2.0	Diment (1996); Dunne (1995)
Donlin Creek, Alaska	323	2.9	Rhyolite sills/dikes, I	Veins, veinlets	Ag, As, Sb, Hg	Abs	Py, Apy, Sbn	Qtz, Ser, Carb, Clay	Immiscible H_2O-NaCl brine and vapour (CO_2) T >550; later H_2O-CO_2-NaCl, T =150-260	~0.5/~2.1	Ebert et al. (2000)
Shotgun, Alaska	~1 M oz		Granite stock, I	Stockwork and breccia	Bi, Te, Mo, As, Cu	0.73	Apy, Po, Lo, Py, Ccp, Sch	Ab, Ser, Qtz, Carb	Immiscible H2O-NaCl brine S >40, vapour (CO2) T =350-650	~0.5/~2.2	Rombach and Newberry (2001)
Kidston, Australia	94	1.48	Rhyolite porphyry stock, I>M	Breccias and sheeted veins	Bi, Mo, W, As, Te, Zn, Cu, Pb, Sn	?	Py, Po, Apy, Bim, Ccp, Sph, Mol, Gal	Qtz, Ser, Carb	Immiscible H_2O-NaCl brine and vapour (CO_2) T ~400-540; late H_2O-NaCl, S < 10, T =170-350	~0.8/~3.0	Baker and Andrew (1991)
Vasilkovskoe, Kazakstan	80	3.7	Granodiorite pluton, I	Sheeted	As, Sb, W, Pb, Cu, Bi, Te	?	Py, Po, Bim, Ccp, Sph, Gal, Mol, Sbn, Sch	Ab, Ser, Qtz, Carb	CO_2-H_2O-NaCl, S = <11, T =150-250	>1.0/>3.0	Spiridonov (1996)
Dublin Gulch, Yukon	50.3	0.93	Granodiorite pluton, I	Sheeted	Bi, Te, Mo, As, Sb,W, Pb, Cu	0.89	Py, Po, Apy, Bim, Sch, Gal, Pb-Bi-Te S	Ksp>Ab, Qtz, Ser, Carb	Early CO_2-H_2O-NaCl-CH_4, T =250-350; late low XCO_2,H_2O-NaCl S =5-15, T =150-250	>1.1/>3.5	Maloof et al. (2001)
Mokrsko, Czech Rep.	66	1.5	Granodiorite pluton, I	Sheeted	As, Bi, Te, Mo, W, Sb	?	Py, Po, Apy, Mol, Sch, Bim	Ab, Amp, Bt, Qtz	CO_2-H_2O-NaCl, S = <10, T =330 ± 20	~1.5/~5.0	Boiron et al. (1995)
Fort Knox, Alaska	158	0.83	Porphyritic granite pluton, I	Sheeted	Bi, Te, Mo, As, Sb,W	0.86	Apy, Py, Sbn, Sch, Po, Lo, Mol, Bim	Ab, Qtz, Ser, Carb	CO_2-H_2O-NaCl-CH_4, S = 2-9, T =300-480	>1.5/>5.0	McCoy et al. (1997)
Pogo, Alaska	10	~15	Granite, aplites, I	Flat lenses	Bi, Te, As, Ag, Cu, Pb	0.89	Apy, Py, Po, Lo, Bim	Bi, Qtz, Ser, Carb	CO_2-H_2O-CH_4, S < 10, T =300-600	>1.7/>5.0	Smith et al. (1999)
Salave, Spain	~15	~2	Granodiorite pluton, I	Disseminated (greissen)	As, Sb, Mo, W, Zn, Cu	?	Mol, Sph, Gal, Cep	Ab, Ser, Carb	CO_2-H_2O-NaCl	?	Harris (1980)
Timbarra, Australia	13	0.95	Granodiorite pluton, I>M	Disseminated	Bi, Mo, Sb, As, Ag	0.69	Mol, Bim, Py, Apy	Ab, Qtz, Ser, Carb	CO_2-H_2O-NaCl, S < 10, T =200-400	~2.0/~7.0	Mustard (2001)
Jilau, Tajikstan	54	1.1	Granodiorite pluton, I	Sheeted	Bi, Te, W, As, Cu	?	Bim, Sch, Cpy, Py, Apy	Qtz, Fsp, Carb, Ser	Early CO_2-H_2O-NaCl-CH_4, T =300-450; late H_2O-NaCl S =2-14, T =130-300	~2.2/~8.0	Cole et al. (2000)

Abbreviations: Ab=Albite, abs = no bismuth reported, Apy = arsenopyrite, Bim = bismuthinite, Bt = biotite, Carb = carbonate, Ccp = chalcopyrite, Fsp = felspar, Gal = galena, I = ilmenite series, I>M = ilmenite series more abundant than magnetie series, Ksp = K felspar, Lo = loellingite, M = magnetite series, Mol = molybdenite, Po = pyrrhotite, Py = pyrite, Qtz = quartz, S = salinity, Sbn = stibnite, Sch = scheelite, Ser = sericite, Sph = sphalerite, T = temperature, ? Au/Bi not reported

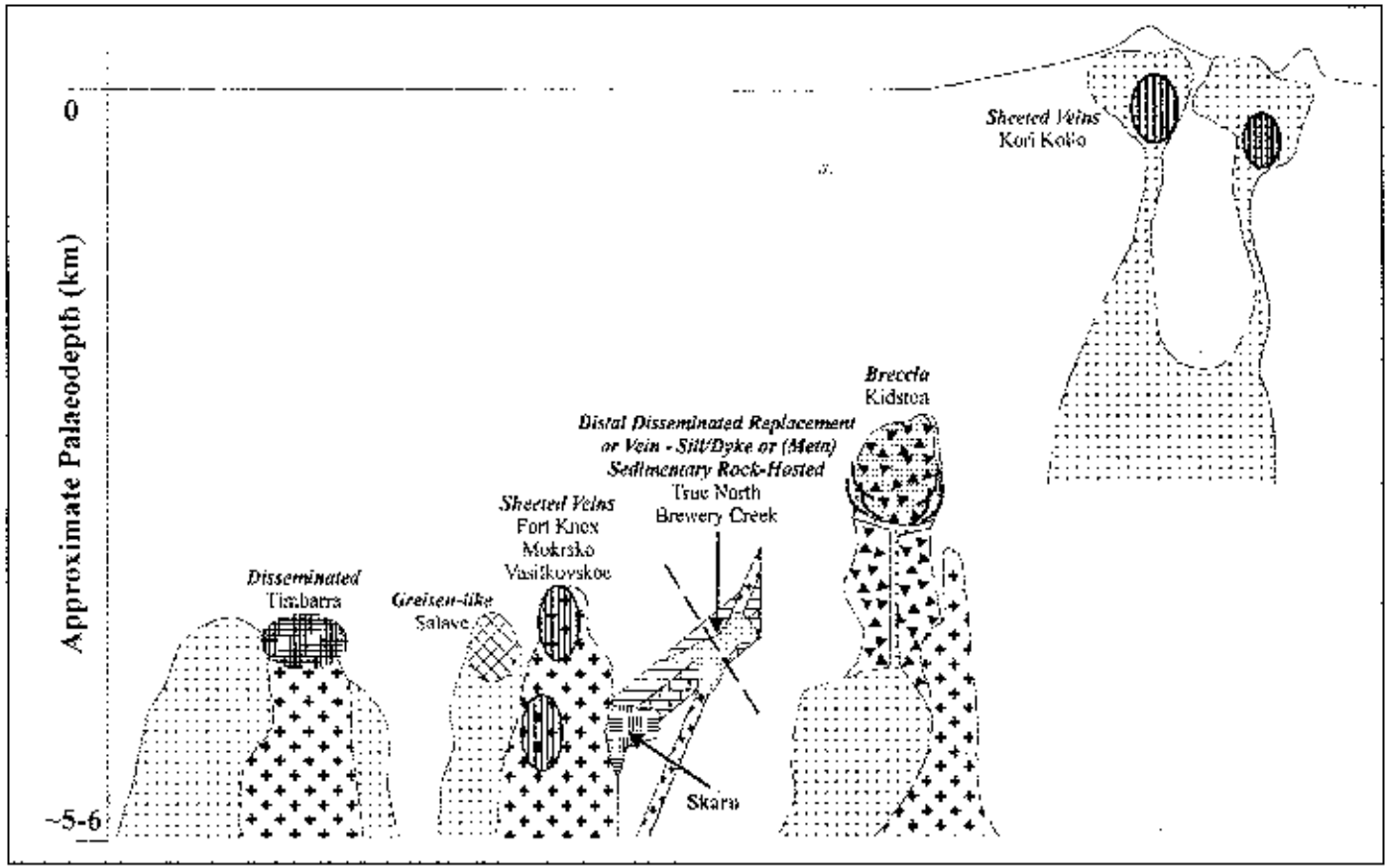

Figure 1 Schematic model from Thompson et al. (1999) showing the different styles of gold deposits in relation to emplacement depth of their genetically related intrusions. Figure 1 suggests that mineralisation may form discontinuously over vertical intervals of approximately 6Km.

3. Intrusion characteristics

Intrusions associated with intrusion-related gold deposits are relatively reduced I-type felsic intrusions (Thompson & Newberry 2000). The intrusions being predominantly felsic, are typically granite to granodiorite in composition (Thompson et al. 1999). The igneous centres associated with intrusion-related gold deposits typically form multiphase complexes that were rapidly emplaced and cooled quickly (Lang & Baker 2001). These complexes include batholiths, large or small plutons, irregular plugs, dome complexes, or swarms of dykes and sills (Lang et al. 2000; Newberry 2000; Thompson et al. 1999). Intrusions are surrounded by contact metamorphic aureoles that vary widely in size (Figure 4).

3.1 Tectonic Setting

It is agreed upon in the literature (Baker, T. 2002; Baker, T. & Lang 1999; Lang & Baker 2001; Lang et al. 1997; McCoy et al. 2002; Thompson et al. 1999) that intrusion-related gold deposits occur in a continental setting well inboard of convergent plate margins, however, the tectonic environment in which these deposits form is poorly understood. Other proposed tectonic settings have included back-arc, foreland fold-thrust, collisional, post collisional and magmatic arc environments (Goldfarb et al. 2000; Thompson et al. 1999) Studies on the Tintina gold belt by Flanigan et al. (2000) have illustrated spatial and temporal variations in the tectonic environment across a plutonic province containing multiple intrusion-related gold deposits. According to Thompson et al (1999) most intrusion-related gold deposits formed above or within old, typically cratonic, continental crust. It can be assumed that no one tectonic regime can model the formation of intrusion-related gold deposits across or within individual plutonic provinces. Thompson (1999) suggested that siliciclastic (meta)sedimentary sequences seem to provide particularly favourable sites for generation of such magmatic provinces, which range in age from Precambrian to Tertiary. A generalised model for the generation of magmas associated with intrusion related gold systems is illustrated in Figure 2.

3.2 Role of Contamination

Felsic magmas that have high CO_2 contents commonly contain a significant amount of assimilated crust (Baker, T. 2002). This is applicable to those associated with intrusion-related gold deposits (Lang et al. 2000; Lowenstern 2001). Evidence exists for involvement of continental crust in magmas from at least several of the major documented examples, however its affect on metal sourcing, especially gold, is unclear (Thompson et al. 1999). Such magmas will have low Cl/H_2O ratios, <0.035 (Candela & Piccoli 1995). Therefore, the bulk magmatic composition of magmas associated with intrusion-related gold may be at the lower end of the typical NaCl range (~2-10 wt %) and this likely restricts the amount of chlorine available to form brines under immiscible conditions.

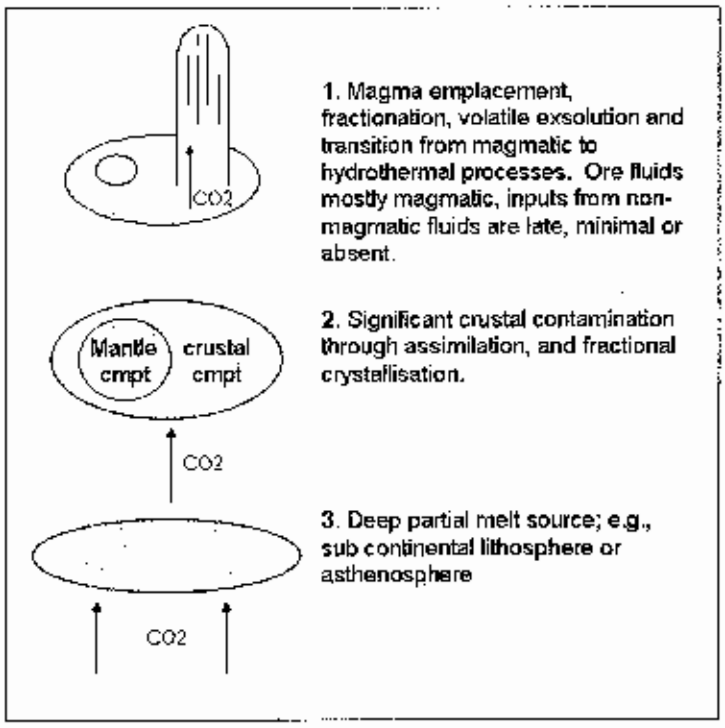

Figure 2 *Schematic model from Lang & Baker (2001) illustrating the important processes responsible for generating magmas associated with intrusion-related gold systems. 3. Generation of primitive melts (dark shades) during partial melting of sub continental lithosphere and/or asthenosphere. 2. Magma rises through crust and undergoes substantial assimilation and fractional crystallisation inferred from Nd and Sr isotopes and geochemistry (Lang et al. 2000). 1. Magma emplacement, further fractionation, and exsolution of CO_2-rich volatile phase resulting in intrusion-related gold mineralisation (Baker, T. & Lang 2001; McCoy et al. 1997; Mustard 2001).*

3.3 Oxidation States

Major deposits of porphyry type (Cu-Au and Au only) are typically associated with highly oxidised, calc-alkaline to alkaline, intermediate (diorite-monzonite) I-type intrusions (Sillitoe 1993). Kaszuba and Wendlandt (2000) have proposed that CO_2 may play an important role in the production of alkali-rich magmas. Intrusion-related gold deposits are related to broadly similar I-type intrusions. However, Thompson (1999) suggested that the relatively reduced character of the gold bearing suites may reflect their passage through thick, upper-crustal sequences of reduced marine siliciclastic rocks. Several of the best documented intrusive-related gold deposits are hosted within rock units of this type. However, the oxidation state of the intrusions associated with intrusion-related gold deposits varies significantly from province to province. Some intrusions contain magnetite whereas others are ilmenite bearing. Thompson et al. (1999) classified most intrusions associated with these deposits as 'reduced, subalkalic, metaluminous, I-type intrusions', with 'intermediate oxidation states around the boundary between the magnetite and ilmenite series' (Figure 3). Magnetite is absent in the Fairbanks district granites, and rare in those in the Yukon, whereas minor amounts of ilmenite are common throughout, suggesting that the intrusions are moderately reduced and assignable to the ilmenite series (McCoy et al. 1997). Low sulphide mineral volume is a common trait of many intrusion-related gold systems. Intrusion-related gold systems are shown to have a reduced lithophile element association (Thompson et al. 1999) as illustrated in Figure 3. This contrasts with deposit types such as porphyry Cu (-Mo-Au), which have higher sulphide contents and a more oxidised chalcophile element association (Figure 3).

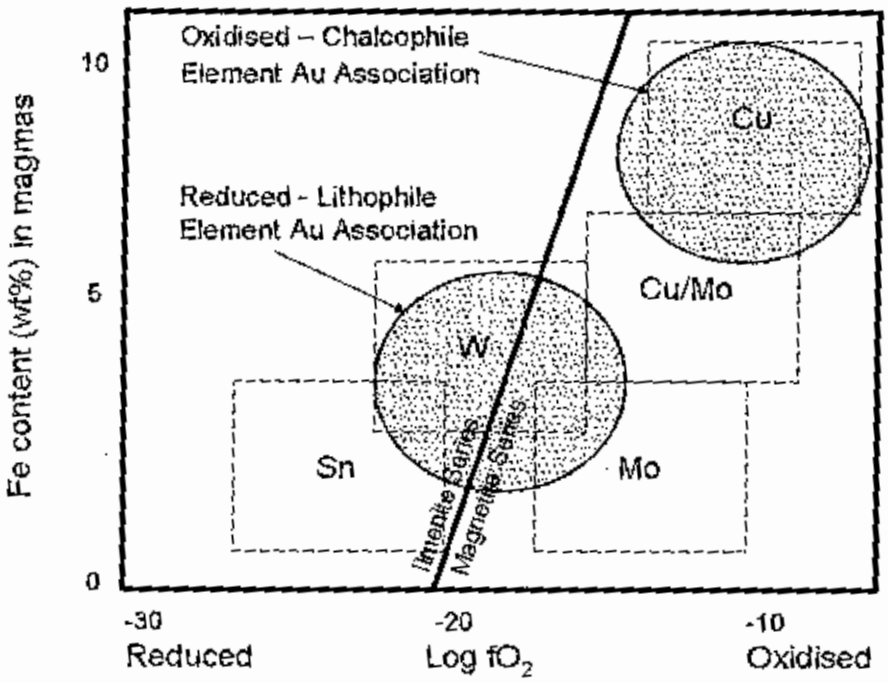

Figure 3 *Schematic plot after Thompson (1999) of degree of fractionation, shown by the Fe content of magmas associated with magmatic-hydrothermal copper, copper-molybdenum, molybdenum, tungsten and tin mineralisation. The generalised position of the moderately reduced, intrusion-related gold style deposits, with their tungsten (partial lithophile) association is highlighted and compared to the position of more typical copper-gold (chalcophile) systems. The approximate boundary between Ishihara's (1977) magnetite- and ilmenite-series magmas is also shown.*

3.4 Textures

Magmatic-hydrothermal transition textures, including miarolitic cavities, interconnected miarolitic textures (IMT's), unidirectional solidification textures (UST's), pegmatites and vein-dykes have been documented in granites associated with deposits, for example Timbarra (Candela & Blevin 1995; Mustard 2001, 2003b, 2003a; Mustard & Ulrich 2004). Magmatic-hydrothermal transition textures suggest evolution of magmatic volatile phases during crystallisation, and support a magmatic origin (Mustard 2003a). The occurrence of large miarolitic cavities (locally 1 to 2 m in diameter) at Emerald Lake, (Tombstone Plutonic Suit, Yukon, Canada) are interpreted as indicative of late stage volatile release while an intrusion was solidifying (Baker, T. & Lang 2001). The occurrence of magmatic-hydrothermal textures implies that these reduced granitoids exsolved magmatic volatiles, which were able to flow through cavities and accumulate in the roof zone of the magma chamber. The occurrence of Au-rich UST's (e.g., Timbarra) implies that these huge volumes of magmatic volatiles carried significant concentrations of metals. Candela and Blevin (1995) proposed that interconnected miarolitic textures develop at pressures less than approximately 2-3 kbars and that the texture is better developed at lower pressures. The major recognised intrusion-related gold deposits all are associated with intrusions that crystallised at pressures less than approximately 2.2 kbars, therefore conforming to this proposal.

4. Fluid/melt characteristics

The evolution of fluid composition in intrusion-related gold deposits is a result of depth (pressure-temperature conditions), and the effects that the behaviour of CO_2 will has on other volatiles in the melt (Baker, T. 2002). For example,
Webster and Holloway (1988) have shown that CO_2 in magmatic volatiles increases the solubility of chlorine and water and therefore the initial fluid exsolved from the melt will be more Cl-rich than later exsolution products. Evidence for such fluid evolution is present at the Emerald Lake and Dublin Gulch deposits, where moderate to high salinity fluids appear to have post-dated earlier low salinity CO_2-rich fluids (Baker, T. & Lang 2001). Nablek & Ternes (1997) documented similar evolution of hydrothermal fluid in the Harney Peak Granite, South Dakota. They interpreted the ore fluid to be entirely derived from magma, based upon isotope data indicating magmatic fluids and comparison with experimental work.

Thompson (1999) preferred a magmatic origin for CO_2-rich fluids in the intrusion-related deposits because of the fluids spatial relationship to intrusions (Figure 1). The presence of CO_2 in melt inclusion, from the Timbarra deposit, Australia (Mustard 2003b) provides direct evidence for a magmatic origin for CO_2. Experimental studies on rhyolitic melts have shown that H_2O is ten times more soluble than CO_2 (Fogel & Rutherford 1990). CO_2 will therefore exsolve from felsic melts earlier and under higher pressures than H_2O (Mustard 2003a). Lowenstern (2001) demonstrated that, after water, CO_2 is the most common gas in volcanic exhalations. It has therefore been suggested by Nablek & Ternes (1997) that when such melts attain fluid saturation, the initial fluid released must be CO_2-rich. Subsequent fluid evolved from the magma will become H_2O-rich and more saline due to higher chloride solubility in aqueous as opposed to carbonic fluid. Intrusions that are emplaced in deeper environments appear to exsolve abundant CO_2, whereas shallower systems typically exsolve saline H_2O-rich fluids more readily (Figure 4).

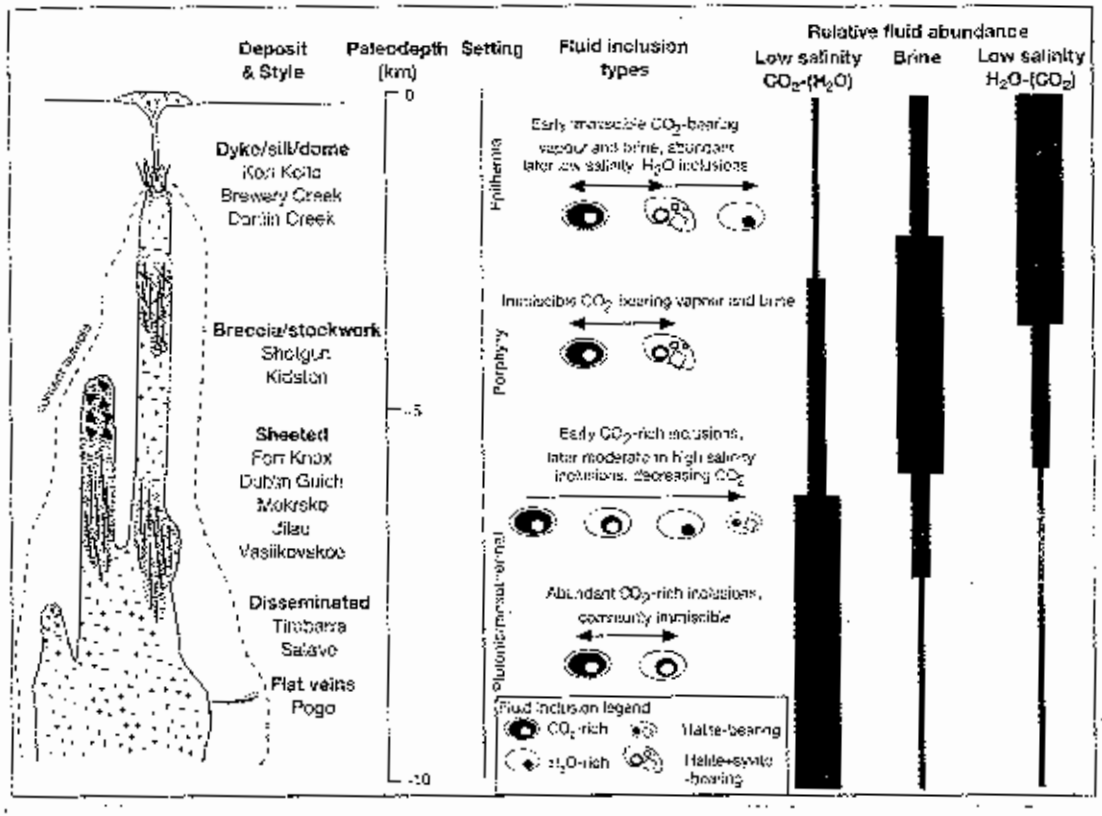

Figure 4 Schematic geological model showing the relationship between intrusion-related gold styles, paleodepth, and hydrothermal fluid types (from Baker (2002) in turn from a combination of Baker and Lang 2001; Lang and Baker 2001; Lang et al. 2001).

The effect of depth on an evolving intrusion' fluid chemistry has been documented in deposits from the Tombstone plutonic suit, Yukon, Canada. Sheeted veins at Mike Lake formed at less than 1 kbar and contain abundant high salinity brines in addition to CO_2-rich fluids. Veins at Emerald Lake and Dublin Gulch contain moderate to high salinity fluids and formed at pressures of >1 kbar, whereas those at Scheelite Dome and MacTung contain only low salinity CO_2-rich fluids and formed at pressures >2kbar (Baker, T. & Lang 2001).

Metal concentrations in melt and fluid inclusions from Timbarra, show Mo, W, Sn, Bi and Au partitioning toward the melt and Cu, Zn, As and Pb (±Sb) moderately to strongly toward the aqueous fluid (Mustard, Ulrich & Mernagh 2004). The characteristic metal assemblage for intrusion-related gold deposits of Au, Bi, As, and Te and to a lesser extent W, Mo, Sn, Pb and Sb, corresponds with this finding. It is therefore logical to assume that these metals would have a common set of genetic processes (source, transport, concentration and deposition).

5. Genesis

5.1 Gold source

According to Thompson et al. (1999), the distinct spatial association with felsic intrusions, combined with the consistent metal signature, suggest a magmatic-hydrothermal origin for intrusion-related gold deposits. Evidence from fluid/melt studies, as previously mentioned, also provides convincing evidence for a magmatic-hydrothermal fluid source. The presence of a Bi-W-As assemblage in several intrusion-related gold regions worldwide is suggestive that a common set of genetic processes was in effect. A range of data including field relationships, geochronology, stable isotopes, fluid inclusions, metal associations and magmatic hydrothermal textures all provided compelling evidence of a magmatic origin for gold at the Timbarra deposit, Australia. The recent detection of gold in silicate-melt inclusions from Timbarra provides yet more critical evidence for this magmatic origin (Mustard & Ulrich 2004).

5.2 Gold concentration

Fractionation of felsic magma may concentrate gold so long as it behaves incompatibly (Cygan & Candela 1995). Burrows and Spooner (1989) have showed that gold was progressively enriched through fractional crystallisation processes in the Val d'Or and Timmins intrusions, Canada. The discoveries of gold in silicate- melt inclusions at the Timbarra deposit, Australia (Mustard, Ulrich & Mernagh 2004) suggest gold preferentially partitioning toward the melt. The presence of gold within melt inclusions from primarily the most fractionated stages of the pluton support this model of incompatible enrichment of gold in late stage granitic melts.

Candela and Blevin (1995) suggested for a high temperature magmatic hydrothermal mineral deposits in, or near, the apical region of a pluton (including intrusion-related gold systems such as Timbarra, Australia) large quantities of the magmatic volatile

phase need to be channelled to the apical region. This in turn must occur before significant cooling to prevent dilution of the aqueous fluid and subsequent dispersal of the ore material. They also illustrated that early establishment of connectivity within melts is favoured by higher initial water concentrations and lower pressures (i.e. higher molar volumes for water).

The degree of enrichment in different metals in and around the intrusions may reflect magma chemistry, proximity of peripheral mineralised zones to intrusions and local conditions of ore formation (Thompson et al. 1999). Evidence for magmatic concentration of gold is the metal association, especially high bismuth (>100ppm and in many cases >1000ppm). The gold-bismuth correlation common in many intrusion-related gold deposits, and vertical and lateral zoning of metals around intrusions support a magmatic hydrothermal origin for mineralisation and CO_2-rich fluids (Thompson et al. 1999).

5.3 Gold transport

Heinrich et al (1999) suggested that Na, K, Fe, Mn, Zn, Rb, Cs, Ag, Sn, Pb, and Tl partitioned into brine (probably as a chloride (Cl^-) complex), whereas Cu, Au and As preferentially partitioned into both the brine and vapour (probably as a bisulphide (HS^-) complex) from micro-analytical studies on inclusions from a range of magmatic-hydrothermal ore deposits. At Timbarra, all inclusions are low salinity thus Au transport as a Cl^- complex is unlikely. However, in shallow systems (e.g. Korri Kollo) saline fluids are much more abundant and thus Au transport by a Cl^- complex is feasible. S preferentially fractionates into the vapour phase and therefore Au transport as an HS^- complex is probable (Mustard 2003b). Seward (1991) proposed Au as likely to be transported as a bisulphide complex due to the reduced conditions and low salinity of the fluids. Bismuth is likely to be transported and precipitated in a similar way, given its strong correlation with gold in deeper systems such as Fort Knox, Dublin Gulch and Pogo (Baker, T. 2002). Chloride complexing may be important in shallow systems such as the Shotgun deposit (Baker (2002). A strong correlation exists between gold and bismuth regardless of fluid type. A potential increase in metal (gold) bearing bisulphide complexes can occur due to the early

release of CO_2 from a melt (Baker, T. 2002). Ore forming fluids may therefore be generated over a range of depths (pressures and temperatures). CO_2 in ore forming systems may promote unmixing and the formation of a vapour phase, causing H_2S to fractionate in to the vapour phase and act as a ligand for metals including Au (Lowenstern (2001).

5.4 Gold deposition

The importance of magmatic-hydrothermal transition textures on gold deposition is highlighted by the presence in many Yukon systems (Lang & Baker 2001; Lang et al. 2000) and at Timbarra (Mustard 2001) of late stage, mineralised aplites and pegmatites that grade laterally, and with time, to gold bearing quartz veins. 'These observations suggest that the ore-forming fluids were concentrated in late phases of crystallising intrusions' (Lang & Baker 2001). The melt and fluid inclusion relationships at Timbarra (Mustard 2003a) are consistent with entrapment of late stage melt with an associated high magmatic volatile content. Gold is likely to be transported as an HS^- complex in the vapour phase and deposited by crystallisation processes. Coulson et al. (2001) has shown that substantial changes in volatile activities accompany even subtle igneous fractionation in these systems and may account for instability in gold complexing and result in deposition.

Candela (1991) detailed three possible models for the behaviour of the magmatic volatile phase during crystallisation:

1. Rise of buoyant plumes of bubbles + liquid ± crystals in the crystallisation interval, transporting volatiles toward the top of the chamber;
2. Connectivity of magmatic volatile-phase volumes in the crystallisation interval, which may also promote upward flow of the magmatic volatile phase near the solidus; and
3. Little to no buoyancy or connectivity occurs; the magmatic volatile phase remains in a dispersed, trapped state in the crystallised pluton; the cooled, subsolidus magmatic volatile phase may mix with exogenous aqueous fluids when the pluton reaches temperatures low enough for thermoelastic cracking.

Baker & Lang (2001) have suggested that a variety of fluid processes may have been responsible for gold precipitation in the Tombstone-Tungsten magmatic belt including immiscibility and/or release of an evolving magmatic fluid. This may also be the case for other documented intrusion-related gold deposits. The most studied gold bearing species $Au(HS)_2^-$, AuHS and $AuCl_2^-$ will all precipitate out gold as a result of decreasing temperature, for example, during crystallisation (cooling). HS^- as the likely transport complex for gold in these systems in addition will precipitate gold as a result of an fO_2 decrease (reduction) and/or sulphide deposition.

The sulphide and ore mineral paragenesis within fractures from Dublin Gulch comprises early molybdenite, followed by galena, lead-bismuth ± antimony sulfosalts, bismuthinite, native bismuth, and gold. The late fractures and associated fill contain scheelite, arsenopyrite, pyrrhotite, and pyrite. Therefore, the gold and related bismuth minerals are interpreted to have formed after initial quartz-K-feldspar veining event, and its associated scheelite and early sulphide minerals. This is consistent with the hypothesis that deposition of early sulphides may have been a catalyst to gold deposition.

In the Fairbanks district, Alaska, gold first occurs in greater than ppm concentrations in pegmatite veins within the "causative" intrusions (McCoy et al. 1997; McCoy et al. 2002). Timbarra (Mustard 2001) and Fort Knox (Bakke 1995), among other deposits (Lang et al. 2000) share a similar paragenetic sequence for structurally controlled mineralisation, including early aplite dikes, vein-dikes and quartz-molybdenite veins, followed by fracturing and formation of later comb and chalcedonic quartz veins. This magmatic hydrothermal evolution is typical of intrusion-related gold deposits (Lang et al. 2000; Thompson et al. 1999), i.e., from truly magmatic textures (miarolitic cavities and UST's) to magmatic-hydrothermal veins.

5.5 Alteration

Typical alteration associated with intrusion-related gold systems is fracture controlled and rarer pervasive alteration that can include felspathic, sericitic, silicic, greisen, calc-silicate, and/or advanced argillic. Systems dominated by sheeted veins (e.g. Fort Knox and Mokrsko) are characterised by macroscopically visible alteration restricted

to narrow envelopes around individual sheeted veins. This implies a very confined fluid flux. However, in some deposits (e.g. Salave) intensely pervasive alteration zones are widespread and textually destructive, implying that less focussed fluid flow also occurs.

At the Dublin Gulch deposit (Yukon, Canada) there are consistent variations in vein assemblages and alteration throughout the sheeted vein complex. Variations along the length of veins suggest progressive changes in fluid chemistry and subsequent mineral deposition during a single vein forming event (Maloof, Baker & Thompson 2001).

5.6 Conclusion

The aqueous complexes responsible for metal transport in these deposits are uncertain due to the presence of variable fluid types i.e. high salinity, low salinity and CO_2-rich etc. However, it seems reasonable to assume that gold in shallow systems (e.g., Korro Kollo) where saline fluids prevail, is transported as a chloride complex, and gold in deeper systems (e.g. Fort Knox), that lack saline fluids and is transported as a bisulphide complex.

Metal concentration processes are important in restricting dispersal of ore material and formation of uneconomic disseminations. In the case of Timbarra, timing of magmatic volatile migration and crystallisation was an important factor. A number of factors, including magma composition, distances from mineralised zones to the intrusion, and fluid composition, seem to play important roles in ore concentration.
Gold deposition appears to be the result of magma fractionation and crystallisation processes. Cooling may be the primary depositional mechanism assuming gold is transported as an HS^- complex in the vapour phase.

The effect of structural controls on intrusion-related gold deposits is lacking. Knowledge from more studied structurally controlled deposit types such as orogenic lode gold, suggest deposit location and geometry (on all scales), fluid pathways, emplacement of intrusions, localisation of alteration and ore, could all be influenced by regional and local stress regimes. Structural controls are worthy of further study with respect to intrusion-related gold mineralisation.

6. Exploration strategies

6.1 Regional Scale

Prospective regions may be evaluated and potentially determined using a geographic information system (GIS) and/or data base approach. The inputs being parameters of intrusive-related gold deposit, common features including: tectonic setting, favourable intrusive bodies/provinces, and/or intrusion-related tungsten-tin provinces.

Exploration for intrusion-related gold should be conducted in continental settings well inboard of a convergent plate margins, however, considerations should also include back-arc, foreland fold-thrust, collisional, post collisional and magmatic arc environments. Due to the level of uncertainty, tectonic setting should not be considered crucial in defining an exploration model but could be utilised in initial regional based investigation.

Felsic magmatic provinces would be most prospective, in which intrusions are characterised by a lower oxidation state spanning the boundary between magnetite and ilmenite series. Airborne geophysical techniques may be useful in locating favourable granite types. For example ilmenite series granites can be identified through their low magnetic signature.

Known intrusion-related tungsten-tin provinces represent highly prospective areas for intrusion-related gold mineralisation because the presence of lithophile metals
(Figure 3) shows that magmatic and post-magmatic processes favourable to metal concentration were active at the present erosion level (Thompson et al. 1999). These areas typically lack previous exploration targeting of intrusive-related gold style mineralisation. Areas of alluvial gold workings in particular determining their source of gold also represent potential targets.

Multiple mineralised centres in any province would require screening, as examples of intrusion-related gold suggest that major gold concentrations may be restricted to an individual deposit (e.g. Korri Kollo), discrete parts of provinces (eg. Georgetown block in northern Queensland) or mineralisation may be widespread (e.g. Tombstone Plutonic Suite, Yukon and Alaska). Screening would be required at variable scales, more detailed where mineralisation is widespread to prioritise targets.

6.2 Local scale

Geochemical prospecting should focus on key pathfinder elements in addition to gold itself that collectively characterise intrusion-related gold mineralisation. Elements most useful would include Au, Bi, As, and Te and to a lesser extent W, Mo, Sn, Pb and Sb. Au and Bi would be especially useful due to their documented correlation in many intrusion-related gold deposits (eg. Dublin Gulch, Fort Knox and Pogo). Gold and bismuth have paired mineralogy at high temperatures and are best correlated and most useful in exploration for deep and/or intrusion proximal deposits (McCoy et al. 2002). Intrusive units spanning granite to granodiorite in composition are most favourable targets. Whole rock geochemistry should also focus on targeting those elements (in addition to gold itself) characteristic of intrusion-related gold and/or which correlate best with gold as mentioned above.

Use of ground based geophysical techniques, such as magnetic susceptibility surveys, could potentially delineate and map intrusions undercover. Some deposits, for example Timbarra, form in the apical region of intrusions due to the migration and entrapment of the magmatic volatile phase transporting metals. Mapping and identification of this region through magnetic surveys could potentially identify such zones and/or most fractionated parts of an intrusion.

Field recognition of magmatic-hydrothermal transition textures including miarolitic cavities, interconnected miarolitic textures, unidirectional solidification textures, pegmatites and vein-dykes. These textures are important for looking at fractionation, magmatic-hydrothermal transition, alteration and vein generation history. For example miarolitic cavities, interconnected miarolitic textures, unidirectional

solidification textures, pegmatite's and vein-dykes present in many intrusion-related gold deposits suggest evolution of magmatic volatile phases during crystallisation and support a magmatic origin. In some intrusion-related gold deposits ore minerals are found in these zones, for example, mineralisation occurs in miarolitic cavities at Timbarra (Thompson et al. 1999).

Fluid inclusion studies have useful implications for ore deposit research and exploration. Fluid inclusion studies can be used to determine temperature, salinity pressure and depth of formation. Melt inclusions are also important in these systems and can give important information on magma composition, metal source and on the volatile phase. Studies of volatile composition may be useful in determining key factors responsible for metal transport and ore deposition, and identify chemical disequilibrium. Intrusion-related gold mineralising fluids are typically characterised by early CO_2 rich fluids of between ~300-~400°C and later cooler (~<300°C) saline brines of between ~5-15 wt% NaCl. Fluid inclusion studies should focus on determining composition (of multiple generations if present), pressure (depth of formation) and temperature of entrapment. Figure 4 (Baker, T. 2002) illustrates the relationship between deposit styles, paleodepth, and hydrothermal fluid types and may be essentially used as a basic exploration model for this style of deposit.

Identification of alteration assemblages surrounding veins and rarer pervasive alteration could be used to delineate prospective vein generations. Recognition of metal bearing fluid compositions would determine likely alteration assemblages.
With possible alteration assemblages including feldspathic, sericitic, silicic, greisen, calc-silicate, and/or advanced argillic differentiation of barren compared to metal bearing veins (or zones), exploration based solely on alteration, would be difficult. A more typical alteration assemblage of carbonate and feldspar is common with the addition of clay alteration typical of shallow systems (<3km, <1 kbar). The restricted nature of alteration in most intrusion-related gold systems makes alteration a less effective tool for targeting prospective zones. Further detailed study into alteration assemblages within these systems may however, improve the effectiveness of alteration as an exploration tool.

References

Baker, EM & Andrew, AS 1991, 'Geologic, fluid inclusion, and stable isotope studies of the gold-bearing breccia pipe at Kidston, Queensland, Australia', *Economic Geology*, vol. 86, pp. 810-30.

Baker, T 2002, 'Emplacement depth and carbon dioxide-rich fluid inclusions in intrusion-related gold deposits', *Economic Geology and the Bulletin of the Society of Economic Geologists*, vol. 97, no. 5, pp. 1111-7.

Baker, T & Lang, JR 1999, 'Geochemistry of hydrothermal fluids associated with intrusion hosted gold mineralization, Yukon Territory', in CJ Stanley, AH Rankin, RJ Bodnar, J Naden, BWD Yardley, AJ Criddle, RD Hagni, AP Gize, J Pasava, AJ Fleet, R Seltmann, C Halls, M Stemprok, B Williamson, RJ Herrington, RET Hill, HM Prichard, F Wall, CT Williams, I McDonald, JJ Wilkinson, D Cooke, NJ Cook, BJ Marshall, PG Spry, K Zaw, LD Meinert, K Sundblad, PW Scott, SHB Clark, E Valsami-Jones, NJ Beukes, HJ Stein, JL Hannah, F Neubauer, DJ Blundell, DHM Alderton, MP Smith, S Mulshaw & RA Ixer (eds), *Proceedings of the ... Biennial SGA Meeting, vol.5*, pp. 17-9.

---- 2001, 'Fluid inclusion characteristics of intrusion-related gold mineralization, Tombstone tungsten magmatic belt, Yukon Territory, Canada', *Mineralium Deposita*, vol. 36, no. 6, pp. 563-82.

Bakke, AA 1995, 'The Fort Knox "porphyry" gold deposit: structurally controlled stockwork and shear quartz vein, sulfide poor mineralization hosted by a Late Cretaceous pluton, east-central Alaska.' in TG Schroeter (ed.), *Porphyry deposits of the northwestern cordillera of North America*, Can Inst Min Metall Spec, vol. 46.

Boiron, MC, Barakat, A, Cathelineau, M, Durisova, J & Moravcek, P 1995, 'Microfissural ore fluid migration: The example of a granodiorite-hosted gold deposit (Mokrsko, Bohemia)', in J Pasava, B Kribek & K Zak (eds), *Mineral deposits: From their origin to their environmental impacts, A.A. Balkema, Rotterdam Brookfield, Prague, 1995, Proceedings*, 3rd Biennial SGA Meeting, pp. 97-100.

Burrows, DR & Spooner, ETC 1989, 'Relationships between Archean gold quartz vein shear-zone mineralisation and igneous intrusions in the Val d'Or and Timmins areas, Abitibi subprovince, Canada.' *Economic Geology*, vol. 84, pp. 424-44.

Candela, PA 1991, 'Physics of aqueous phase evolution in plutonic environments', *American Mineralogist*, vol. 76, pp. 1091-.

Candela, PA & Blevin, PL 1995, 'Do some miarolitic granites preserve evidence of magmatic volatile phase permeability?' *Economic Geology and the Bulletin of the Society of Economic Geologists*, vol. 90, pp. 2310-6.

Candela, PA & Piccoli, PM 1995, 'Model ore-metal partitioning from melts into vapour and vapour/brine mixtures', in JFH Thompson (ed.), *Magmas, fluids, and ore deposits*, Mineralogical Association of Canada Short Course Series, vol. 23, pp. 101-28.

Cole, A, Wilkinson, JJ, Halls, C & Serenko, TJ 2000, 'Geological characteristics, tectonic setting, and preliminary interpretations of the Jilau cold-quartz vein deposit, Tajikistan', *Mineralium Deposita*, vol. 35, pp. 600-18.

Coulson, IM, Dipple, GM & Raudsepp, M 2001, 'Evolution of HF and HCl activity in magmatic volatiles of the gold-mineralized Emerald Lake Pluton, Yukon Territory, Canada', *Mineralium Deposita*, vol. 36, pp. 594-606.

Cygan, GL & Candela, PA 1995, 'Preliminary study of gold partitioning among pyrrhotite, pyrite, magnetite, and chalcopyrite in gold-saturated chloride solutions at 600 to 700°C, 140 MPa (1400 bars)', in JFH Thompson (ed.), *Magmas, fluids, and ore deposits.*, Min Assoc Can Short Coarse Ser, vol. 23, pp. 129-37.

Diment, R 1996, 'Brewery Creek gold deposit, in Yukon exploration and geology: Field work report for 1995, Whitehorse, Yukon, Indian, and Northern Affairs Canada', *Exploration and Geological Services Division*, pp. 89-97.

Diment, R & Craig, S 1998, 'Brewery Creek gold deposit, central Yukon', in *Yukon Exploration Geology 1998*, Exploration and Geological Services Division, Yukon Region, Indian and Northern Affairs Canada, pp. 225-30.

Dunne, KPE 1995, 'Brewery Creek: Preliminary fluid inclusion study: Unpublished consultant report to Yukon Geology Program and Vicery Mining Pty., Vancouver B.C., Vicerory Mining Pty., 6p'.

Ebert, S, Miller, L, Petsel, S, Dodd, S & Kowalczyk, P 2000, 'Geology, mineralisation, and exploration at the Donlin Creek project, southwest Alaska', in TL Tucker & MT Smith (eds), *The Tintina gold belt: Concepts, exploration, and discoveries*, British Columbia and Yukon Chamber of Mines, Cordilleran Roundup 2000, pp. 99-114.

Flanigan, B, Freeman, C, McCoy, D, Newberry, RJ & Hart, CJR 2000, 'Paleo-reconstruction of the Tintina gold belt - implications for mineral exploration', in TL Tucker & MT Smith (eds), *The Tintina gold belt: concepts, exploration and discoveries.*, British Columbia and Yukon Chamber of Mines, vol. Special Volume 2, pp. 35-48.

Fogel, RA & Rutherford, MJ 1990, 'The solubility of carbon dioxide in rhyolite melts: A quantitative FTIR study.' *American Mineralogist*, vol. 75, pp. 1311-26.

Goldfarb, RJ, Hart, CJR, Miller, L, Farmer, GL & Groves, D 2000, 'The Tintina gold belt - a global perspective.' in TL Tucker & MT Smith (eds), *The Tintina gold belt: concepts, exploration and discoveries.*, British Columbia and Yukon Chamber of mines, vol. Special Volume 2.

Harris, M 1980, 'Gold mineralisation at the Salavae gold prospect Northwest Spain.' *Trans Inst Mining Metall, Appl Earth Sci*, vol. B89:B1-B4.

Harris, R & Gorton, R 1998, 'The True North project, Alaska.' in G Walton & J Jambor (eds), *Pathways '98 Extended Abstract Volume*, British Columbia and Yukon Chamber of Mines and the Society of Economic Geologists, pp. 80-2.

Heinrich, CA, Gunther, D, Audetat, A, Ulrich, T & Frischknect, R 1999, 'Metal fractionation between magmatic brine and vapor, determined by microanalysis of fluid inclusions', *Geology*, vol. 27, pp. 755-8.

Hollister, VF 1992, 'On a proposed plutonic porphyry gold deposit model', *Nonrenewable Resor*, vol. 1, pp. 293-302.

Kaszuba, JP & Wendlandt, RF 2000, 'Effect of carbon dioxide on dehydration melting reactions and melt compositions in the lower crust and the origin of alkaline rocks', *J Petrol*, vol. 41, no. 3, pp. 363-86.

Lang, JR & Baker, T 2001, 'Intrusion-related gold systems; the present level of understanding', *Mineralium Deposita*, vol. 36, no. 6, pp. 477-89.

Lang, JR, Baker, T, Hart, CJR & Mortensen, JK 2000, 'An exploration model for intrusion related gold systems.' *Soc Econ Geol News*, vol. 40, no. 1, pp. 7-75.

Lang, JR, Thompson, JFH, Mortensen, JK, Baker, T, Sillitoe, RH & Anonymous 1997, 'Intrusion-related Au mineralization associated with lithophile elements; an under-recognized metallogenic association', in *Abstracts with Programs - Geological Society of America*, Geological Society of America (GSA), Boulder, vol. 29, p. 358.

Lowenstern, JB 2001, 'Carbon dioxide in magmas and implications for hydrothermal systems', *Mineralium Deposita*, vol. 36, no. 6, pp. 490-502.

Maloof, TL, Baker, T & Thompson, JFH 2001, 'The Dublin Gulch intrusion-hosted gold deposit, Tombstone plutonic suite, Yukon Territory, Canada', *Mineralium Deposita*, vol. 36, no. 6, pp. 583-93.

McCoy, DT, Newberry, RJ, Severin, K, Marion, P, Flanigan, B & Freeman, C 2002, 'Paragenesis and metal associations in interior Alaska gold deposits; an example from the Fairbanks district', *Mining Engineering*, vol. 54, no. 1, pp. 33-8.

McCoy, DT, Newberry, RJ, Layer, PW, DiMarchi, JJ, Bakke, A, Masterman, JS & Minehane, DL 1997, 'Plutonic related gold deposits of interior Alaska.' in RJ Goldfarb & LD Miller (eds), *Ore deposits of Alaska*, Soc Econ Geol News, vol. 9.

Moraveck, P 1995, 'The Mokrsko gold deposit', in P Moraveck (ed.), *Gold deposits of the central SW part of the Bohemian massif*, 3rd Biennial SGA Meeting, Prague, Excursion Guide, pp. 33-61.

Mustard, R 2001, 'Granite-hosted gold mineralization at Timbarra, northern New South Wales, Australia', *Mineralium Deposita*, vol. 36, no. 6, pp. 542-62.

---- 2003a, 'The magmatic-hydrothermal transition at Timbarra: Implications for the genesis of intrusion-related gold deposits.' in DGEc al (ed.), *Mineral Exploration Sustainable Development*, Millpress, Rotterdam, Netherlands, 2003, vol. 1, pp. 355-8.

---- 2003b, 'Carbon dioxide bearing melt inclusions within a gold-mineralized felsic granite', in DGEe al (ed.), *Mineral Exploration Sustainable Development*, Millpress, Rotterdam, Netherlands, 2003, vol. 1, pp. 351-4.

Mustard, R & Ulrich, T 2004, 'A melt-inclusion study on the behaviour of gold and other metals (Sn, W, Mo, Bi, As, Cu, and Sb) during fractional crystallisation of a felsic magma', in *Dynamic Earth: Past, Present and Future*, Geological Society of Australia, vol. Abstacts 73, p. 103.

Mustard, R, Ulrich, T & Mernagh, T 2004, 'The partitioning of gold and other metals between coexisting silicate melt and CO_2-rich low-salinity aqueous fluid at the magmatic-hydrothermal transition', in *Dynamic Earth: Past, Present and Future*, Geologicial Society of Australia, vol. Abstracts 73, p. 104.

Nablek, PI & Ternes, K 1997, 'Fluid inclusions in the Harney Peak granite, Black Hills, South Dakota, USA: implications for solubility and evolution of magmatic volatiles and crystallization of leucogranite magmas', *Geochim Cosmochim Acta*, vol. 61, pp. 1447-65.

Newberry, RJ 2000, 'Mineral deposits and associated Mesozoic and Tertiary igneous rocks within the interior and adjacent Yukon portions of the "Tintina gold belt": a progress report.' in TL Tucker & MT Smith (eds), *The Tintina gold belt: concepts, exploration and discoveries.*, British Columbia and Yukon Chamber of Mines., vol. Special Volume 2, pp. 59-88.

Newberry, RJ, McCoy, DT & Brew, DA 1995, 'Plutonic-hosted gold ores in Alaska: igneous versus metamorphic origins.' *Resour Geol Spec Issue*, vol. 18, pp. 57-100.

Newberry, RJ, Burns, LE, Solie, DN & Clautice, KH 1988, 'A revised geologic model for the North Star gold belt, interior Alaska: progress report.' *Division of Geological and Geophysical Surveys Public-Data File*, pp. 88-23.

Petersen, EU & Fitzmayer, JR 1998, 'The alunite-sericite association: A new type of epithermal precious metal deposits', *Geological Society of America Program with Abstracts*, vol. 30, p. A127.

Seward, TM 1991, 'The hydrothermal geochemisrty of gold.' in RP Foster (ed.), *Gold metallogeny and exploration*, Glasgow, Blackies, pp. 165-209.

Sillitoe, RH 1991, 'Intrusion related gold deposits', in RP Foster (ed.), *Gold metallogeny and exploration.*, Blackie, Glasgow., pp. 165-209.

---- 1993, 'Gold-rich porphyry copper deposits: Geological model and exploration implications.' in RV Kirkham, WD Sinclair, RI Thorpe & JM Duke (eds), *Mineral deposit modeling*, Geol Assoc Can, vol. Spec Pap 40, pp. 465-78.

Smith, M, Thompson, JFH, Bressler, J, Layer, PW, Mortensen, JK, Abe, I & Takaoka, H 1999, 'Geology of the Liese Zone, Pogo property, east-central Alaska', *SEG Newsletter no. 38*.

Spiridinov, EM 1996, 'Granite rocks and gold mineralisation of North Kazahkstan', in V Shatov, R Seltmann, A Kremenetsky, B Lehmann, V Popov & P Ermolov (eds), *Granite related ore deposits of central Kazahkstan and adjacent areas*, Glagol Publishing House, St Petersburg, pp. 197-217.

Thompson, JFH & Newberry, RJ 2000, 'Gold deposits related to reduced granitic intrusions', *Reviews in Economic Geology*, vol. 13, pp. 377-400.

Thompson, JFH, Sillitoe, RH, Baker, T, Lang, JR & Mortensen, JK 1999, 'Intrusion-related gold deposits associated with tungsten-tin provinces', *Mineralium Deposita*, vol. 34, no. 4, pp. 323-34.

Webster, JD & Holloway, JR 1988, 'Experimental constraints on the partitioning of Cl between topaz rhyolite melt and H_2O and $H_2O + CO_2$ fluids: New implications for granite differentiation and ore deposition.' *Geochim et Cosmochim Acta*, vol. 51, pp. 2091-105.

Appendix B

Enterprise Vein long projection

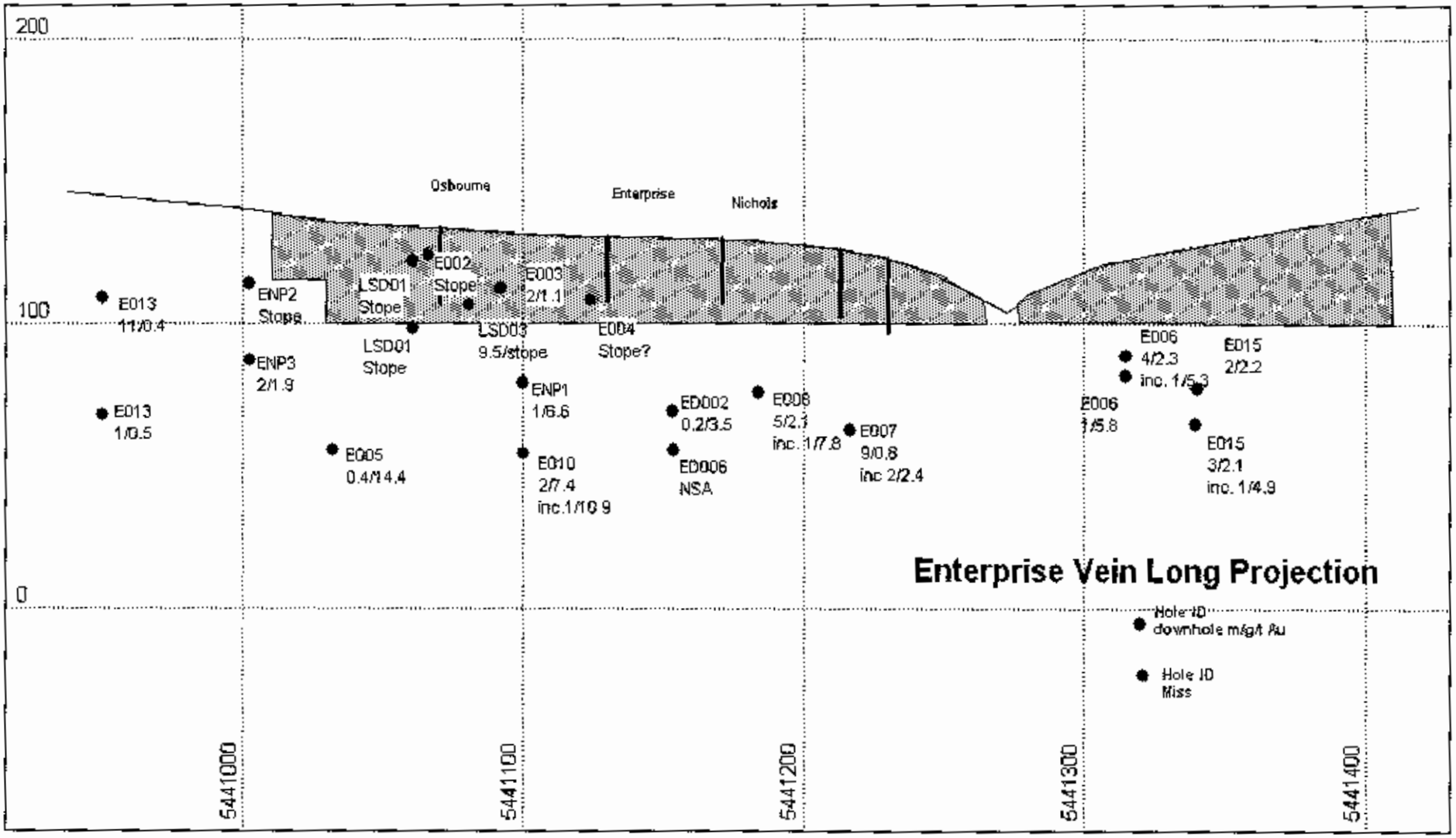
200
100
0
Osbourne
Enterprise
Nichols
E013
11/0.4
E013
1/0.5
ENP2
Stope
ENP3
2/1.9
E005
0.4/14.4
LSD01
Stope
E002
Stope
LSD01
Stope
LSD03
9.5/stope
E003
2/1.1
E004
Stope?
ENP1
1/6.6
E010
2/7.4
inc.1/10.9
ED002
0.2/3.5
ED006
NSA
E008
5/2.3
inc. 1/7.8
E007
9/0.8
inc 2/2.4
E006
4/2.3
inc. 1/5.3
E006
1/5.8
E015
2/2.2
E015
3/2.1
inc. 1/4.9
Enterprise Vein Long Projection
Hole ID
downhole m&g/t Au
Hole ID
Miss
5441000
5441100
5441200
5441300
5441400

Appendix C

Drill logs

- E005
- ED002
- ED003
- ED006
- PD001
- PD002

Hole Number:		E005																					Logged by Nicholas Fitzpatrick 05/2004
FROM	TO		Mineralisation/veins														Structure						Additional Comments
(m)	(m)	Rock Type	Colour	Weathering	Mineral 1	Style 1	Amount 1	Mineral 2	Style 2	Amount 2	Mineral 3	Style 3	Amount 3	Mineral 4	Style 4	Amount 4	Structure 1	CA Structure 1	Structure 2	CA Structure 2	Texture 1	Texture 2	
56	59.8	GRAND	G	Y	Qtz	Vn	10	Mo	B	2	Mic	D	<10										Granodiorite with Qtz veins 1cm wide minor Mo and Sericite alteration envelopes
59.8	59.88	VEIN	W		Qtz	Vn	25																Vein growth inot void later infill by mafic dyke
59.88	61.05	GRAND	G		Qtz	Vn	10	Mo	B	2													Granodiorite with Qtz veins 1cm wide minor Mo
61.05	61.11	MAFIC	Bk		Fld	Ph	20																Intrusive mafic vein dyke - nothing cross cuts (late)
61.11	61.8	GRAND	G		Qtz	Vn	10	Po	B	Tr													Granodiorite, mafic xenoliths (15%)
61.8	61.94	VEIN	W		Qtz	Vn																	Barron Qtz vein
61.94	62.95	GRAND	DG		Ser	D	10																Mafic xenoliths, Gneissic contact (white musc.) with underlying felsic phase, rock brocken up.
62.95	63.53	FELSIC	W																				Felsic intrusive phase, visible quartz, feldspar ± sericite
63.53	66.75	GRAND	DG		Qtz	Vn	20	Fld	Vn	<5													Veinlets with chlorite and sericite alt. envelopes and veins with chlorite alteration envelopes
66.75	67.85	GRAND	Gn		Qtz	Vn	10	Ep	Vn	2	Chl	Pv	20	Ser	Pv	5							Altered granodiorite
67.85	69.31	GRAND	DG		Qtz	Vn	5	Ser	Pv	2													<5% Mafic xenoliths
69.31	70.25	GRAND	DG		Qtz	Vn	20																Chlorite altered granodiorite with Qtz veins
70.25	70.65	FELSIC	W																				Felsic intrusive phase, gneissic contact and posible UST contact
70.65	72.45	GRAND	DG		Qtz	Vn	15	Mo	B	2	Phg	D	15										Small mafic xenoliths, phlogopite alteration, minor moly in veins
72.45	73.7	GRAND	DG		Qtz	Vn	10	Ep	D	5	Chl	D	20										Altered granodiorite, chlorite and biotite alteration
73.7	83.5	GRAND	DG		Qtz	Vn	20																Phlogopite common, mafic xenolith
83.5	83.6	VEIN	W		Qtz	Vn	95+	Po	B	2	Py	B	2										Biotite alteration envelope around vein, mafic xenolith
83.6	86.9	GRAND	G		Qtz	Vn	10	Mo	B	<5													Dendritic Molybdenum growth in Qtz vein
86.9	90.2	GRAND	Gn		Qtz	Vn	<5	Chl	Pv	30													Phlogopite and biotite alteration arounf Mo vein
90.2	92.15	GRAND																					Chlorite altered granodiorite
92.15	96.3	GRAND			Qtz	Vn	5	As	Vn	4													Chlorite altered Granodiorite with massive sulphide Qtz vein
96.3	99	GRAND	DG		Qtz	Vn	10																Mafic in colour granodiorite - Biotite alteration? Inc. proporton of mafics
99	101.5	GRAND	DG		Qtz	Vn	5																Mafic xenolith, phlogopite alteration

101.5	103.5	GRAND																						Conc of large biotites at the contact with underlying intrusive phase.
103.5	103.55	MAFIC	Bk																					Mafic intrusive vein dyke
103.55	104.15	GRAND	Gn		Qtz	Vn	10																	Veinlets with sericite alteration envelopes
104.15	104.25	FELSIC	W																					Felsic clot? Feldspar and qtz, minor mafics and sulphides
104.25	109.4	GRAND	G		Qtz	Vn	10	Po	B	2	Mo	B	2	Py	B	2								Minor bands of biotite alteration (veinlets?), mafic xenolith
109.4	109.64	VEIN	W		Qtz	Vn	98																	Qtz vein with felspar and white mica alteration at margins
109.64	110.23	GRAND	G		Qtz	Vn	5																	Abundant phlogopite ~20%
110.23	110.41	VEIN	W		Qtz	Vn																		Alteration zonation vein-biotite-feldspar-granodiorite
110.41	113.2	GRAND	G		Qtz	Vn	10	Po	B	2	Py	B	2	Mo	B	2								Minore Qtz veins containing minor Po, Mo and Py
113.2	113.55	GRAND	Gn		Qtz	Vn	5	Chl	Pv	20	Ser	Pv	5											Visible white mica ~10%
113.55	118.6	GRAND	G/Bl		Qtz	Vn	10																	Granodiorite, with abundant phlogopite, veinlets with chlorite alteration
118.6	120.45	GRAND			Qtz	Vn	15																	Chlorite sericite altered granodiorite, 3 vein generations:1 vein with biotite along margin cut by samller alteration forming vein
120.45	123.37	GRAND			Qtz	Vn	5																	Granodiorite containing mafic xenolith
123.37	123.38	VEIN	W																					Aplite vein, clear sugary texture
123.38	130	GRAND			Qtz	Vn	5																	
130	130.5	VEIN	W		Mo	B	2	Ser	Sel	?	Chl	Sel	?											Sericite and chlorite alt. envelope around 2cm wide vein
130.5	133.4	GRAND			Qtz	Vn	<5																	Small 1cm3 biotite 'clots', Qtz veins with sericite halos
133.4	133.75	GRAND	G/Bl		Qtz	Vn	25																	Sericite and chlorite ± muscovite alt. envelope around vein
133.75	141	GRAND	G/Bl		Qtz	Vn	5																	
141	148.8	GRAND			Qtz	Vn	10	Po	Vn	<5														Altered granodiorite (Chl and Ser) veinlets with sericite alteration halos
148.8	153	GRAND			Qtz	Vn	10																	Altered granodiorite, Biotite clots, carbonate veins (weathered to orange), sericite alt. halos
153	155	GRAND			Qtz	Vn	5																	Abundant veinlets with alt selvages
155	165.35	GRAND			Qtz	Vn	5																	Qtz veins 2-3cms wide with chl? Alt. halos
165.35	167.3	GRAND			Qtz	Vn	10																	Biotite rich granodiorite, Carbonate veins altering to orange, sericite haloes
167.3	173.85	GRAND			Qtz	Vn	10																	Biotite rich granodiorite, with biotite clots

173.85	175	GRAND			Qtz	Vn	15																Pervasive Chl-Ser alt, carbonate vein with Ser alt halos
175	176	GRAND	Bk		Qtz	Vn	10	Phg	D	20	Mus	D	5										Qtz veins brocken up by overprinting pervasive biotite alteration
176	170.5				Qtz	Vn	10																Biotite clots
170.5	179.5				Qtz	Vn	10																Chlorite and Sericite alteration around veins
EOH																							

Hole Number:		ED002																					Logged by Nicholas Fitzpatrick 26/05/2004
FROM	TO		Mineralisation/veins														Structure						Additional Comments
(m)	(m)	Rock Type	Colour	Weathering	Mineral 1	Style 1	Amount 1	Mineral 2	Style 2	Amount 2	Mineral 3	Style 3	Amount 3	Mineral 4	Style 4	Amount 4	Structure 1	CA Structure 1	Structure 2	CA Structure 2	Texture 1	Texture 2	
35.5	38.7	GRAND	G		Qtz	Vn	2																Granodiorite with minor Qtz veins, Interstitial biotite
38.7	40.3	GRAND	G/Gn		Qtz	Vn	3	Chl	Pv	5	Ser	Pv	5										Silica-chlorite-sericite altered granodiorite
40.3	44	GRAND	G		Qtz	Vn	5	Po	Vn	2	Po	D	1	As	Vn	1							Veins in stockwork arrangement
44	44.2	FELSIC	W		Qtz	D	5	Po	D	1													Felsic dyke cont. minor Qtz clasts (5mm) and Po - finer grained than surrounding granodiorite
44.2	45.4	GRAND	G		Qtz	Vn	2																Chl altered granodiorite cut by veins and mafic dyke
45.4	45.5	VEIN	W		Qtz	Vn	98	Mo	B	2													Qtz vein containing minor Mo (as blebs/patches)
45.5	47	GRAND	G		Qtz	Vn	10	Ser	Pv	10	Mo	Vn	1										Weakly Ser altered granodiorite with Qtz-Mo veins
47	48.3	GRAND	G		Qtz	Vn	10																Aplite vein, biotite clots (cm scale), felsic clots
48.3	51.1	GRAND	G		Qtz	Vn	10	Mo	B	2													Granodiorite with minor Qtz-Mo vein cutting barron Qtz vein
51.1	51.7	GRAND	G		Qtz	Vn	2	Ser	Pv	5	Chl	Pv	5										Chlorite-Sericite altered granodiorite
51.7	54.8	GRAND	G		Qtz	Vn	5	Po	B	2													Biotite clots, veins with coarse feld-Qtz margins (UST?)
54.8	55	GRAND	G		Qtz	Vn	60	Crb	Vn	25	Ser	Sv	15										Qtz-Carbonate vein with sericite selvage
55	57.9	GRAND	G		Qtz	Vn	10	Mo	B	2													Granodiorite with Qtz±Mo veins upto 5cm
57.9	58.8	LOSS																					CORE LOSS
58.8	62	GRAND	G		Qtz	Vn	10	Ser	Pv	10	Py	D	2	Mo	B	1							Silica-Sericite-Pyrite altered granodiorite, carbonate patches, Qtz-Mo veins
62	66.5	GRAND	B		Qtz	Vn	2	Po	D	Tr													Feldspar-Biotite-Hornblende? rich granodiorite
66.5	67.2	GRAND	G		Qtz	Vn	5	Ser	Pv	10	Py	D	2										Roch chips (Fault), Silica-Sericite-Pyrite altered granodiorite
67.2	67.4	VEIN	W		Qtz	Vn	90	As	Vn	5													Laminated Qtz-Aspy vein (gold bearing)
67.4	67.7	GRAND			Qtz	Vn	5	Ser	Pv	10	Py	D	2										
67.7	69.5	GRAND	DG		Qtz	Vn	2																
69.5	69.7	FAULT			Qtz	Vn	5	Ser	Pv	10	As	Vn	5										Displaced Qtz vein, Py-Aspy on fault surface, Sercite selvage
69.7	73.2	GRAND			Qtz	Vn	10	Po	B	1	Mo	B	1										Feldspar-Biotite-Hornblende? Rich granodiorite, minor Qtz veins (Qtz-Po and Qtz-Mo veins)

73.2	74.3	GRAND	G		Ser	Pv	10	Chl	Pv	10													Silica-sericite-chlorite altered granodiorite + selective replacement of felspars by sericite
74.3	77.4	GRAND			Qtz	Vn	5	Chl	Sv	2													Felsic clot? Within feldspar-biotite-hornblende granodiorite
77.4	77.9	VEIN			Qtz	Vn	90	Po	B	2	As	B	2										Qtz vein with distinct coarse (in comparison to host) selvage. Phlogopite common.
77.9	87.6	GRAND	G		Qtz	Vn	1																Granodiorite: 50% Qtz, 30+%Feldspar, 20% Biotite (Phlogopite comprising >=50% of est. biotite)
87.6	89.2	GRAND	G		Qtz	Vn	15	?	Sv	2													Granodiorite with Qtz veinlets with alteration selvage (Sericite or chlorite?), Qtz zone
89.2	90.7	GRAND	G																				Granodiorite
90.7	92	GRAND	Gn		Qtz	Vn	5	Qtz	Pv	10	Ser	Pv	5										Intensely Silica-sericite altered granodiorite
92	97.1	GRAND			Qtz	Vn	2	Po	B	Tr													Granodiorite, biotite spots, minor Qtz-Po veins
97.1	97.7	MAFIC	DG																		Porph		Dark grey, porphyritic mafic dyke - felspathic margins
97.7	101.1	GRAND	G		Qtz	Vn	1																Weakly (Chl±Ser) altered granodiorite
101.1	101.6	FAULT			Ser	Pv	5	Qtz	Pv	10	Py	Vn	2										Silicified fault with Silica-Ser alteration halo, minore Pyrite vein
101.6	102.1	GRAND	G		Ser	Pv	2	Qtz	Pv	5													Silica-sericite altered granodiorite
102.1	102.6	FAULT																					Brittle Fault chlorite-sericite altered halo
102.6	103.6	GRAND	G		Ser	Pv	2	Qtz	Pv	5													Silica-sericite altered granodiorite
103.6	104	FAULT			Qtz	Vn	5	Ser	Pv	15													Brittle Fault chlorite-sericite altered halo
104	104.7	GRAND	G		Qtz	Vn	5																Granodiorite with minore Qtz veins
104.7	107.5	GRAND			Qtz	Vn	5	Ser	Pv	10	Po	D	Tr										Patchy silica-sericite-pyrrhotite altered granodiorite, Po orientated along veinlets, large biotite clot
107.5	111.5	GRAND	G		Qtz	Vn	10	Ser	Sv	5	Py	D	Tr										Granodiorite with Qtz-Sericte veinlets/Qtz rich zones/ biotite spots, phlogopite common
111.5	112.4	VEIN	W		Qtz	Vn	70											Vn	5				Qtz vein (or aplite?)
112.4	113.2	GRAND	G		Qtz	Vn	2																Weakly (Chl±Ser) altered granodiorite
113.2	113.8				Qtz	Vn	20	Ser	Sv	2													Flowbanded granodiorite, Qtz veinlets all oriented the same way, Qtz-Musc veins
113.8	117	GRAND	DG		Qtz	Vn	2	Ser	Pv	2													Weakly altered granodiorite
117	117.7	FAULT			Qtz	Vn	5	Chl	Pv	15	Py	D	Tr										Chl altered granodiorite with remnant Qtz vein containing Pyrite
117.7	122.8	GRAND			Qtz	Vn	2	Ser	Pv	2													Moderately altered granodiorite, Selective chlorite replacement of biotite, patchy sericite alteration, biotite spots

122.8	123.2	VEIN			Qtz	Vn	30	Ser	Pv	10	Py	Vn	1	Mo	B	Tr							Sericite altered granodiorite, Qtz veins with traces of Po and/or Mo
123.2	127.2	GRAND			Ser	Pv	2																Weakly Sericite altered granodiorite
127.2	139.8	GRAND			Qtz	Vn	5	Po	B	2													Mafic xenolith cut by Qtz vein which it's self is cut by a Qtz vein
139.8	140	GRAND			Qtz	Vn	95	Ser	Sv	5													Qtz vein and veinlets sericite selvage in granodiorite
EOH																							

Hole Number:		ED003																						Logged by Nicholas Fitzpatrick 28/05/2004
FROM	TO		Mineralisation/veins															Structure						Additional Comments
(m)	(m)	Rock Type	Colour	Weathering	Mineral 1	Style 1	Amount 1	Mineral 2	Style 2	Amount 2	Mineral 3	Style 3	Amount 3	Mineral 4	Style 4	Amount 4	Structure 1	CA Structure 1	Structure 2	CA Structure 2	Texture 1	Texture 2	
0	7.4	SOIL	R	Y																			Deeply weathered colluvial scree with Qtz clasts
7.4	20.9	NO CORE																					LOSS OF CORE
20.9	23.9	GRAND																					Weathered granodiorite fragments intermixed with clay
23.9	25.4	GRAND			Qtz	Vn	5	Chl	Sel	Tr	Mo	B	Tr										Granodiorite: 50% Qtz, 20% feldspar, 30% mafics (biotite) and small biotite spots (clots?)
25.4	26.9	GRAND																					Weathered rock fragments (granodiorite)
26.9	29.8	GRAND			Qtz	Vn	5	Chl	Sel	Tr													Granodiorite with composition as above
EOH																							

Hole Number:		ED006																						Logged by Nicholas Fitzpatrick 27/05/2004
FROM	TO		Mineralisation/veins															Structure						Additional Comments
(m)	(m)	Rock Type	Colour	Weathering	Mineral 1	Style 1	Amount 1	Mineral 2	Style 2	Amount 2	Mineral 3	Style 3	Amount 3	Mineral 4	Style 4	Amount 4	Structure 1	CA Structure 1	Structure 2	CA Structure 2	Texture 1	Texture 2	
40.5	44.9	GRAND	G		Qtz	Vn	2	As	Vn	1													Granodiorite, approximate composition: 45% Qtz, 30% felspar, 25% Biotite (interstitial to euhedral-subhedral Qtz and feldspar crystals), rare phlogopite, minor Qrtz Aspy veins
44.9	46	GRAND	G/W		Qtz	Vn	1	Ser	Sv	5													Weakly altered granodiorite with Qtz veinlets/microveins
46	46.4	VEIN	W		Qtz	Vn	90	As	Vn	5	Py	Vn	Tr										Qtz vein containing stockwork Aspy (minor Py) stockwork veining
46.4	47.7	GRAND	D/G		Qtz	Vn	15	Mo	B	5	Po	B	2	Cpy	Vn	Tr	Ser	Sv	10				Hornblende-biotite-feldspar granodiorite
47.7	50.3	GRAND	D/G		Qtz	Vn	2	Po	B	Tr	Ser	Sv	5										Mafic granodiorite with minor Qtz veining and associated sericite alteration, biotite clots in the Qtz vein
50.3	55.95	GRAND	D/G		Qtz	Vn	10	Mo	B	2	Po	Vn	Tr										Mafic granodiorite with Qtz-Mo±Po veins, alteration selvage comprising feldspar and biotite, mafic xenolith? Containg 5mm epidotes and surrounded by an alteration selvage
55.95	56.4	GRAND	G		Qtz	Vn	25	Mo	B	10	Ser	Pv	10	Py	Vn	2							Brittle fault in a pervasively silica-sericte and chlorite altered granodiorite, 2cm quartz vein with irregular margins cut by veinlets
56.4	57.2	GRAND	G		Qtz	Vn	25	Mo	B	10	Swr	Pv	10	Py	Vn	2	As	B	Tr				Diffuse grain boundaries (colliform?), Qtz-Mo vein not causing alt., microveinlets with strong sericite alt. selvages
57.2	58.2	GRAND	G/W		Qtz	Vn	5	Ser	Sv	5													Granodiorite (~50% Qtz, ~30% feldspar, ~20% biotite), microveins
58.2	59.4	GRAND	G		Qtz	Vn	10	Ser	Pv	20	Mo	B	2	Chl	Pv	15							Possible fault (rock brocken up) sericite-chlorite altered granodiorite with minor quartz veining
59.4	59.8	GRAND	G		Qtz	Vn	5																Granodiorite weak selective alt. of biotite to chlorite.
59.8	60.6	FAULT	G		Qtz	Vn	2	Chl	Pv	15	Ser	Pv	→	Ser	Ser	20							Brittle fault zone, Ser-Chl alt. granodiorite with minor quartz veins and veinlets
60.6	67.6	GRAND	G		Qtz	Vn	5	Ser	Sv	2													Granodiorite with mafic xenoliths and biotite spots

67.6	70.3	GRAND	G		Qtz	Vn	15	Mo	B	2	Py	B	Tr										Granodiorite with Qtz-Mo veins with Qtz-felspar selvages
70.3	71.1	GRAND	Gn		Qtz	Vn	5	Ser	Sv	15	Chl	Sv	5										Sericite>Chlorite altered granodiorite with distinct vein selvages
71.1	74.5	GRAND	G		Qtz	Vn	5	Mo	B	2	Po	B	Tr										Granodiorite with Qtz-Mo veins with Qtz-felspar selvages
74.5	75	VEIN	W		Qtz	Vn	50																Qtz veins with complex cross cutting relations
75	75.5	GRAND	G		Qtz	Vn	5	Ser	Sv	20	Chl	Sv	10	Po	Vn	2							Granodiorite with Qtz±Po veins and feldspar selvages
75.5	77.2	GRAND	G		Qtz	Vn	5																Granodiorite with minor Qtz veins and feld. Selvages
77.2	80.6	GRAND			Qtz	Vn	10	Py	Vn	2	Mu	Py	2	Ser	Py	15	Chl	Py	15				Sericite-chlorite-muscovite altered granodiorite with Qtz-Py veins, carbonate veins and 3cm fault zone
80.6	85.35	GRAND	G/Gn		Qtz	Vn	10	Ser	Sv	10	Po	B	2										Granodiorite, Qtz-Po veins with sericite selvages
85.35	85.6	VEIN	W		Qtz	Vn	95	Mo	B	5													Qtz vein with minor moly. Spots and quartz-feldspar margin
85.6	86	GRAND	G		Qtz	Vn	2																Granodiorite with minor veining, common phlogopite
86	87.4	GRAND			Qtz	Vn	15	Ser	Pv	25	Mo	B	Tr	As	Vn	5	Phg	D	20				Veining in almost stockwork arrangement, Qtz and minor As veins, Phlogopite common in host
87.4	88.5	GRAND	G		Qtz	Vn	2	Ser	Sv	2													Pervasive phlogopite alteration: 40% phlogopite, 30% Qtz, 30% feldspar
88.5	89.2	GRAND	Gn		Qtz	Vn	5	Py	B	Tr	As	Vn	Tr	Ser	Pv	25+							Sericite altered granodiorite with minor Qtz±As veins
89.2	91.5	GRAND	G		Qtz	Vn	2																Granodiorite: 20% interstitial biotite, feld>Qtz
91.5	96.2	MAFIC	B		Qtz	Cl	10	Qtz	Vn	5	Ser	Sv	15	Mu	Pv	5	Po	B	2		Porph		Mafic dyke? Porphytitic texture, clasts of quartz, clasts of surrounding host (granodiorite)
96.2	97.4	GRAND	LG		Qtz	Vn	15																Granodiorite with mafic spots
97.4	97.8	MAFIC	B		Qtz	Cl	10														Porph		Mafic interval, clasts of quartz and minor feldspar
97.8	102.3	GRAND	G		Qtz	Vn	5																Minor mafic zones, aplite vein, biotite spots
102.3	102.6	MAFIC	B																				Mafic zone (not the same as overlying), more equigranular
102.6	103.7	GRAND	B		Qtz	Vn	2																Granodiorite, quartz patch with large needles (biotite) ~1.5cm long, UST?
103.7	107.5	MAFIC/G	B		Qtz	Vn	10																Flowbanding in mafic granite: horbblende-feld-biotite rich intrusive, finer grained at contact with above unit

107.5	112	MAFIC/G	B		Qtz	Vn	5	Ser	P	5													~2m from contact marked by biotite altered granodiorite, feld-Qtz selvages around veins and microveins
112	112.7	VEIN	W		Qtz	Vn	60	Ser	Sv	15	Mo	B	Tr										Qtz vein cross-cut be veinlet causing alteration
112.7	114.8	MAFIC	B		Qtz	Vn	5	Ser	Sv	15	Po	B	Tr								Porph		Mafic interaval, porphyritic quartz clasts and quartz veins
114.8	115.4	FELSIC	W		Qtz	Vn	20	Ser	Sv	20													Felsic granodiorite, aplite vein surrounded by pervasive sericite alteration (selvage)
115.4	131.2	GRAND	B		Qtz	Vn	10	Po	B	Tr	Mo	B	Tr	Ser	Sv	5							Mafic in appearance, granodiorite?, Qtz veins with feld biotite selvages and other veins with sericite selvages, some minor zones of intense sericite alteration containing trace amonts of Po
131.2	132.2	GRAND			Qtz	Vn	10	Chl	Pv	20	Ser	Pv	10	Po	B	Tr							Chlorite-sericite altered granodiorite with Qtz-Po veining
132.2	134	GRAND			Qtz	Vn	10	Ser	Pv	50	Chl	Pv	10	Po	B	Tr					Brecci		Intense sericite alteration, rock brecciated
134	134.3	FAULT			Qtz	Vn	5	Ser	Pv	50+													Intense sericite alteration, fault zone
134.3	135.8	GRAND			Qtz	Vn	5	Chl	Pv	10	Ser	Pv	5										Granodiorite with minor Chl-Ser alteration
135.8	138.8	GRAND			Qtz	Vn	10	As	V	5													Muscovite-sericite altered granite, stockwork sulphide veining of As
EOH																							

Hole Number:		PD001																					Logged by Nicholas Fitzpatrick 13/07/2004
FROM	TO		Mineralisation/veins															Structure						Additional Comments
(m)	(m)	Rock Type	Colour	Weathering	Mineral 1	Style 1	Amount 1	Mineral 2	Style 2	Amount 2	Mineral 3	Style 3	Amount 3	Mineral 4	Style 4	Amount 4	Structure 1	CA Structure 1	Structure 2	CA Structure 2	Texture 1	Texture 2	
5.7	7.7	SED	Bk	Y																			Weathered Mathinna Group (MG) sediments
7.7	10.1	SED/GRAND	R	Y																			Weathered MG, with rare <20cm intevals of weathered granite
10.1	11.6	SED/GRAND	R	Y																			Weathered MG, with <1% weathered granite intervals, unconsolidated zones possible faults
17	19.1	SED	Bk																				Weathered MG, with minor fesh silt/mud stone
19.1	22.1	SED	Bk																				Start of fresh rock, core brocken up into ~2cm clasts
22.1	24.9	GRAND	G		Qtz	Vg	<1	Chl	Sel	40+	Py	D	Tr										Granodiorite selective alt. of feldspars to chlorite, Vugs upto 4cm in size cont. dendritic Qtz growth, Aplite veinapparent width 3cm Qtz along margins, Py on fracture surfaces, Small inc of sed rare
24.9	26.6	SED	Bk		Qtz	Vn	Tr																MG core broken up but rock fresh, sulphides along fracture surfaces, rare granite inc. cm scale with cooked MG margins 0.5cm deep purple in colour
26.6	~28	NO CORE																					
~28	29.8	GRAND	G		Py	Fr	2																Granodiorite 50% Qtz, 40% feldspar (alt. to chlorite), 10% interstitial mafics, Pyrite in fractures (veins?)
29.8	31.7	SED	Bk																				MG, pyrite along fracture surfaces
31.7	34.4	GRAND	G																				<1% veinlets with alt. halos, contain sulphides, pyrite along fracture surfaces
34.4	40.1	SED	Bk		Qtz	Vn	1																MG, Qtz vein barron - deformed blebs of felsic material possibly oriented along bedding
40.1	41.5	GRAND	G		Ep	Sel	10	Chl	Sel	10													Granodiorite with selective alteration of feldspars
41.5	42	FAULT																					Fine unconsolidated sand - fault pug
42	43.5	SED/GRAND																					Zone of intermixed MG and Granodiorite, very subtle boundaries (not sharp), deformed Qtz bands (veins?)
43.5	51	SED	Bk		Qtz	Vn	2	Py	Vn	Tr	As	Vn	Tr										MG with slightly deformed barron Qtz veins and minor pyrite ± arsenopyrite veinlets

51	54	SED/GRAND	Bk/G		Crb	Vn	2																	MG containing varying sized zones (1cm-10cm) of granodiorite, and carbonate veining
54	62.5	SED	Bk/G		Crb	Vn	5+	Qtz	Vn	Tr	Qtz	D	1											MG, with Granodiorite inc. <5%, Purple alteration (pyroxene?), Qtz zone 15cm x 5cm (with almost aplite texture), 5% sulphide veinlets
62.5	63.1	GRAND	G		Crb	Vn	<3	Chl	Sel	15+														Granodiorite with concentration of sulphides along contact with underlying MG, sharp contact
63.1	66	SED	Bk																					Purple alteration (pyroxene?)
66	66.5	GRAND	G																					Blurred contacts, washed out look, not a crisp texture
66.5	69.5	SED	Bk																					MG with rare granodiorite inc. with washed out texture
69.5	74.5	GRAND	G		Crb	Vn	15																	Poor contact with MG granodiorite dark in clour at bounday, colour doesn't distinguish granodiorite-MG contact, texture only used to define contact, More interstitial mafics ~20%
74.5	80.5	SED	Bk		Crb	Vn	2																	Veins with alteration halos
EOH																								

Hole Number:		PD002																					Logged by Nicholas Fitzpatrick 13/07/2004
FROM	TO		Mineralisation/veins														Structure						Additional Comments
(m)	(m)	Rock Type	Colour	Weathering	Mineral 1	Style 1	Amount 1	Mineral 2	Style 2	Amount 2	Mineral 3	Style 3	Amount 3	Mineral 4	Style 4	Amount 4	Structure 1	CA Structure 1	Structure 2	CA Structure 2	Texture 1	Texture 2	
~18.5	25.1	GRAND	W	Y	Py	D	Tr																Intensely weathered granodiorite. ~20% Qtz crystals remaining content altered to clays. Trace diss. Sulphides. Granodiorite appears to be altered
25.1	28.1	SAND	W	Y																			Unconsolidated sed result from weathering. Fault?
28.1	~34.9	GRAND	W	Y	Qtz	Vg	<1	Py	D	Tr													Weathered granodiorite, Coherant fragments, >50% Qtz, remainder alt. to clays, mafics unrecognisable. NB: Py apperas to be inc. down hole i.e. toward vein
~34.9	35.6	VEIN	G	Y	Qtz	Vn	25	As	Vn	70	Cpy	Vn	<5										Brecciated vein, Appers to be larger mineralised Qtz vein(s) cut be smaller sulphide veinlets, Orientation of larger As veins (apparent thickness 1cm) is subparallel
35.6	36.5	GRAND			Qtz	Vn	<5	Py	Vn	Tr													Weathered granodiorite, Biotite (phlogopite) crystals remain
36.5	36.6	FAULT																					Unconsolidated granite - fault pug
36.6	37.7	GRAND	G	Y	Qtz	Vn	<2	As	Vn	Tr	Py	D	Tr										Weathered granodiorite with minor diss. Py
37.7	38.6	VEIN	G		Qtz	Vn	20	As	Vn	70	Cpy	Vn	5	Py	Vg	5							Visual estimate of vein orientation ~20° off core axis, Qtz veins at least tow orientations: subparallel to core and earlier crosscutting. As in subparallel veins, Qtz vugs along centre of some veins contain Py precipitant
38.6	40.6	GRAND		Y	Qtz	Vn	5	As	Vn	2	Py	D	Tr										As makin up large >50% of at least 2 Qtz veins remaining Qtz veins are barron, Qtz vugs common in veins and at separate bodies 1cm x 1cm, all minerals in granodiorite other than Qtz weathering to clays
40.6	~45	GRAND			Py	Fr	5																Becoming less weathered i.e. fresh, Py along fracture surfaces (late precipitant), Granodiorite: 30% feldspars weathering to clay, ~40% Qtz, 20% Biotite (as phlogopite), ~10% Chlorite
Hole started 18.5m EOH at 45m on 12th July 2004 continuing to ~140m																							

Appendix D

Magnetic Susceptibilty

- E005
- ED002
- ED006
- PD001
- PD002

DDH E005: MAGNETIC SUSCEPTIBILITY 10^{-3} SI UNITS

(m)	10^{-3} SI units	(m)	10^{-3} SI units	(m)	10^{-3} SI units
56	2.63	109	1.46	162	1.91
57	1.19	110	1.08	163	0.66
58	0.16	111	1.64	164	1.86
59	0.27	112	0.76	165	1.97
60	0.13	113	2.37	166	0.40
61	0.26	114	0.89	167	1.75
62	0.18	115	0.80	168	0.78
63	0.03	116	0.41	169	0.62
64	0.19	117	2.79	170	0.40
65	0.32	118	1.42	171	0.48
66	0.13	119	2.77	172	1.82
67	0.20	120	1.07	173	0.40
68	0.07	121	0.35	174	0.28
69	0.03	122	1.83	175	1.31
70	0.00	123	0.27	176	0.14
71	0.12	124	1.15	177	0.42
72	0.16	125	2.73	178	1.58
73	0.43	126	0.06	179	0.78
74	0.24	127	0.58		
75	0.10	128	0.96		
76	0.08	129	0.55		
77	0.16	130	0.22		
78	0.20	131	0.70		
79	0.15	132	0.24		
80	0.55	133	1.29		
81	0.31	134	0.14		
82	0.22	135	1.51		
83	1.49	136	0.70		
84	0.79	137	0.79		
85	0.59	138	1.79		
86	1.59	139	0.23		
87	0.94	140	0.98		
88	1.33	141	0.95		
89	3.22	142	0.93		
90	2.84	143	0.88		
91	2.56	144	0.06		
92	0.60	145	0.41		
93	0.22	146	0.60		
94	0.08	147	0.14		
95	2.62	148	0.18		
96	1.16	149	0.60		
97	1.98	150	1.15		
98	2.89	151	1.24		
99	1.12	152	2.07		
100	0.94	153	1.08		
101	0.37	154	0.81		
102	0.45	155	1.65		
103	1.22	156	2.41		
104	0.71	157	1.51		
105	1.10	158	1.92		
106	1.34	159	2.11		
107	1.23	160	0.85		
108	0.77	161	1.99		

DDH ED002: MAGNETIC SUSCEPTIBILITY 10^{-3} SI UNITS

(m)	10^{-3} SI units	(m)	10^{-3} SI units
36	0.27	89	0.11
37	0.33	90	0.27
38	0.28	91	0.62
39	0.15	92	0.19
40	0.25	93	0.24
41	0.23	94	0.58
42	0.38	95	0.61
43	0.87	96	0.53
44	0.4	97	0.93
45	0.62	98	0.21
46	0.11	99	0.14
47	0.12	100	0.23
48	0.26	101	0.54
49	0.14	102	0.38
50	0.23	103	0.52
51	0.3	104	0.63
52	0.19	105	0.55
53	0.14	106	0.43
54	0.2	107	0.12
55	0.2	108	1.32
56	0.13	109	0.28
57	0.22	110	0.2
58	0.11	111	0.32
59	0.17	112	0.4
60	0.21	113	0.32
61	0.19	114	0.12
62	0.7	115	0.1
63	0.21	116	0.12
64	0.16	117	0.09
65	0.27	118	0.08
66	0.7	119	0.08
67	0.02	120	0.17
68	0.59	121	0.25
69	0.66	122	0.17
70	0.09	123	0.17
71	0.3	124	0.16
72	0.37	125	0.13
73	0.52	126	0.12
74	0.21	127	0.28
75	0.79	128	0.11
76	0.21	129	0.4
77	0.25	130	0.12
78	0.67	131	0.02
79	0.76	132	0.12
80	0.31	133	0.16
81	0.21	134	0.15
82	1.05	135	0.1
83	0.17	136	0.11
84	0.13	137	0.17
85	0.12	138	0.1
86	0.13	139	0.11
87	0.27	140	0.17
88	0.24		

DDH ED006: MAGNETIC SUSCEPTIBILITY 10^{-3} SI UNITS

(m)	10-3 SI units	(m)	10-3 SI units
41	0.12	94	0.27
42	0.17	95	0.48
43	0.16	96	0.18
44	0.16	97	0.06
45	0.18	98	0.31
46	0.55	99	0.25
47	0.2	100	0.23
48	0.09	101	0.1
49	0.12	102	0.11
50	0.13	103	0.46
51	0.07	104	3
52	0.1	105	0.45
53	0.03	106	1.19
54	0.15	107	0.23
55	0.12	108	0.04
56	0.06	109	0.5
57	0.07	110	0.35
58	0.09	111	0.39
59	0.01	112	0.26
60	0.12	113	1.09
61	0.52	114	0.49
62	0.14	115	0.27
63	0.14	116	0.11
64	0.14	117	0.23
65	0.15	118	0.16
66	0.13	119	0.6
67	0.22	120	0.85
68	0.08	121	0.29
69	0.2	122	0.41
70	0.44	123	0.56
71	0.08	124	0.53
72	0.21	125	0.24
73	0.1	126	0.55
74	0.16	127	0.4
75	0.23	128	0.29
76	0.13	129	0.33
77	0.09	130	0.79
78	0.3	131	0.23
79	0.06	132	0.15
80	0.16	133	0.14
81	0.18	134	0.08
82	0.13	135	0.75
83	0.26	136	0.08
84	0.22	137	0.12
85	0.15	138	0.15
86	0.12	139	0.11
87	0.15		
88	0.26		
89	0.25		
90	0.24		
91	0.12		
92	0.83		
93	0.17		

DDH PD001: MAGNETIC SUSCEPTIBILITY 10^{-3} SI UNITS

(m)	10^{-3} SI units	(m)	10^{-3} SI units
13	0.06	69	0.01
17	0.12	70	0.58
18	0.15	71	1.35
19	0.07	72	2.71
22	0.05	73	0.81
23	0.12	74	2.84
24	0.15	75	0.4
25	0.38	76	0.38
26	0.24	77	0.16
28	0.13	78	0.22
29	0.11	79	0.3
30	0.34	80	0.25
31	0.38		
32	0.25		
32.5	0.14		
33	0.57		
33.5	1.35		
34	0.16		
35	0.32		
36	0.27		
37	0.26		
38	0.28		
39	0.2		
40	0.27		
41	0.26		
42	0.17		
43	0.13		
44	0.29		
45	0.59		
46	0.12		
47	0.2		
48	0.18		
49	0.22		
50	0.28		
51	0.27		
52	0.42		
53	0.25		
54	0.18		
55	0.4		
56	0.46		
57	0.63		
58	0.92		
59	0.29		
60	0.42		
61	0.33		
62	0.61		
63	2.14		
63.5	0.27		
64	0.29		
65	0.36		
66	0.87		
67	1.1		
68	0.31		

DDH PD002: MAGNETIC SUSCEPTIBILITY 10^{-3} SI UNITS

(m)	10^{-3} SI units
28.5	0.1
29	0.03
29.5	0.19
30	0.18
30.5	0.08
31	0.07
31.5	0.03
32	0.03
32.5	0.16
33	0.1
33.5	0.1
34	0.09
34.3	0.08
34.6	0.08
34.9	0.13
35.2	0.12
35.5	0.26
35.8	0.06
36.1	0.11
36.6	0.11
38.5	0.13
37.1	0.15
37.25	0.12
37.4	0.15
37.55	0.16
37.7	0.16
38	0.12
38.3	0.09
38.6	0.14
38.9	0.15
40	0.18
40.1	0.12
40.6	0.12
40.95	0.15
41.3	0.2
41.4	0.18
41.9	0.14
42.4	0.12
42.9	0.11
43.1	0.09
43.35	0.5
43.6	0.38
44	0.19
45	0.31

Appendix E

XRF method

Summary of X-Ray Fluorescence (XRF) Analysis

School of Earth Sciences, University of Tasmania **Phil.Robinson 29/03/2000**

Instrument	Philips PW1480 X-Ray Spectrometer
X-Ray Tubes	3kW max. ScMo anode side window. Elements analysed: Majors, S and Y, Rb, U, Th, Cu, Pb, Zn, Ni, As, Bi, Co, Ga, Tl, Se, W, Br
	3kW max. Au anode side window. Elements analysed: Nb, Zr, Sr, Ba, Cr, V, Sc, La, Ce, Nd, Sb, Sn
	3kW max. Rh anode side window. Elements analysed: Mo, occasionally Nb
Crystals:	LiF 200, LiF 220, PX-1 (for Na and Mg), PE002, Ge111
Collimators:	Coarse (0.7mm) and fine (0.3mm) with auxiliary (0.14mm)
Detectors:	Gas flow proportional counter with P10 gas (10% methane in argon) and Scintillation Counter.

Sample Changer: Philips 30 position sample holder

Sample Preparation

Major Elements: Fusion discs prepared at 1100 degreesC in 5%Au/95%Pt crucibles
0.77g sample, 4.125g Norrish Flux (Lithium borates/La2O3 mix), 0.055g LiNO3 for silicates.Platinum/gold moulds used for cooling.
Sulphide bearing samples have a mix with more LiNO3 as oxidising agent and the mix is preignited at 700 degreesC for 10 minutes. Ore samples and ironstones use 12/22 flux and a higher flux/sample ratio. Dolomites and limestones need pure lithium tetraborate as a flux.

Trace Elements Pressed powder pills (3.5 tonnes/cm^{-2}) with 10 grams sample.
Binder used is PVP-MC.

Corrections

Corrections for mass absorption are calculated using Philips X40 software with De Jongh's calibration model and Philips (or CSIRO) alpha coefficients. Compton scattering is also used for many trace elements.

Calibration

Pure element oxide mixes in pure silica, along with international and Tasmanian standard rocks are used. Numerous checks of standard rocks and pure silica blanks are run with each program.

Appendix F

FeO method

FeO analysis method

Conducted by Amdel Limited

FeO analysis was achieved by digesting a known weight of sample in a reducing atmosphere with Hydrochloric Acid and a few drops of Hydrofluoric Acid. This is attained by adding a scoop of Sodium Bicarbonate to the sample before adding the acid. A rubber bung is fitted to the flask this has a vent opened to the atmosphere. After digestion it is cooled and titrated with standard Potassium Dichromate solution using Barium Diphenylamine Sulphonate Indicator as an indicator.

Appendix G

Whole-rock geochemistry

Sample ID	ED2.3	ED2.4	ED2.12	ED2.13	E5.1	E5.2	E5.4	E5.7	EG.10	E5.12	E5.13	ED6.1	ED6.11a	ED6.14	PD1.1	ED6.11b
Lithology	AVD	FHB	FBQ	FQ	FBQ	FQ	FQ	VD	AVD	FQ	FBQ	FHB	FHB	FHB	FBQ*	PVD
SiO2 wt %	77.85	65.99	66.60	76.61	66.84	77.88	79.20	58.95	78.96	76.97	63.43	65.76	67.89	58.58	65.12	71.69
TiO2	0.02	0.49	0.46	0.04	0.48	0.07	0.09	0.70	0.03	0.12	0.54	0.49	0.43	1.04	0.54	0.49
Al2O3	12.00	16.06	15.61	12.47	15.90	11.81	12.41	15.85	10.70	12.21	16.52	15.98	15.26	15.66	16.35	12.85
Fe2O3			-0.11		0.06	-0.07								0.27	1.80	
FeO			4.10		3.60	0.60								7.40	2.40	
FeOtot	0.54	4.29	4.00	0.59	3.65	0.54	0.68	5.49	0.74	0.82	4.61	4.15	3.50	7.60	4.02	3.54
Fe2O3tot	0.60	4.77	4.45	0.66	4.06	0.60	0.75	6.10	0.82	0.91	5.13	4.61	3.89	8.44	4.47	5.24
MnO	0.01	0.08	0.06	0.01	0.06	0.01	0.03	0.10	0.02	0.01	0.04	0.08	0.06	0.14	0.05	0.06
MgO	0.15	2.13	1.82	0.17	2.16	0.29	0.26	3.82	0.16	0.42	2.07	2.25	1.95	3.59	2.35	2.52
CaO	0.86	4.27	3.58	0.96	3.79	1.03	0.45	5.99	1.93	1.88	4.50	4.33	3.90	5.19	2.39	2.34
Na2O	3.47	4.28	4.14	3.66	3.94	3.30	4.40	4.28	4.07	4.23	4.04	4.13	4.11	3.67	3.63	3.58
K2O	4.48	1.53	1.69	4.66	1.52	3.63	1.47	1.15	1.64	1.63	1.55	1.60	1.48	1.93	1.77	2.15
P2O5	0.01	0.16	0.14	0.01	0.14	0.02	0.02	0.25	0.01	0.04	0.18	0.14	0.13	0.35	0.15	0.11
Loss inc. S-	0.77	0.58	1.59	0.74	1.11	1.10	1.02	2.39	1.71	1.50	1.60	0.61	0.73	1.12	2.85	0.92
Total	100.22	100.34	100.13	100.00	99.99	99.74	100.09	99.58	100.04	99.93	99.59	99.99	99.83	99.71	99.66	100.02
S	0.10	0.04	0.33	0.05	0.07	0.01	0.05	0.34	0.05	0.08	0.82	0.01	0.10	0.71	1.64	0.04
Mo ppm	1	<1	65	66	24	4	23	2	3	51	1	1	97	25	<1	71
Sb	<2	<2	<2	<2	<2	<2	<2	<2	<2	<2	<2	<2	<2	<2	<2	<2
Sn	<1.5	<1.5	<1.5	<1.5	<1.5	<1.5	<1.5	3	2	<1.5	2	<1.5	<1.5	<1.5	2	<1.5
Nb	3	9	8	4	8	5	3	8	5	4	7	9	8	13	8	11
Zr	50	112	104	55	102	80	54	121	88	64	109	105	100	180	120	116
Sr	109	460	423	58	472	148	151	781	150	222	527	443	414	499	397	263
Ba	456	601	553	660	498	700	574	518	256	629	417	553	533	677	381	481
Sc	<2	12	11	<2	12	<2	<2	17	2	3	14	12	11	18	13	11
V	3	99	86	3	93	10	12	156	6	22	104	99	83	198	107	88
Y	4	13	12	7	9	10	7	15	7	8	15	13	11	21	14	12
U	6	4	4	5	2	9	6	3	16	6	2	3	4	3	2	3
Rb	70	54	66	62	69	61	43	57	40	41	70	49	50	82	94	83
Th	18	10	9	15	8	23	21	8	23	19	6	8	7	4	6	9
Pb	14	9	7	20	6	14	9	5	10	7	6	7	6	7	8	7
As	4	<3	<3	<3	<3	<3	80	<3	<3	<3	<3	<3	<3	<3	5	<3
Bi	<2	<2	<2	<2	<2	<2	<2	<2	<2	<2	<2	<2	<2	<2	<2	<2
Zn	4	69	57	5	45	17	9	54	4	10	38	58	47	102	36	43
Cu	21	12	65	8	14	4	6	47	13	19	135	6	25	202	64	9
Ni	5	16	11	5	16	4	4	47	9	4	10	18	15	22	17	21
W	<2	<2	16	<2	5	<2	3	87	<2	4	163	<2	<2	3	<2	<2

Abbreviations: AVD = Aplite 'vein' dyke, FBQ = Feldsepr-biotite-quartz granodiorite, FBQ* = Feldspar-biotite-quartz granodiorite from the Potoroo prospect, FeO* = total Fe, FHB = Feldspar-hornblende-biotite granodiorite, PVD = porphyritic 'vein' dyke, QF = quartz feldspar granodiorite.

Appendix H

Microprobe data

- **Plagioclase feldspar**
- **Biotite**
- **Hornblende amphibole**

Plagioclase feldspar

Sample #	ED2.2	ED2.2	ED2.12	ED2.12	ED2.12	ED2.12	ED6.14	ED6.15
Hole	ED002	ED002	ED002	ED002	ED002	ED002	ED006	ED006
Depth	44	44	97.2	97.2	97.2	97.2	103.7	103.7
P_2O_5	0.0079	0.0231	0.0097	0.0283	0.0012	0.0058	-0.0057	0.0167
SiO_2	59.0352	57.0894	60.9766	57.7434	53.8063	60.1273	55.957	59.3882
TiO_2	0.0081	0.0163	0.0114	0.0228	-0.0016	-0.0179	0.0049	0.0196
Al_2O_3	24.2129	25.7965	23.6423	25.6306	27.8861	24.0612	26.6483	24.4235
Cr_2O_3	0.0035	-0.005	0.004	-0.0005	-0.0229	0.006	0.007	0.0005
Fe_2O_3	0.0746	0.1039	0.064	0.2728	0.0648	0.0762	0.1064	0.0861
MgO	0.012	0.0074	0.0083	0.0224	0.0044	0.0083	-0.0224	0
CaO	6.6895	8.1795	5.7859	7.9128	10.8499	6.2275	9.1546	6.5716
MnO	0.0157	-0.0253	0.0087	-0.0135	0.0053	0.0053	0.0196	-0.0126
SrO	0.0095	0.0159	0.0024	0.0581	0.064	0.0238	0.0655	0.0286
BaO	0.0899	0.0889	0.1368	0.0675	0.0304	0.0362	0.1009	0.0578
Na_2O	7.4282	6.3999	7.8707	6.7036	5.0098	7.7096	6.1439	7.5354
K_2O	0.3703	0.2923	0.3083	0.2651	0.1549	0.3149	0.1651	0.1341
Total Ox	97.9573	98.0132	98.829	98.7276	97.877	98.6019	98.3732	98.2621
O=	0	0	0	0	0	0	0	0
Total Ox	97.9573	98.0132	98.829	98.7276	97.877	98.6019	98.3732	98.2621
P	0.001	0.004	0.001	0.004	0	0.001	0	0.003
Si	10.754	10.428	10.964	10.473	9.917	10.853	10.225	10.762
Ti	0.001	0.002	0.002	0.003	0	0	0.001	0.003
Al	5.198	5.554	5.01	5.479	6.057	5.119	5.739	5.216
Cr	0.001	0	0.001	0	0	0.001	0.001	0
Fe	0.01	0.014	0.009	0.037	0.009	0.01	0.015	0.012
Mg	0.003	0.002	0.002	0.006	0.001	0.002	0	0
Ca	1.306	1.601	1.115	1.538	2.142	1.204	1.792	1.276
Mn	0.002	0	0.001	0	0.001	0.001	0.003	0
Sr	0.001	0.002	0	0.006	0.007	0.002	0.007	0.003
Ba	0.006	0.006	0.01	0.005	0.002	0.003	0.007	0.004
Na	2.624	2.267	2.744	2.357	1.79	2.698	2.177	2.648
K	0.086	0.068	0.071	0.061	0.036	0.073	0.038	0.031
Total Cat	19.993	19.948	19.93	19.969	19.963	19.966	20.005	19.957

Biotite microprobe

Sample #	ED2.2	ED2.2	ED2.2	ED2.2	ED2.12	ED2.12	ED6.14
Hole	ED002	ED002	ED002	ED002	ED002	ED002	ED006
Depth	44	44	44	44	97.2	97.2	103.7
V_2O_5	0.002	-0.0076	0.0199	-0.0033	-0.0116	0.0054	-0.0065
SiO_2	35.6241	36.6034	35.4619	36.293	35.8763	36.3024	35.6637
TiO_2	2.4655	3.1163	3.7925	3.9672	3.5697	2.3065	4.5746
ZrO_2	0.0224	-0.0558	-0.0222	0.1779	-0.0669	0.0223	-0.0223
Al_2O_3	13.941	13.8472	13.6161	13.9356	13.9478	14.2908	13.4731
Cr_2O_3	0.0431	0.0098	0.0292	0.0723	-0.0084	-0.0194	-0.0098
MgO	10.9797	10.725	10.2622	10.0026	10.3671	10.2372	9.6826
CaO	0.0363	0.0156	0.0034	-0.0259	0.0294	0.0449	-0.0345
MnO	0.3037	0.3309	0.3965	0.4269	0.2249	0.2275	0.2202
FeO	19.3453	19.0963	19.0583	19.432	19.1035	20.4986	19.5224
ZnO	-0.0183	-0.0162	0.0465	-0.0233	0.0386	0.0354	0.0253
BaO	0.1403	0.313	0.3084	0.2522	0.4072	0.1433	0.4317
H_2O	3.1846	3.2004	3.202	3.3299	3.2286	3.2051	3.2767
Na_2O	0.0983	0.093	0.1075	0.0791	0.0612	0.1298	0.1068
K_2O	8.2555	9.2022	9.3558	9.3025	9.5649	9.6061	9.0989
F	0.4501	0.5472	0.4348	0.3057	0.4367	0.4977	0.3112
Cl	0.1118	0.1259	0.1345	0.1388	0.1442	0.1674	0.139
Total Ox	95.0036	97.2261	96.2296	97.7156	97.0002	97.7204	96.5261
O=F , Cl	0.2148	0.2588	0.2134	0.16	0.2164	0.2474	0.1624
Total Ox	94.7888	96.9673	96.0162	97.5555	96.7838	97.4731	96.3637
V	0	0.002	0.002	0.004	0.002	0.001	0.004
Si	6.235	6.286	6.178	6.2	6.196	6.249	6.182
Ti	0.324	0.402	0.497	0.51	0.464	0.299	0.596
Zr	0.002	0	0	0.015	0	0.002	0
Al	2.876	2.803	2.796	2.806	2.839	2.899	2.752
Cr	0.006	0.001	0.004	0.01	0	0	0
Mg	2.865	2.746	2.665	2.548	2.669	2.627	2.502
Ca	0.007	0.003	0.001	0	0.005	0.008	0
Mn	0.045	0.048	0.059	0.062	0.033	0.033	0.032
Fe	2.831	2.743	2.777	2.776	2.759	2.951	2.83
Zn	0	0	0.006	0	0.005	0.005	0.003
Ba	0.01	0.021	0.021	0.017	0.028	0.01	0.029
OH	3.718	3.666	3.721	3.795	3.719	3.68	3.789
Na	0.033	0.031	0.036	0.026	0.021	0.043	0.036
K	1.843	2.016	2.079	2.027	2.107	2.11	2.012
F	0.249	0.297	0.24	0.165	0.239	0.271	0.171
Cl	0.033	0.037	0.04	0.04	0.042	0.049	0.041
Total Cat	21.077	21.102	21.12	21	21.128	21.236	20.979

Hornblende amphibole

Sample #	ED2.2	ED2.2	ED2.2	ED2.2	ED2.12	ED2.12	ED2.12	ED2.12
Hole	ED002	ED002	ED002	ED002	ED002	ED002	ED002	ED002
Depth	44	44	44	44	97.2	97.2	97.2	97.2
SiO_2	42.7848	46.0998	50.3885	49.305	49.5675	50.6	50.6897	49.8835
TiO_2	1.6189	1.2175	0.587	0.6159	0.5944	0.1073	0.3571	0.4002
ZrO_2	-0.0201	0.0652	0.005	0.0402	0.0452	-0.0101	0.0605	0.0555
Al_2O_3	12.4092	7.7341	3.1887	4.2211	3.1967	3.0321	3.5185	3.7044
Cr_2O_3	0.0582	0.0225	0.0245	0.0263	0.0103	-0.0094	-0.0094	0.0038
MgO	13.6071	11.5273	12.7886	12.3971	11.6228	12.0765	12.8916	12.4041
CaO	11.0703	10.0885	11.2272	10.6812	10.0183	10.7452	10.5691	10.2606
MnO	0.1752	0.58	0.8152	0.8982	0.4601	0.5352	0.7692	0.7789
FeO	11.3944	16.2535	15.6875	16.183	18.5273	16.8463	16.4108	16.7136
ZnO	-0.0061	0.0435	0.0184	0.0564	0.0129	0.0225	0.0293	0.0661
SrO	-0.0345	-0.0624	-0.0141	-0.0777	-0.037	-0.0632	-0.0353	-0.0371
BaO	0.1002	0.0917	0.0781	0.094	0.1188	0.081	0.0822	0.0982
H_2O	1.7507	1.7256	1.8321	1.7768	1.7518	1.7944	1.7636	1.7857
Na_2O	2.47	1.4831	0.4831	0.5519	0.7164	0.3954	0.6695	0.6386
K_2O	0.3149	0.2634	0.2656	0.3346	0.2708	0.1954	0.2565	0.2815
F	0.3493	0.3242	0.1486	0.2276	0.2392	0.1759	0.3016	0.2137
Cl	0.0251	0.0287	0.0185	0.0424	0.0438	0.0356	0.0422	0.0282
Total Ox	98.1283	97.5484	97.5567	97.4518	97.1963	96.6428	98.4114	97.3165
O=F , Cl	0.1527	0.143	0.0668	0.1054	0.1106	0.0821	0.1365	0.0964
Total Ox	97.9756	97.4054	97.4899	97.3464	97.0857	96.5607	98.2749	97.2201
Si	6.672	7.327	7.921	7.799	7.921	8.041	7.927	7.896
Ti	0.19	0.146	0.069	0.073	0.071	0.013	0.042	0.048
Zr	0	0.005	0	0.003	0.004	0	0.005	0.004
Al	2.281	1.449	0.591	0.787	0.602	0.568	0.648	0.691
Cr	0.007	0.003	0.003	0.003	0.001	0	0	0
Mg	3.163	2.731	2.997	2.923	2.769	2.861	3.005	2.927
Ca	1.85	1.718	1.891	1.81	1.715	1.829	1.771	1.74
Mn	0.023	0.078	0.109	0.12	0.062	0.072	0.102	0.104
Fe	1.486	2.16	2.062	2.141	2.476	2.239	2.146	2.212
Zn	0	0.005	0.002	0.007	0.002	0.003	0.003	0.008
Sr	0	0	0	0	0	0	0	0
Ba	0.006	0.006	0.005	0.006	0.007	0.005	0.005	0.006
OH	1.821	1.829	1.921	1.875	1.867	1.902	1.84	1.885
Na	0.747	0.457	0.147	0.169	0.222	0.122	0.203	0.196
K	0.063	0.053	0.053	0.068	0.055	0.04	0.051	0.057
F	0.172	0.163	0.074	0.114	0.121	0.088	0.149	0.107
Cl	0.007	0.008	0.005	0.011	0.012	0.01	0.011	0.008
Total Cat	18.488	18.138	17.852	17.91	17.908	17.792	17.909	17.89

Hornblende amphibole

Sample #	ED6.14	ED6.14	ED6.14	ED6.14
Hole	ED006	ED006	ED006	ED006
Depth	103.7	103.7	103.7	103.7
SiO2	48.9062	51.9247	50.9585	51.3442
TiO2	0.6164	0.4083	0.4708	0.3829
ZrO2	0.0252	0.0505	-0.0101	0.0808
Al2O3	5.0493	2.1949	2.5282	2.6297
Cr2O3	-0.0113	0.0009	-0.0009	0.0019
MgO	12.4234	13.7076	13.2075	13.231
CaO	10.7087	11.126	10.3501	10.9946
MnO	0.6085	0.6469	0.8327	0.6055
FeO	15.7463	14.9007	15.8172	15.5401
ZnO	0.0259	0.0034	0.0675	0.0232
SrO	-0.0372	-0.0105	-0.0035	-0.0352
BaO	0.1005	0.0669	0.0682	0.1111
H2O	1.7904	1.8205	1.7981	1.8299
Na2O	0.8216	0.4384	0.4762	0.4759
K2O	0.3211	0.1898	0.1341	0.1925
F	0.2127	0.2053	0.1958	0.1745
Cl	0.0334	0.0234	0.036	0.0134
Total	97.3895	97.7084	96.9408	97.6312
O=F , Cl	0.0971	0.0917	0.0906	0.0765
Total	97.2925	97.6167	96.8502	97.5547
Si	7.719	8.093	8.041	8.035
Ti	0.073	0.048	0.056	0.045
Zr	0.002	0.004	0	0.006
Al	0.939	0.403	0.47	0.485
Cr	0	0	0	0
Mg	2.923	3.185	3.107	3.087
Ca	1.811	1.858	1.75	1.843
Mn	0.081	0.085	0.111	0.08
Fe	2.078	1.942	2.087	2.034
Zn	0.003	0	0.008	0.003
Sr	0	0	0	0
Ba	0.006	0.004	0.004	0.007
OH	1.885	1.893	1.893	1.91
Na	0.251	0.132	0.146	0.144
K	0.065	0.038	0.027	0.038
F	0.106	0.101	0.098	0.086
Cl	0.009	0.006	0.01	0.004
Total	17.952	17.793	17.808	17.808

Appendix I

Fluid inclusions

ID	Type	Class	Shape	Size	Fill	Te	Tm_ice	Td	Th_CO_2	Phase	Tm_clathrate	Th_total	EqWt%NaCl	Density
A1	CO2	Primary	Faceted	10	0.7	-62	2		24.5	Liquid	7	360	5.7631	0.719
A4	CO2	Primary	Faceted	5	0.7					Liquid		340		
A10	CO2	Primary	Faceted	10	0.7	-30	-1.5		17.5	Liquid	10	400	0	0.7994
C20	CO2	Primary	Rounded	10	0.7	-60.5				Liquid	9.9	380		
C21	CO2	Primary	Faceted	10	0.7	-50	-2			Liquid	8.5	380		
D1	CO2	Primary	Rounded	5	0.7	-55			27	Liquid	8.4	330	3.2074	0.6775
D2	CO2	Primary	Faceted	5	0.7	-30			27	Liquid	7.3	330	5.2343	0.6775
D3	CO2	Primary	Rounded	5	0.7		-8.3		27	Liquid	7.9	320	4.1461	0.6775
D4	CO2	Primary	Rounded	5	0.7		-8.3		27	Liquid	8.4	330	3.2074	0.6775
D5	CO2	Primary	Faceted	5	0.7	-36			27	Liquid	7.9	300	4.1461	0.6775
D6	CO2	Primary	Faceted	5	0.7	-49			27	Liquid	7.9	330	4.1461	0.6775
E1	CO2	Primary	Faceted	10	0.5	-20	-9		13.5	Liquid	9.5	430	1.0365	0.8346
E2	CO2	Primary	Faceted	10	0.7	-20			22	Liquid	9.5	380	1.0365	0.7518
E3	CO2	Primary	Faceted	10	0.5				17	Liquid	7		5.7631	0.8041
E4	CO2	Primary	Faceted	5	0.7	-50	-1		17	Liquid	9	380	2.0417	0.8041
E5	CO2	Primary	Faceted	5	0.7	-50	-1		17	Liquid	9	380	2.0417	0.8041
E8	CO2	Primary	Faceted	5	0.5		-1			Liquid	9			
E20	CO2	Primary	Rounded	10	0.5	-35			27.1	Liquid	12.5			0.6756
F1	CO2	Primary	Faceted	5	0.5	-25	6.5		10	Liquid	7.5	366	4.8762	0.8619
F2	CO2	Primary	Faceted	10	0.7	-20	6.5		12.5	Liquid	7.5	450	4.8762	0.8427
F20	CO2	Primary	Faceted	5	0.5		-8		27	Liquid	4.6		9.6481	0.6775
F21	CO2	Primary	Rounded	5	0.5		-3		27	Liquid	6		7.4548	0.6775
F22	CO2	Primary	Rounded	5	0.5		1.8		27	Liquid	8		3.9607	0.6775
F23	CO2	Primary	Rounded	5	0.5	-32	-7		27	Liquid	2		13.2313	0.6775
F24	CO2	Primary	Faceted	10	0.5	-58.5	5		27	Liquid	8		3.9607	0.6775
G20	CO2	Primary	Faceted	10	0.5	-49	2.5		18	Liquid	9.8	384	0.4184	0.7946
G21	CO2	Primary	Faceted	5	0.7				17	Liquid	9.8	476	0.4184	0.8041
G22	CO2	Primary	Faceted	5	0.7				17	Liquid	9.8	384	0.4184	0.8041
G23	CO2	Primary	Faceted	10	0.7		7		19.9	Liquid	9.8	358	0.4184	0.7754
H1	CO2	Primary	Faceted	10	0.5	-61.4	4.2	260	23.3	Liquid				0.7355
H2	CO2	Primary	Faceted	10	0.7	-50	5	260	23.3	Liquid				0.7355
H20	CO2	Primary	Faceted	10	0.5	-50	2	310	29	Liquid	8.4		3.2074	0.6309
H21	CO2	Primary	Faceted	5	0.5	-45.5		310	22	Liquid	7.6		4.6954	0.7518

ID	Type	Class	Shape	Size	Fill	Te	Tm_ice	Td	Th_CO_2	Phase	Tm_clathrate	Th_total	EqWt%NaCl	Density
H22	CO2	Primary	Faceted	5	0.5			310		Liquid	7.6			
H23	CO2	Primary	Rounded	5	0.5	-45.5		310	19	Liquid	7.6		4.6954	0.7847
H24	CO2	Primary	Faceted	5	0.7	-45.5		310	23	Liquid	7.6		4.6954	0.7394
H25	CO2	Primary	Rounded	5	0.5	-45.5		310	18	Liquid	7.6		4.6954	0.7946
I1	CO2	Primary	Faceted	10	0.5	-52	5.3		25	Vapour	8.5	290	3.0162	0.2425
I2	CO2	Primary	Faceted	5	0.5	-50	5.3		27.2	Liquid	8.5	349	3.0162	0.6736
I3	CO2	Primary	Faceted	5	0.5	-50	5.3		27.2	Liquid	8.5		3.0162	0.6736
I4	CO2	Primary	Faceted	5	0.5	-50	5.3		27.2	Liquid	8.5	349	3.0162	0.6736
K1	CO2	Primary	Faceted	10	0.5	-57	2		26	Liquid	6.5	390	6.6224	0.6956
L1	CO2	Primary	Faceted	10	0.5	-52	-5.6		22.5	Liquid	8.7	370	2.63	0.7457
L2	CO2	Primary	Faceted	10	0.7	-51.5	-4		22.5	Liquid	8.8	300	2.4351	0.7457
L3	CO2	Primary	Faceted	10	0.7					Liquid		300		
M20	CO2	Primary	Faceted	5	0.95	-55	-2		13.1	Vapour	8.3	415	3.3975	0.1501
M21	CO2	Primary	Faceted	5	0.9				13.1	Liquid		355		0.8379
M22	CO2	Primary	Faceted	5	0.9				15.1	Liquid				0.8212
N1	CO2	Primary	Faceted	5	0.5		4		20	Liquid	6.8	450	6.1101	0.7743
N2	CO2	Primary	Faceted	5	0.5	-47	4		20	Liquid	6.8	450	6.1101	0.7743
N3	CO2	Primary	Faceted	5	0.5	-39	4		20	Liquid	6.8	450	6.1101	0.7743
N4	CO2	Primary	Faceted	10	0.5	-30	0	439	18.4	Liquid	6.8		6.1101	0.7907
N5	CO2	Primary	Faceted	5	0.5		2.7		20	Liquid	6.8	450	6.1101	0.7743
N6	CO2	Primary	Rounded	10	0.7	-37	2	443	23.4	Liquid	6.8		6.1101	0.7342
N7	CO2	Primary	Faceted	5	0.5			400		Liquid	6.8	390		
N20	CO2	Primary	Faceted	5	0.5	-33	-3		18	Liquid	1.1		14.3382	0.7946
N21	CO2	Primary	Faceted	5	0.5				18	Liquid	5		9.0415	0.7946
N22	CO2	Primary	Faceted	5	0.5				18	Liquid	8		3.9607	0.7946
P1	CO2	Primary	Faceted	10	0.5	-50	2	360	25	Vapour	6.9		5.9372	0.2425
P2	CO2	Primary	Faceted	10	0.7	-47	2	300	25	Vapour	6.9		5.9372	0.2425
P3	CO2	Primary	Faceted	10	0.7	-40	2		26	Vapour	6.4	368	6.791	0.2557
P21	CO2	Primary	Faceted	5	0.7				28	Liquid	7.3	350	5.2343	0.6566
R1	CO2	Primary	Faceted	5	0.5		2		27	Liquid	5	395	9.0415	0.6775
R2	CO2	Primary	Faceted	10	0.5		2	300	27	Liquid	5		9.0415	0.6775
R3	CO2	Primary	Faceted	10	0.7		2	470	27	Liquid	8		3.9607	0.6775

ID	Type	Class	Shape	Size	Fill	Te	Tm_ice	Th_aq	Td	Phase	Tm_clathrate	Th_total	EqWt%NaCl	Density
A2	V+L	Primary	Faceted	5	0.7	-60	-5	286.5		Liquid	-5	286.5	7.8185	0.8155
A3	V+L	Primary	Faceted	5	0.7			343		Liquid		343		0.6005
A4	V+L	Primary	Faceted	5	0.5			340		Liquid		340		0.6105
A5	V+L	Primary	Faceted	5	0.7			360		Liquid		360		0.5282
A11	V+L	Primary	Faceted	5	0.7	-45	-1	400		Liquid	10.5	400	1.6515	0.4877
A12	V+L	Primary	Faceted	5	0.7		-0.4	386		Liquid	10.5	386	0.662	0.5039
A13	V+L	Primary	Faceted	5	0.5			386		Liquid		386		0.317
B20	V+L	Primary	Rounded	5	0.5	-50	-0.5	331		Liquid	8.5	331	0.8274	0.6449
B21	V+L	Primary	Faceted	5	0.5		4.9	370		Liquid	9	370		0.5334
B23	V+L	Primary	Faceted	5	0.5			380		Liquid		380		0.317
D20	V+L	Primary	Faceted	10	0.95	-9.5	-4.8	12.5		Liquid	0	12.5	7.5355	1.0534
D21	V+L	Primary	Faceted	5	0.7			400		Liquid		400		0.317
D22	V+L	Primary	Faceted	5	0.5		-7.5	379		Liquid	12.1	379	11.1005	0.7102
D23	V+L	Primary	Faceted	5	0.6		-7.5	390		Liquid	12.1	390	11.1005	0.6913
G1	V+L	Primary	Irregular	5	0.7		-10	420		Liquid	10	420	13.945	0.6854
H3	V+L	Primary	Faceted	5	0.9	-30	-5.3	209		Liquid	-3	209	8.2372	0.9187
H4	V+L	Primary	Faceted	5	0.9	-55	-5.3	205		Liquid	3	205	8.2372	0.9231
H5	V+L	Primary	Faceted	5	0.9			199		Liquid		199		0.8658
L20	V+L	Primary	Faceted	10	0.5	-55	-8	347		Liquid	8.5	347	11.7023	0.7698
L21	V+L	Primary	Faceted	5	0.7		-4	322		Liquid	4.8	322	6.3737	0.7422
L22	V+L	Primary	Faceted	5	0.7		-4	322		Liquid	9	322	6.3737	0.7422
L23	V+L	Primary	Faceted	5	0.5		-4	322		Liquid		322	6.3737	0.7422
L24	V+L	Primary	Faceted	10	0.5		-8	395		Liquid		395	11.7023	0.6921
M1	V+L	Primary	Faceted	5	0.5		-2.5	380		Liquid		380	4.0743	0.5896
M2	V+L	Primary	Faceted	5	0.5	-30		380		Liquid	11.2	380		0.317
M3	V+L	Primary	Faceted	5	0.7	-44	-2.5	328		Liquid		328	4.0743	0.7
M4	V+L	Primary	Faceted	5	0.9			357		Liquid		357		0.5438
O20	V+L	Primary	Faceted	10	0.7	-50	-4.5		383	Liquid	7			
S1	V+L	Primary	Faceted	10	0.5	-35	4	400		Liquid	9.5	400		0.4478
S2	V+L	Primary	Faceted	10	0.5		5	400		Liquid	9.5	400		0.4478

ID	Type	Class	Shape	Size	Fill	Te	Tm_ice	Th_aq	Phase	Tm_clathrat	Th_total	EqWt%NaCl	Density
B1	V+L	Secondary	Faceted	5	0.75	-65	-2.5	363	Liquid	0	363	4.0743	0.6279
B2	V+L	Secondary	Faceted	2.5	0.5		-5	310	Liquid	7	310	7.8185	0.7798
B6	V+L	Secondary	Faceted	5	0.5		-5	245	Liquid	7	245	7.8185	0.8723
B7	V+L	Secondary	Faceted	5	0.5			315	Liquid	7	315		0.6793
B8	V+L	Secondary	Faceted	5	0.5		-5	325	Liquid	7	325	7.8185	0.7556
C1	V+L	Secondary	Rounded	5	0.5			303	Liquid	5	303		0.7062
C2	V+L	Secondary	Faceted	2.5	0.5		-6.25	250	Liquid	11	250	9.5179	0.8811
C3	V+L	Secondary	Faceted	2.5	0.5		-5	295	Liquid	5.9	295	7.8185	0.8029
C4	V+L	Secondary	Faceted	2.5	0.5			295	Liquid	5.9	295		0.7226
C6	V+L	Secondary	Faceted	2.5	0.75		-6.25	289	Liquid	11	289	9.5179	0.8297
I20	V+L	Secondary	Faceted	5	0.8		-7.6	178	Liquid		178	11.2223	0.9733
I21	V+L	Secondary	Faceted	5	0.75		-7.6	178	Liquid		178	11.2223	0.9733
I22	V+L	Secondary	Faceted	5	0.75		-8.4	178	Liquid		178	12.1713	0.9804
J2	V+L	Secondary	Faceted	2.5	0.9			170	Liquid	-0.6	170		0.8975
J3	V+L	Secondary	Faceted	5	0.8		-6.2	209	Liquid	-5.3	209	9.4522	0.9282
J4	V+L	Secondary	Rounded	2.5	0.75		-6.2	209	Liquid	-5.3	209	9.4522	0.9282
P20	V+L	Secondary	Faceted	5	0.5			347	Liquid	2	347		0.5861
P22	V+L	Secondary	Faceted	5	0.7	-30	-4.5	295	Liquid	2	295	7.1054	0.7951
P23	V+L	Secondary	Rounded	2.5	0.5			300	Liquid	7.3	300		0.7125
P24	V+L	Secondary	Rounded	2.5	0.5	-37	-1.5	246	Liquid	6.8	246	2.4692	0.8227
Q1	V+L	Secondary	Faceted	5	0.5	-50	2.7	340	Liquid	5	340		0.6102
Q2	V+L	Secondary	Faceted	5	0.75		-10	340	Liquid		340	13.945	0.8072
Q20	V+L	Secondary	Faceted	5	0.75		-8	326	Liquid	5	326	11.7023	0.801
Q21	V+L	Secondary	Faceted	5	0.75	-55	-8	289	Liquid	2.5	289	11.7023	0.8519

ID	Type	Class	Shape	Size	Fill	Te	Tm_ice	Th_aq	Td	Phase	Tm_clathrate	Th_total	EqWt%NaCl	Density
C22	V+L+S	Secondary	Faceted	10	0.5		-5		406	Liquid	8.3			
O1	V+L+S	Secondary	Faceted	10	0.5				369	Liquid				
T1	V+L+S	Secondary	Faceted	10	0.5	-63	-8.6	375		Liquid	2	550	12.4019	0.7355
T20	V+L+S	Secondary	Faceted	10	0.5	-50	-4			Liquid	1			
T21	V+L+S	Secondary	Faceted	10	0.5					Liquid	2			
U1	V+L+S	Secondary	Faceted	10	0.95	-15	-10			Liquid	0			
U2	V+L+S	Secondary	Faceted	5	0.95		-10			Liquid	0			
U20	V+L+S	Secondary	Faceted	5	0.7	-25.5	-9			Liquid	-5			
V1	V+L+S	Secondary	Faceted	5	0.95	-23	-10		220	Liquid	-7			
V20	V+L+S	Secondary	Faceted	10	0.7	-20	-10			Liquid	-0.5			
W1	V+L+S	Secondary	Faceted	5	0.5	-30	-15			Liquid	2			
W20	V+L+S	Secondary	Faceted	10	0.5	-34.6	-13		300	Liquid	7.6			
X1	V+L+S	Secondary	Faceted	5	0.5	-35	-8			Liquid				
X20	V+L+S	Secondary	Faceted	5	0.7		-13			Liquid				

Appendix J

Sulphur isotope analyses

Sulphur Isotope Analysis

CSL No.	Sample ID	Drill Hole	Depth (m)	Mineral	Weight (mg)	Yield (mmHg)	$\delta^{34}S$ (wrt CDT) permil
9111	S1	E005	85	mo	15.6	23.0	**0.17**
9112	S2	E005	85	mo	15.5	26.4	**0.83**
9113	S3	E005	93.8	aspy	15.7	22.0	**-0.36**
9114	S4	E005	93.8	aspy	14.6	13.8	**0.28**
9115	S5	E005	111.5	po	15.3*	25.8	**0.44**
9116	S6	E005	111.5	po	17.6	35.0	**1.78**
9117	S7	E005	141.5	py	10.8	24.4	**2.25**
9118	S8	E005	145	py	11.6	23.8	**2.43**
9119	S9	E005	145	aspy	17.0	18.4	**2.07**
9120	S10	E005	147	mo	9.3*	7.8	**1.40**
9121	S11	ED006	94	po	13.1	20.4	**0.93**
9122	S12	ED002	77.4	po	16.0	27.6	**1.31**

Abbreviations: mo = molybdenite, aspy = arsenopyrite, po = pyrrhotite, m = metres, mg = milligrams, * = all sample used.